

HYD-RESPONSES: daily hydro-meteorological catchment-level time series to analyse HYDrological drought dynamics in RESPONSE to (cumulative) water deficits in Swiss catchments.

Christoph Nathanael von Matt^{1,2}, Benjamin David Stocker^{1,2}, and Olivia Martius^{1,2}

¹Institute of Geography, University of Bern, Bern, Switzerland

²Oeschger Center for Climate Change Research, University of Bern, Bern, Switzerland

Correspondence: Christoph Nathanael von Matt (christoph.vonmatt@unibe.ch)

Abstract.

The HYD-RESPONSES dataset (<https://doi.org/10.5281/zenodo.14713274>; von Matt et al., 2026) provides new daily catchment-level time series for key hydro-meteorological variables necessary to study drought conditions, including precipitation, snow water equivalent, temperature, soil moisture, (potential) evaporation, and streamflow. The dataset covers 184 small to large Swiss catchments of the surface water monitoring network operated by the Federal Office for the Environment (FOEN). The catchments range across a variety of streamflow regime types, mean altitudes, biogeographic regions, and anthropogenic influences. The dataset comprises daily mean streamflow observations obtained from the Federal Office for the Environment (FOEN), complemented by daily hydrometeorological variables aggregated at the catchment scale. Complementary variables are derived from from spatially gridded products provided by MeteoSwiss (Spatial Climate Analyses), the WSL Institute for Snow and Avalanche Research SLF (SPASS), SLF (OSHD), and the European Centre for Medium-Range Weather Forecasts ECMWF (ERA5-Land reanalysis).

In addition, derived indicators describing snowfall, snowmelt, (potential) water balance and streamflow are provided. Deficits related to precipitation, evaporation, and streamflow are quantified using both standardized and non-standardized (drought/deficit) indices. Standardized indices include the SPI, SPEI and SMRI and are provided on multiple aggregation scales from 1 to 24 months (mostly in 3-monthly steps). Non-standardized indices are provided as cumulative (water) deficits in (potential) water balance (CWD and PCWD) and streamflow (CQD). For all variables and indices, the climatology and the (standardized) anomalies are available on various time scales (daily, monthly, seasonal, and yearly). Drought event time series containing drought event numbers and drought event durations, are provided for streamflow droughts identified by using two percentile-based event definitions (fixed and variable threshold) and for cumulative water deficits (CWD, PCWD and CQD).

Detailed catchment descriptors covering hydro-climatological and hydro-terrestrial aspects as well as streamflow characteristics are provided for all catchments. The dataset can be used to study weather-driven streamflow extremes, to train data-driven machine-learning algorithms, to study drought propagation, and for comparative analyses of catchment responses in disturbed and undisturbed catchments. The dataset is compatible with the recently published "Catchment Attributes and MEteorology for Large-sample Studies" dataset for hydrological Switzerland (CAMELS-CH) and with additional catchment descriptors

1 Introduction

In recent years, the frequency of droughts has increased in Europe and Switzerland with notable drought years in 2003, 2011, 2015, 2018, 2020. Most recently, in 2022, conditions were characterized as unprecedented in terms of compound heat and
30 drought in the last 500 years over large parts of Europe (BAFU, 2016; BAFU et al. (Eds.), 2019; BUWAL, BWG, Me-
teoSchiweiz, 2004; Scherrer et al., 2022; Tripathy and Mishra, 2023). Under climate change, this trend is likely to continue
with projected increases in drought frequency, dry spell duration, and drought severity for both individual and combined
drought types (Brunner et al., 2019c, a; Calanca, 2007; Kotlarski et al., 2023; Muelchi et al., 2021a; von Matt et al., 2024).
Increasing drought impacts on various sectors are expected. This has prompted Swiss national authorities to establish a na-
35 tional drought early warning system (DEWS, see <https://www.trockenheit.admin.ch/en>; BAFU (Eds.), 2021; CH2018, 2018;
Haile et al., 2020; Henne et al., 2018; Naumann et al., 2021; Brunner et al., 2019a; Otero et al., 2023; Ranasinghe et al., 2021;
Tschurr et al., 2020; BAFU, 2022; Swiss Confederation, 2025).

Droughts are an inherently multivariate phenomenon with often non-linear propagation from meteorological conditions to im-
pacts on ecosystems, infrastructure, and economy. Individual drought events may differ in their hydro-climatological, hydro-
40 meteorological, hydro-terrestrial and anthropogenic drivers (Brunner et al., 2023; Hao and Singh, 2015; Mishra and Singh,
2010; Zhou et al., 2021; Floriancic et al., 2020; Massari et al., 2022). The consideration of multiple hydro-climatic, hydro-
meteorological, hydro-terrestrial and anthropogenic (disturbance) factors is therefore key to understand catchment-specific
drought responses and sensitivities and to provide information for drought early warning, preparations, and interventions (e.g.,
Apurv et al., 2017; Apurv and Cai, 2020; Baez-Villanueva et al., 2024; Brunner et al., 2022, 2021; Ding et al., 2021; Peña-
45 Angulo et al., 2022; Peña-Gallardo et al., 2019; Sutanto and Van Lanen, 2022; Tjrdeman et al., 2018; Van Lanen et al., 2013;
Savelli et al., 2022; Van Loon and Laaha, 2015; von Matt et al., 2024).

High-resolution observational datasets provide a unique opportunity to combine multiple hydro-meteorological variables to
analyze and monitor drought dynamics and the evolution of drought impacts of individual events at the catchment-level. For
example, the propagation of meteorological to hydrological droughts or the evolution of droughts from the development to the
50 recovery phase can be studied (Brunner et al., 2021; Brunner and Chartier-Rescan, 2024; Parry et al., 2016; Raposo et al., 2023;
Brocca et al., 2024a; Brunner et al., 2021; Stocker et al., 2023; Poussin et al., 2021). The Federal Office for Climatology and
Meteorology (MeteoSwiss) provides a suite of high-resolution essential climate variables spatially interpolated to a regular grid
from a dense measurement station network (MeteoSwiss, 2024). Further, new high-resolution snow climatologies produced by
both MeteoSwiss and the WSL Institute for Snow and Avalanche research SLF have recently become available, providing a
55 unique opportunity to analyze the long-term influence of snow processes, which are crucial for streamflow (drought) generation
in Alpine catchments in Switzerland (Staudinger et al., 2014, 2017; Avanzi et al., 2024; Brunner et al., 2023; Koehler et al.,
2022; Michel et al., 2023; Marty et al., 2025).

Observation-based evapotranspiration and soil moisture data is sparse in Switzerland. Hence, information on these variables is often extracted from hydrological model simulations (Brunner et al., 2021; Melsen and Guse, 2019; Samaniego et al., 2013, 2018). The ERA5-Land reanalysis dataset, provided by the European Centre for Medium-Range Weather Forecasts (ECMWF) (Muñoz-Sabater et al., 2021), offers a compromise between high spatial resolution and long temporal coverage and is better suited for hydro-meteorological analyses and modelling over more complex terrain such as Switzerland than the ERA5 reanalysis datasets (Muñoz-Sabater et al., 2021). A frequently used approach for analyzing drought propagation from meteorological (precipitation) to agricultural (soil moisture) and hydrological (streamflow and/or groundwater) droughts relies on standardized drought indices based on e.g., precipitation and/or evaporation (by using the standardized precipitation index (SPI) or the standardized precipitation evaporation index (SPEI) (Raposo et al., 2023; Barker et al., 2016; Peña-Gallardo et al., 2019; Zhou et al., 2021). These standardized drought indices are typically aggregated over varying retrospective time scales (months to years) and are useful proxies for various factors that determine catchment-scale water balances, including soil moisture, streamflow, groundwater, and snow processes (Bachmair et al., 2018; Tschurr et al., 2020; European Commission, 2020; Cammalleri et al., 2019; Staudinger et al., 2014). Longer aggregation scales hereby reflect response scales of storage components with longer memory, while shorter scales reflect streamflow and/or soil moisture in smaller catchments, mainly influenced by pluvial processes (Bachmair et al., 2018; Baez-Villanueva et al., 2024; Haslinger et al., 2014; Myronidis et al., 2018; Staudinger et al., 2014; Tschurr et al., 2020; WMO and GWP, 2016; Yihdego et al., 2019; Cammalleri et al., 2019; Bachmair et al., 2016; European Commission, 2020). Standardized drought indices are now widely used in DEWS (Bachmair et al., 2016; Kchouk et al., 2022; Raposo et al., 2023; Tjrdeman et al., 2020) and will also be used in the Swiss DEWS (L. Benelli, pers. comm.).

Recent studies focused on assessing the benefits of non-standardized (deficit) indices in tracking the drought propagation signal across drought types (see e.g., Brunner and Chartier-Rescan, 2024; Sur et al., 2020; Wu et al., 2020). Non-standardized indices provide physically interpretable and consistent information on deficits which remain inter-comparable across systems (Van Loon, 2015; Raposo et al., 2023; Wu et al., 2020). Examples are the Hydrological Anomaly Index (HAI), the Water Balance Drought Index (WBDI), the cumulative water deficits (CWD), and the potential cumulative water deficit (PCWD) (Stocker et al., 2023; Sur et al., 2020; Wu et al., 2020). Non-standardized indices allow direct quantification of (precipitation) deficits or surpluses associated with the drought propagation into and recovery from a (hydrological) droughts (Wu et al., 2020) and hence provide valuable information for proactive water management and decision-making (Xu et al., 2023; Parry et al., 2018).

Here, we present a novel dataset with high-resolution observational daily catchment-level time series for key hydro-meteorological variables (including precipitation, snow water equivalent, temperature, soil moisture, (potential) evaporation and streamflow), standardized and non-standardized (drought/deficit) indices (SPI, SPEI, SMRI, CWD, PCWD, CQD) and (streamflow) drought events covering 184 small to large catchments in Switzerland. The HYD-RESPONSES dataset can be combined with existing hydro-meteorological time series datasets and catchment descriptors such as CAMELS-CH (Höge et al., 2023a), which provides large-sample hydro-meteorological data for hydrologic Switzerland (i.e., all catchment areas that drain into Switzerland) and is the Swiss version of the "Catchment Attributes and MEteorology for Large-sample Studies"

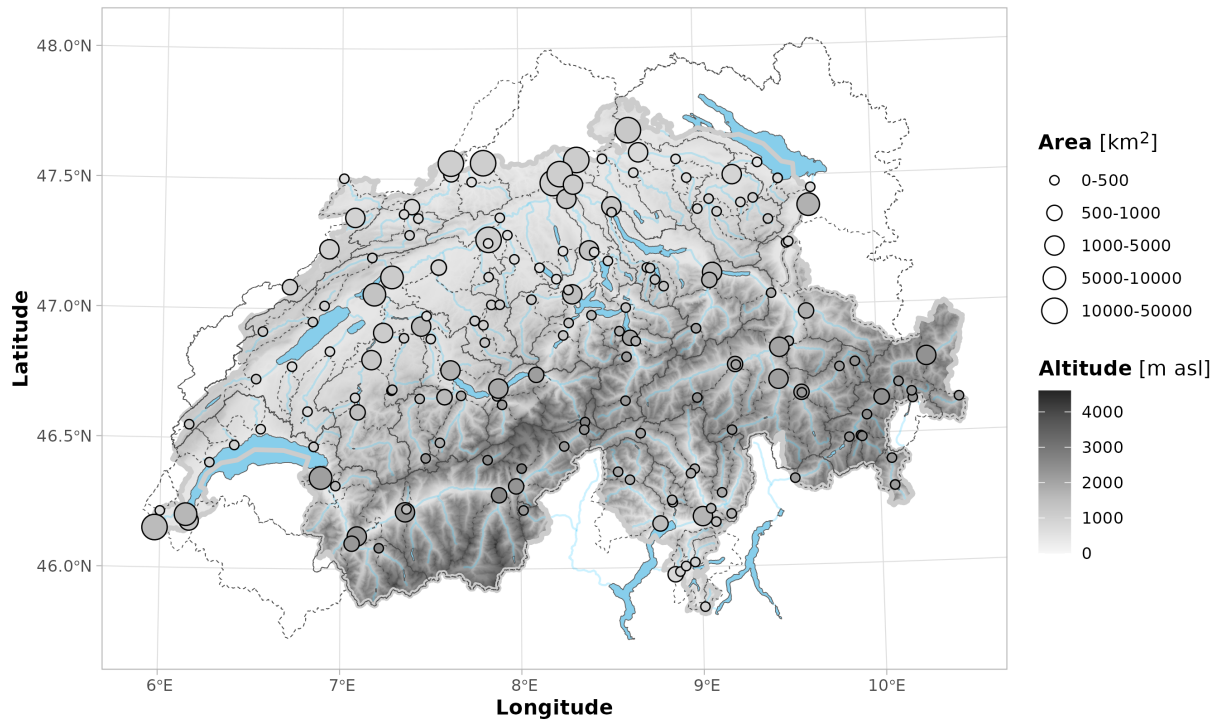


Figure 1. Overview of the study area and catchments included in the HYD-RESPONSES dataset. Catchment outlets (circles) are coloured by mean catchment altitude [m a.s.l.] and the point size scales with the catchment area [km²]. Dashed lines show the catchment outlines. Generalized streamflow networks and lakes are shown in light blue.

(CAMELS; see e.g., Clerc-Schwarzenbach et al., 2024). The remaining paper is structured as follows: In section 2 the study region and the catchments are presented. Section 3 introduces all datasets used to compile the HYD-RESPONSES dataset. Section 4 elaborates on the processing of hydro-meteorological data. Section 5 is the analogue for the processing and extraction of catchment descriptors. Section 6 finally discusses the dataset and points to potential caveats and cautionary notes while section 7 presents multiple complementary datasets which are valuable in combination with the HYD-RESPONSES dataset. Section 8 provides a concluding summary. Three exemplary use cases to illustrate the nature and potential of the HYD-RESPONSES dataset are provided in Appendix A.

100 2 Study region and catchments

The 184 catchments (Fig. 1) provided in the HYD-RESPONSES dataset span a wide range of catchment areas (0.56–35'878 km²), glaciation percentages (0–56 %), altitude ranges (467–2937 m a.s.l.) and 18 streamflow regime types (see Fig. 2). Roughly two thirds of the catchments 64.7 % (n=119) are small to mid-size with an area of between 10 km² and 500 km². Only 9 (4 %) catchments are smaller than 10 km² and 56 (30.4 %) catchments are larger than 500 km². The dataset contains

105 eight very large catchments with areas between 10000 km² and 50000 km² (max. area = 35'878 km²), associated with the three
largest rivers in Switzerland: Aare, Rhine and Rhone. Most catchments (82.5 %) have less than 5 % glaciated area. In terms of
mean catchment height (elevation), the catchments are distributed relatively equally between 500 and 2500 m a.s.l. (see Fig.
2c). Only eight catchments are higher than 2500 m a.s.l. and only one catchment is at very low elevation (catchment Wiese,
Basel). Streamflow regime types were classified and adjusted by the FOEN based on data from the Hydrological Atlas of
110 Switzerland Table 5.2 (https://hydrologischeratlas.ch/downloads/01/content/Tafel_52.pdf). Catchments smaller than 500 km²
are characterized by considering mean altitude and catchment glaciation percentage to reflect the contribution of specific
streamflow (drought) generating processes (glacial, nival, pluvial). Catchments larger than 500 km² are generally classified
as *mixed regime* (>500 km²) type and contain catchments characterized by a combination of streamflow (drought) generating
processes. For more information see also Aschwanden and Weingartner (1985) and Fig. 2e.

115 Note that 12.5 % (n=23) of the catchments have at least 5 % of catchment area lying outside of the Swiss national borders as the
dataset consists of catchments of the entire hydrological Switzerland (catchments that drain in(to) Switzerland). Furthermore,
the Swiss streamflow monitoring network is designed such that multiple measurement stations may be located along the
same river. As a result, upstream catchments can be nested within larger downstream catchments, leading to hierarchical
dependencies.

120 **3 Input data products**

In this section, the input datasets used to produce and compile the HYD-RESPONSES dataset are presented and reference
literature for further reading and more detailed information is provided. Original data products are provided by the Federal
Office for Climatology and Meteorology (MeteoSwiss), the Federal Office for the Environment (FOEN), the Swiss Federal
Office of Topography (Swisstopo), the Federal Office for Agriculture (FOAG), the WSL Institute for Snow and Avalanche
125 Research (SLF) and the European Centre for Medium-Range Weather Forecasts (ECMWF).

3.1 Catchment-level time series data from streamflow observations

Daily average streamflow measurements at the catchment outlet were provided by the FOEN via the Hydrological Service
(www.hydrodaten.admin.ch) for more than 200 stations. The data availability is station-specific and depends on the installation
and FOEN-internal data quality checking. The HYD-RESPONSES dataset only provides a subset of 184 catchments and
130 considers only stations for which an analysis of hydrological drought dynamics in response to cumulative water deficits was
deemed to be meaningful in correspondence with the FOEN (Caroline Kan; see Fig. 1). These are stations that provide reliable
streamflow (Q) time series and are associated with a physical/natural catchment. Stations are therefore excluded if they i)
only provide water-level information (no Q, 3 stations), ii) are not part of the main streamflow measurement network (e.g.,
stations from other networks such as the National Surface Water Monitoring Programme (NAWA BAFU, 2023), 4 stations), iii)
135 secondary stations (11 stations), iv) stations with potential return streamflow (= negative Q values, 2 stations), v) Q measured
at derivations (2 stations), vi) stations without watershed delineation (i.e., subterranean; 1 station) and vii) uncertainties in time

Table 1. (Spatially gridded) Data products used for the time series extraction. Full variable names and associated units are provided in Table B1 (glossary) in Appendix B. Note that the variable short names correspond to the layer/product names in the respective dataset.

Dataset	Variables	Period	Spatial resolution	Temporal resolution	Producer
Spatial Climate Analyses	TabsD, RhiresD	1961–2023	1 × 1 km	daily	MeteoSwiss
	TminD, TmaxD, SrelD	1971–2023			
Snow Climatology for Switzerland (SPASS)	SWECLQMD	1961–2022	1 × 1 km	daily	MeteoSwiss & SLF
Climatological snow data since 1998 (OSHD)	swee, romc	1998–2023	1 × 1 km	daily	SLF
ERA5-Land	tp, t2m, e, pev, smlt, sd, ssr, ro, sro, swvl1, swvl2, swvl3, swvl4	1950–2023	0.1 × 0.1° (ca. 9 × 9 km)	hourly	ECMWF
Streamflow time series	Q	Station specific	catchment-level (outflow point data)	daily	FOEN

series composition due to displacement and/or temporarily missing Q of contributing stations (4 stations). The complete list of stations included is provided in Tables B6, B7, B8, B9 and B10 in Appendix B.

3.2 Catchment-level time series data derived from spatially gridded products

140 Hydro-meteorological variables used in this study were compiled from multiple complementary data sources, combining station-based spatial climate analyses, dedicated snow model products, and reanalysis data (Table 1). This multi-source approach allows both comprehensive coverage of relevant variables and comparative analyses between different data products.

Meteorological variables derived from station-based observations were obtained from the high-resolution (1 × 1 km) spatial climate analyses provided by MeteoSwiss (MeteoSwiss, 2024). These include average 2 m temperature (TabsD), daily minimum and maximum 2 m temperature (TminD, TmaxD), daily precipitation sums (RhiresD), and daily sunshine duration (SrelD) (Frei, 2014; Frei and Schär, 1998; MeteoSwiss, 2021a, b, c). Data availability is product-specific and covers the period 1961–2023 for RhiresD and TabsD and 1971–2023 for TminD, TmaxD, and SrelD. The spatial climate analyses generally cover the Swiss territory only, with the exception of RhiresD, which also includes catchments outside Switzerland that drain through Swiss territory. Note that RhiresD is not available for catchments covering regions in France and Italy before 1992 due to limited meteorological station availability and reduced data reliability (MeteoSwiss, 2021a). Catchments with substantial

areas in these regions should therefore be treated with caution or excluded from analyses prior to 1992 (see Sect. 6.2).

155 Snow water equivalent (SWE) data were compiled from two independent high-resolution (1×1 km) snow datasets. The primary source is the spatial Snow Climatology for Switzerland (SPASS) developed jointly by MeteoSwiss and SLF (Michel et al., 2023; Marty et al., 2025). This dataset provides modelled and bias-corrected daily SWE for September 1961–September 2022, derived using the SnowQM model based on TabsD and RhiresD. The SnowQM model is presented in detail in Michel et al. (2023). The spatial coverage is restricted to Switzerland. A second snow dataset is derived from the Swiss Operational Snow-Hydrological model system (OSHD), provided by WSL (SLF), which supplies SWE and modelled snowmelt runoff for
160 the period 1998–2022 (Mott, 2023; Mott et al., 2023).

All remaining hydro-meteorological variables, including evaporation, potential evaporation, soil moisture, and additional variables overlapping with the datasets described above, were extracted from the ERA5-Land reanalysis provided by ECMWF (Muñoz-Sabater et al., 2021). Several variables are thus available from multiple sources and are retained in the
165 HYD-RESPONSES dataset to enable inter-product comparisons. Variables covered by more than one data source include air temperature (TabsD, TminD and TmaxD from MeteoSwiss, t2m from ERA5-Land), precipitation (RhiresD from MeteoSwiss, precipitation from ERA5-Land), snow water equivalent (SWE; from SPASS, OSHD, and ERA5-Land) and modelled snowmelt (from OSHD and ERA5-Land). Additional ERA5-Land-specific variables include soil water volume (swvl) at four depths, total solar radiation (ssr), total runoff (ro), and surface runoff (sro). Detailed variable descriptions are provided in the dataset
170 documentation on Zenodo (von Matt et al., 2026). A glossary for the variable abbreviations is provided in Table B1.

ERA5-Land data are available at hourly resolution for the period 1950—2023 via the Copernicus Climate Data Store (CDS) (<https://cds.climate.copernicus.eu/datasets/reanalysis-era5-land>). ERA5-Land consists of numerical model output from the ECMWF land surface model which itself is driven by downscaled and elevation-corrected meteorological forcing from
175 ERA5 (Muñoz-Sabater et al., 2021). The higher spatial resolution ($0.1 \times 0.1^\circ$, approximately 9×9 km) results in an enhanced soil moisture representation and river discharge estimations making ERA5-Land more suitable for analyses based on the hydrological cycle than ERA5 (Muñoz-Sabater et al., 2021).

The procedures used to extract time series from all gridded datasets are detailed in Section 4.

180 3.3 Catchment-level time-invariant data (catchment descriptors)

Datasets used to compile an extensive set of catchment descriptors include station metadata and information on time series availability and homogeneity provided by the FOEN as well as spatial (polygon) data on hydro-terrestrial characteristics (e.g., soil characteristics, hydro-geology) provided by the FOEN, FOAG and Swisstopo (see Table 2). Most information is available from www.opendata.swiss, the FOEN Hydro-Service (www.hydrodaten.admin.ch), or can be downloaded and inspected via

Table 2. Data products used to extract catchment descriptors.

Dataset	(Extracted) Variables	Producer
Digital soil suitability maps of Switzerland	soil wetness, soil depth, permeability, water holding capacity, nutrient content and skeletal content	FOAG
Hydrogeological map of Switzerland	aquifer type (loose or solid rock), aquifer genesis and aquifer productivity	FOEN
Lithological map for Switzerland	dominant rock type classes (loose, sedimentary and crystalline rock)	Swisstopo
Springs and swallow holes in karst regions	number of springs (per km ²)	FOEN
swissTLM3D Hydrography	Drainage density	Swisstopo
Biogeographic regions of Switzerland	Biogeographic regions	FOEN
Catchment metadata	time series availability, breakpoint analysis, area, mean height, outlet coordinates and streamflow regime type	FOEN

185 www.map.geo.admin.ch (Swisstopo). Direct links to the datasets are provided below and in section *Code and data availability*.

The digital soil suitability maps of Switzerland provide information on a set of different soil characteristics assessed on 25 different geological and geomorphological units which are further discriminated by different landscape elements depending on aspect, slope and bedrock. The maps were first assessed in 1980 and revised in 2000 (BLW, 2022; Swisstopo, 2020). The
 190 different soil characteristics include soil wetness, soil depth, permeability, water storage capacity, nutrient content and skeletal content.

The hydro-geological map of Switzerland provides information on groundwater resources in Switzerland (Schürch et al., 2007), including information on aquifer type (loose or solid rock), aquifer genesis and aquifer productivity. The map was originally produced and published for the Hydrological Atlas of Switzerland (HADES, <https://hydrologischeratlas.ch/>). The
 195 hydro-geological information was further complemented with the lithological map for Switzerland (produced by Swisstopo), which provides a general overview of dominant rock type classes (loose, sedimentary and crystalline rock). The maps are available via opendata.swiss (hydrogeological map, lithological map) or can also be accessed via the Hydrological Service of the FOEN (<https://www.bafu.admin.ch/bafu/de/home/themen/wasser/zustand/karten/geodaten.html>). The number of springs and swallow holes in karstic regions provides additional information related to aquifers and the contribution of subsurface
 200 water storage. The layer provides main discharge source locations in karstic regions and is available via opendata.swiss (produced by FOEN). The swissTLM3D Hydrography provides topological information on the different water bodies of Switzerland (including flowing and stagnant waters) and originates from the swissTLM3D dataset provided by and accessible

Basic catchment characteristics

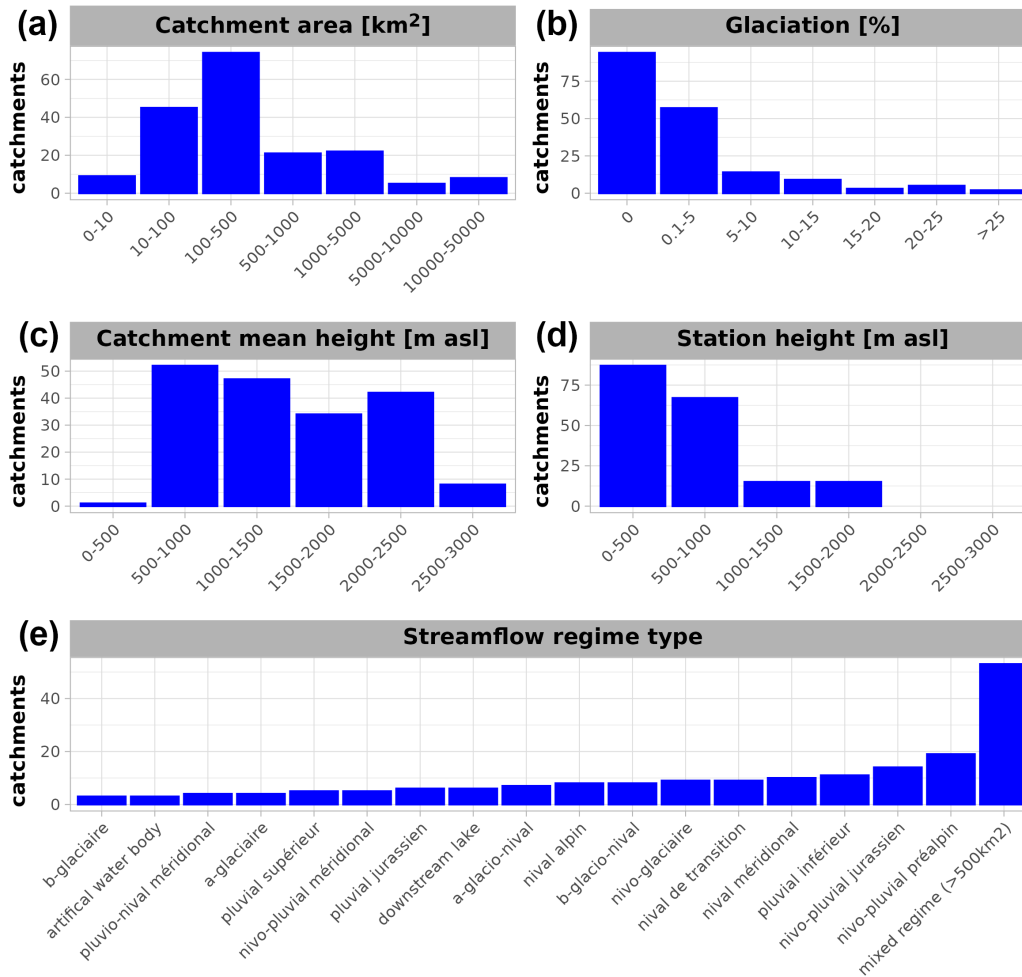


Figure 2. General catchment characteristics provided by the FOEN. **a)** Catchment area in km², **b)** Glaciation percentage (of catchment area), **c)** catchment mean height [m a.s.l.], **d)** height of the streamflow gauge measurement station [m a.s.l.] and **e)** streamflow regime types. The Y-axis shows the number of catchments in each category.

via Swisstopo.

The biogeographic regions of Switzerland provide six regions differentiated by similarity of flora, fauna, bryophytes and ornithological information as well as homogeneous surface water catchments (BAFU (Eds.), 2022). Biogeographic (eco-)regions often correspond well to catchment groups with similar streamflow regime types and are therefore frequently used for catchment regionalization (e.g., Jehn et al., 2020; Guo et al., 2021). The biogeographic regions are available via opendata.swiss.

Finally, general information on the gauging stations and streamflow time series (availability and homogeneity) were provided as accompanying (meta-)data by the FOEN. Time series homogeneity was derived by the FOEN using breakpoint tests following the method of Bai and Perron (1998). Breakpoints are identified by partitioning the time series based on the number of potential breakpoints and subsequent modeling of the time series by piecewise linear regression (see Bai and Perron, 1998). The optimal breakpoints are found by minimization of the sum of squared residuals. Resulting breakpoints are indicative to changes in the mean annual 7d mean flow (M7Q) and were further plausibilized by the FOEN based on catchment meta information and known (potentially) relevant anthropogenic influences such as the construction of (reservoir) dams, hydropower and wastewater treatment plants (for more information see BAFU, 2024). General station information includes catchment area, mean catchment height (elevation), glaciation percentage, outlet coordinates and streamflow regime type (among others) (see Figs. 1 and 2). Catchment outlines (polygons provided by the FOEN) and catchment outlets (point shapes) are provided in the coordinate system CH1903/LV03 (EPSG:21781).

220

Note that the digital soil suitability maps, swissTLM3D hydrography, biogeographic regions of Switzerland as well as information on springs and swallow holes in karst regions are restricted to Swiss national territory. Catchments with a significant area outside of Switzerland should be treated with caution regarding descriptive variables extracted from these datasets (see Sect. 5 for a comprehensive overview on extracted descriptors). The hydrogeological and lithological maps of Switzerland to a large extent also cover areas outside of Switzerland. Only catchments of the Rhine (catchments 2091, 2143, 2288, 2289) and Wiese (catchment 2199) are not entirely covered. However, with a coverage of at least >94%, descriptors extracted from these datasets may still prove valuable for these catchments.

225

Methodological details on the extraction and preparation of catchment descriptors are presented in Section 5.

230 **4 Processing of hydro-meteorological data**

This section describes the methodology used for aggregating spatially gridded (time series) data product, the methods used to derive additional indicators, standardized drought indices, and presents the definition and declaration of (hydrological) drought events. Guidance on the reliability of indicators is provided through a three-level classification based on the origin of the underlying data, the extent to which variables rely on (model) assumptions, and the degree of processing applied to derive the hydro-meteorological data, (drought) indices, and events. *Level 1* consists of direct, unaltered measurement data and is therefore considered the most reliable. *Level 2* includes data directly extracted from publicly available spatially interpolated hydro-meteorological datasets and data subjected to only minimal (post-)processing (e.g., temporal aggregation). *Level 3* comprises all variables, indicators, and indices derived by the authors, irrespective of the degree of validation or verification performed. For both *Level 2* and *Level 3* data, additional annotations are provided for variables whose derivation is based on a (strong) modeling component. A summary of the classification is provided in Table 3.

240

The naming of the unaltered variables directly retrieved from measurement data (streamflow) or extracted from spatially

Table 3. Three-level processing classification used for hydro-meteorological data in the HYD-RESPONSES dataset. Note that these classes differ from the satellite data classification

Level	Description
Level 1 (L1)	Direct, unaltered measurement data. These data are considered the most reliable, as they are not subject to interpolation, modeling assumptions, or additional processing.
Level 2 (L2)	Data extracted from publicly available, spatially interpolated hydro-meteorological datasets and data subjected to only minimal post-processing, such as temporal aggregation. Variables whose derivation relies on strong underlying (modeling) assumptions are explicitly annotated.
Level 3 (L3)	Variables, indicators, and indices derived by the authors, irrespective of the degree of validation or verification performed. Variables whose derivation relies on strong underlying (modeling) assumptions are explicitly annotated.

interpolated hydro-meteorological datasets is based on the layer names used in the original input datasets (see variables listed in Table 1 and the glossary provided in Table B1). Derived variables and (standardized) drought indices are named by a suffix representing the type of indicator followed by all contributing variables where ERA5-Land variables are kept in lowercase while variables from other products start with upper-case letters. Naming for derived variables based on the snow products make use of the product name (SPASS) or the combination of product and variable names (OSHD) as identifier for clear distinction. All extracted and derived variables and their suggested reliability level are listed in the Tables B2, B3, B4 and B5 in Appendix B.

Time series of all categories are illustrated in Fig. 6 showing the exceptional drought year 2022 for the example catchment *2034 - Broye, (Payerne, Caserne d'aviation)* located in the western Swiss Plateau region (see catchment contours in Fig. A4). A detailed analysis of the event year 2022 demonstrating the utility of the time series provided in the HYD-RESPONSES dataset is provided in Sect. A2 in Appendix A.

4.1 Time series extraction

Based on the spatially gridded hydro-meteorological input products (see Sect. 3.2), catchment-level time series were extracted using the R-packages *terra* (Hijmans, 2023) and *exactextractr* (Baston, 2023). First, the hourly ERA5-Land data was aggregated to daily resolution following the standards used by the MeteoSwiss spatial climate analyses (e.g., RhiresD and TabsD). For this, instantaneous variables and variables representing accumulations or fluxes are distinguished. For instantaneous variables, we provide daily average values. For variables representing accumulations and fluxes, we provide daily sums. Flux variables (mainly precipitation and evapotranspiration) are aggregated using the same temporal convention as the RhiresD precipitation sums, i.e., from 06 UTC (day) to 06 UTC (day + 1) (see MeteoSwiss, 2021a). Instantaneous variables and ERA5-Land temperature were averaged from 00 UTC to 00 UTC again following the convention used in

equivalent MeteoSwiss products (e.g., TabsD; MeteoSwiss, 2021b). Daily catchment-average time series were then extracted by using the catchment outlines (polygons) provided by the FOEN. Units were homogenized across time series. Both units and full standard variable names are listed in Table B1 (glossary).

The length of the time series depends on the dataset that they were derived from (see Table 1 for details). Streamflow time series are provided for three different catchment-specific time periods: (1) the original time series (entire period), (2) the time series of the most recent gap-free time-period and (3) the most recent homogeneous time series (in case of significant and plausible breakpoints; otherwise equal to the gap-free time series) (see Fig. 3). The breakpoint information is provided by FOEN (see Sect. 3.3). Information on the start of the streamflow monitoring by water level sensor is also provided. The streamflow data should only be considered reliable after the initialization of a sensor. In case of no breakpoints the gap-free period is equal to the homogeneous period. The homogeneous period is usually the shortest (e.g., in case of breakpoints or water level sensor initialization; see for example catchment 2349 in Fig. 3). In the case of gaps but no breakpoints, both the homogeneous and the gap-free periods are identical (see, i.e., catchments 2239, 2386 and 2368 in Fig. 3). Indicators and (non-)standardized (drought/deficit) indices derived from the hydro-meteorological time series are available for the longest common period of all contributing variables.

4.2 Derived indicators

4.2.1 Streamflow

Derived indicators related to streamflow consist of the 7-day average streamflow (moving average) M7Q (Fig. 6i). The M7Q (or M7) is often used in low-flow studies and is also used for the official low-flow statistics in Switzerland by the FOEN (see e.g., BAFU, 2024; Muelchi et al., 2021a; von Matt et al., 2024).

4.2.2 Snow related variables

In addition to variables providing direct information on (modelled) snowmelt, also daily differentiated SWE (Δ SWE) time series are provided for both SPASS and OSHD. Snowfall (Δ SWE > 0) and snowmelt (Δ SWE < 0) time series are provided separately. Note that SWE is reset in the SPASS dataset at the end of every snow year (every September 1st) to avoid unrealistically high accumulation of snow water equivalents (“snow towers”; see Michel et al., 2023). As snowfall and snowmelt were derived from daily differences in SWE (Δ SWE), this reset can result in an artificially large negative Δ SWE value on September 1st that does not represent actual physical snowmelt. To prevent this model artifact from affecting the derived snowmelt time series, Δ SWE values on September 1st were set to missing values and replaced by a linear interpolation using the Δ SWE values from the preceding and following days. Snow-corrected precipitation series ($P + \Delta$ SWE) were calculated by combining time series of total precipitation (RhiresD and ERA5-Land) and Δ SWE time series (SPASS, OSHD) as well as time series with modelled snowmelt information (SPASS, OSHD and ERA5-Land). Negative snow-corrected precipitation amounts (e.g., $RhiresD < \Delta$ SWE) were set to zero.

(Potential) Water balance indicators (P–E and P–PET) were derived by combining the total and snow-corrected precipitation time series with the ERA5-Land evaporation and potential evaporation time series.

4.3 Cumulative water deficits

(Potential) Cumulative water deficits (CWD and PCWD) are non-standardized indicators tracking evaporation-driven deficits in the (potential) water balance. CWD and PCWD were derived from the daily water balance indicator time series (see Sect. 4.2.3) using the *cwd* R-package (Stocker et al., 2023; Stocker, 2021). A deficit starts when the water balance is negative (i.e., $P - E < 0$) and is accumulated as long as the deficit remains uncompensated (deficit > 0). Note that no surplus information is tracked. Once the deficit is compensated, the values remain at zero (CWD = 0). Example time series are shown for both CWD and PCWD in Fig 6k,l. In some cases (especially for P–PET based only on ERA5-Land variables, i.e., $tp-pev$), PCWDs are not compensated each year and can persist over multiple years. Both CWDs and PCWDs are hence also provided on a yearly calculation basis (annual reset on December 31st). Non-standardized indices preserve units (here millimetres) and are physically interpretable in terms of absolute deficit amounts. Cumulative water deficits do not rely on a predetermined calculation time window, which allows the user to track both deficits accumulated over short periods in time (below one month) and deficits accumulated over very long periods.

Water-balance based non-standardized drought indices are widely in use in ecohydrological, land-atmosphere interaction research and catchment-memory studies both with and without temporal resets (see e.g., Biegel et al., 2025; Cui et al., 2022; Stocker et al., 2023). Being more strongly tied to the actual physical water availability, non-compensated CWDs may provide valuable information on carry-over effects in multi-year drought contexts and/or long-term shifts in climatic water balance (Stocker, 2021; Fowler et al., 2022; Saft et al., 2015). PCWDs in contrast are based on potential water balance and (absolute) carry-over deficits should hence be treated with caution. CWD and PCWD time series which are annually reset provide complementary year-to-year information, which may better align in contexts of annual low-flow statistics and allows for a year-to-year comparison across years and catchments.

4.4 Standardized (drought) indices

Standardized (drought) indices depict the anomaly of a deficit over a fixed retrospective time window (e.g., 1 month). The hydro-meteorological indicator time series is first aggregated over the given window and then transformed to a standard normal distribution by fitting a suitable candidate distribution (Tijdeman et al., 2020; Stagge et al., 2015). Standardized indices therefore provide information on both anomalously dry and wet conditions, which are often defined by thresholds corresponding to standard deviations (STD). As such, values below -1 STD indicate drier than normal conditions (moderate droughts), while values above $+1$ STD indicate wetter than normal conditions (moderate wetness) (McKee et al., 1993; Tschurr et al., 2020). The HYD-RESPONSES dataset provides daily time series for three standardized (drought) indices: the Standardized Precipitation Index (SPI, McKee et al., 1993), the Snowmelt and Rain Index (SMRI, Staudinger et al., 2014), and the Standard-

ized Precipitation Evaporation Index (SPEI, Vicente-Serrano et al., 2010). The SPI represents deficits driven by precipitation only (derived from P), while the SMRI tracks deficits in liquid water input originating from both rainfall and snowmelt (derived from $P + \Delta SWE$) accounting for seasonal snowfall and snowmelt dynamics (Staudinger et al., 2014; Baez-Villanueva et al., 2024). The SPEI represents deficits driven by evaporative demand (derived from P-PET) and hence indirectly accounts for temperature effects (Vicente-Serrano et al., 2010; Mwinjuma et al., 2026; Gebrechorkos et al., 2025). Daily time series for all three indices (SPI, SPEI, SMRI) are provided for aggregation windows ranging from 1–24 months (31–730 days). Exemplary SPI and SMRI time series for all aggregation windows are shown in Fig. 6g,h.

All indices were calculated using the *SCI* R-package (Stagge et al., 2015; Gudmundsson and Stagge, 2016) with custom modifications accounting for the daily time series resolution. All candidate distributions provided within the *SCI* R-package (*gamma*, *genlog*, *gumbel*, *lnorm*, *norm*, *gev*, *pe3*, *weibull*) were tested for suitability. The distributions were fitted for each day of the year (DOY) based on the reference period 1991–2020. This results in a fit for each DOY derived from the same (window of) values for each distribution. Monthly SPI fits (SPI-1) are for example based on the 30 daily values up to the specific DOY for each of the 30 years in the reference period 1991–2020. The suitability of candidate distributions was assessed based on three indicators: the Shapiro-Wilks normality tests (*p*-values; Shapiro and Wilk, 1965), the number of flags returned by the fitting function *fitSCI* (see *SCI* R-package; Gudmundsson and Stagge, 2016), and the number of missing and/or implausible values. Implausible values are defined as values above or below ± 3 STD following Stagge et al. (2015). Estimating more extreme standardized index values from a 30-year climatology requires substantial extrapolation of the fitted distribution and is therefore associated with large uncertainty, particularly given the strong temporal autocorrelation of drought indices. Values beyond ± 3 correspond to events with return periods far exceeding the length of the reference record and cannot be robustly quantified (see Stagge et al., 2015).

The returned flags in distribution parameter fitting were mainly related to convergence issues (non-convergence) (flag 3, see *SCI* R-package Gudmundsson and Stagge, 2016). Without a valid fit, the transformation to standardized index values is not possible resulting in missing values on the flagged DOYs in all time series years. As in Staudinger et al. (2014), one best-fitting distribution (over all DOYs) is chosen for all catchments to allow for catchment comparability. The distribution was selected among the distributions satisfying the following conditions: (1) the transformed values are not significantly different from a normal distribution for the majority of catchments (*p*-values > 0.05 for at least 75 % of the catchments), (2) fewer than 5 DOYs flagged and (3) fewer than 50 implausible and/or missing values in the transformed time series (combined consideration of missing values due to flags and unrealistically high/low values). The distribution selection procedure is illustrated for the SPEI in Fig. 4. The results of the Shapiro-Wilks tests (*p*-values) and information on missing/implausible values and flags are also provided in the HYD-RESPONSES dataset and can be used to identify catchments with non-satisfying properties within the overall best-fitting distribution (see Fig. 4). Following Stagge et al. (2015), values of all standardized (drought) indices time series were constrained to the interval $[-3, 3]$ STD.

The *Gamma* distribution was chosen for the SPI for all variables (RhiresD, ERA5-Land), which is consistent with other studies and recommendations of the World Meteorological Organization (WMO) (WMO and GWP, 2016; Stagge et al., 2015; Tschurr et al., 2020; von Matt et al., 2024). The SMRI was fitted by the *genlog* (*lnorm*) distribution for the snow-corrected precipitation

series based on SPASS (ERA5-Land and OSHD). For the SPEI, the *genlog* distribution was found to perform best across time scales (see Fig. 4).

365 SPI, SPEI and SMRI provide complementary (and standardized) information on hydroclimatic variability and drought-related processes facilitating integrated analyses of drought development and propagation and allowing consistent comparisons across catchments, regions and climates (Mwinjuma et al., 2026; Gebrechorkos et al., 2025; Tisdeman et al., 2022). Standardized indices are frequently employed in drought monitoring and early warning systems (DEWS; Tisdeman et al., 2020; Kchouk et al., 2022), drought propagation analysis or as proxy for various storage processes (Haslinger et al., 2014; Cammalleri et al., 2019; Raposo et al., 2023; Peña-Gallardo et al., 2019; Barker et al., 2016). Example use cases for drought event analysis and 370 catchment response patterns are provided in sections A2 and A3 in Appendix A.

4.5 Climatology & Anomalies

Climatologies and anomalies are provided for all time series, including the time series of variables directly extracted from spatially gridded data products with no modifications except for spatial and temporal aggregation where required (see Sect. 4.1), derived indicators (Sect. 4.2), standardized drought indices (Sect. 4.4), and cumulative water deficits (Sect. 4.3 and 4.6). 375 Both climatologies and anomalies are based on the reference period 1991–2020. The climatology is provided for two variants: i) using moving windows and ii) for fixed time windows. The variants are available at the following time scales: daily (only i), monthly (both), seasonal (both), and annual (only ii). The moving window climatology was calculated by using a moving window of 31 days ($day - 15$, $day = 0$, $day + 15$) for the monthly, a 3-month window (91 days) for the seasonal and a 6-month (183 days) window for the extended season time scale. The moving window climatology is calculated for DOYs 1–366 with 380 NA-values set for February 29th in the case of non-leap years. Example time series for monthly anomalies in 2 m temperature, precipitation, evaporation, soil moisture, snow water equivalent, snowmelt and (potential) cumulative water deficits are shown in Fig. 6a-f,m-n.

The regular climatology is available for monthly, seasonal (DJF, MAM, JJA, SON), extended season (May–October, November–March) and annual time scales. Using the moving window climatology, standardized anomalies have been derived by first subtracting the climatological mean (μ) and then dividing by the climatological standard deviation (σ) (also 385 known as *z-scores*). The following climatological statistics are provided: minimum, maximum, mean, median, standard deviation, 5th, 25th, 75th and 95th percentiles. For the 7-day average streamflow series (M7Q) we also provide the 2nd, 10th and 15th percentiles which are frequently used in streamflow drought analysis and monitoring (see e.g., Van Loon, 2015; Stahl et al., 2020; Sarailidis et al., 2019; BAFU, 2025).

390 4.6 Cumulative streamflow deficits

Time series of cumulative streamflow deficits (CQD) were calculated based on negative streamflow anomalies (drought phases) by using the same procedure as for cumulative water deficits (see Sect. 4.3). CQD time series are provided for both fixed and variable threshold definitions. Fixed thresholds (e.g., a constant percentile threshold) are used for critical flow levels that do not change seasonally (e.g., directly linked to physical/actual low-flow or water scarcity situations) whereas variable thresholds

395 (e.g., seasonally varying percentiles) account for seasonality and changing flow regimes, allowing drought phases and deficits to be identified relative to expected (seasonal) conditions ("anomalies", Stahl et al., 2020; Van Loon, 2015; Brunner et al., 2019a; von Matt et al., 2024). Hence, variable threshold definitions are often used to analyse seasonally varying streamflow (drought) generating processes or to understand drought propagation mechanisms (Brunner et al., 2023, 2022; Hammond et al., 2022). For the fixed threshold definition, daily M7Q anomalies were derived for events exceeding the Q347 threshold, defined as the
400 daily flow rate exceeded for 347 days per year (i.e., the 347-day exceedance flow, roughly corresponding to the 5th streamflow percentile; see Sect. 5.3). For the variable threshold definition, daily M7Q anomalies were calculated for the following monthly (31 days) and seasonal (91 days) percentiles: 2nd, 5th, 10th, 15th, 25th, 50th (median) and mean. Cumulative deficits are physically interpretable and in the case of cumulative water deficits [mm] and streamflow deficits [m³/s] also physically comparable in terms of total runoff depth [mm]. Figure 6j shows CQDs for both fixed and variable threshold definitions for the year 2022 for
405 catchment 2034 - Broye, (*Payerne, Caserne d'aviation*).

4.7 Identification of drought events

We define drought events as coherent phases of non-zero deficits for cumulative deficits (CWD, PCWD and CQD) and as negative M7Q-based streamflow anomalies for streamflow droughts. Streamflow drought phases were extracted for the same percentiles and time scales as used for CQDs (see Sect. 4.6), namely for monthly (31 days) and seasonal (91 days) percentiles:
410 2nd, 5th, 10th, 15th, 25th, 50th (median) and the mean. Streamflow events were also extracted for the fixed (yearly) Q347 threshold (see Sect. 4.6 and 5.3).

An event starts on the first day values fall below the threshold value and lasts until values exceed the threshold again (see Fig. 5). For each variant, the event time series consists of consecutively numbered event phases and information on the event duration since the start (i.e., an event with a duration of 5 days is represented in the time series as: "1 1 1 1 1" (event phase number),
415 "1 2 3 4 5" (duration since start)). Additional event characteristics (e.g., lowest value during a phase) can easily be derived by the user in combination with the indicator time series. A minor pooling of hydrological drought events is introduced by using the 7-day average streamflow (M7Q) time series which merges closely succeeding and potentially dependent individual events to one single event as a result of the smoothing of large day-to-day fluctuations (Tallaksen and Van Lanen, 2004; Hisdal and Tallaksen, 2000; Tallaksen et al., 1997; Sarailidis et al., 2019). Streamflow drought events based on both fixed and variable
420 threshold definitions were used for the event shadings in Fig. 6.

5 Catchment descriptors

Catchment descriptors were extracted from spatial datasets containing information on hydro-terrestrial characteristics (e.g., soil suitability maps), catchment (station) metadata (see Sect. 3.3) and the extracted hydro-meteorological time series (e.g., climatology; see Sect. 4.5). All catchment descriptors provide only static (time-invariant) catchment information. Catchment
425 descriptors are provided as single-value catchment-level information. An example use case of catchment grouping/regionalization based on catchment descriptors is presented in Sect. A1 in Appendix A.

5.1 Field-based descriptors

Spatially non-overlapping polygon datasets (e.g., soil suitability maps) typically provide categorized values for variable-specific classes (e.g., soil depth classes are *shallow*, *medium*, *deep*, *very deep*). To extract catchment-level information, polygon-based information was first rasterized to a spatial grid identical to the MeteoSwiss spatial climate analyses grid products (in both extent and resolution). The rasterization was done by using the *rasterize* function of the *terra* R-package (Hijmans, 2023). Each grid cell only contains the value of the category with the largest overlap. The percentage overlap with the catchment area was then assessed for all variable-specific classes by using the *exact_extract* function (as for time series) and adjusting the aggregation function to fractions ("frac"; see Baston, 2023). Catchment area overlap fractions are provided for all categories. Descriptors with multiple classes can also be reduced to a single dominant category represented by the largest percentage overlap ("proportion"). An example is shown for the biogeographic regions in Fig. 7a. Reducing a specific catchment descriptor to one single (dominant) category (e.g., derived via largest overlap percentage) may however lead to a loss in explanatory power as the category with the largest overlap may not necessarily be the most representative or most influential for streamflow (drought) analysis.

5.2 Feature-based descriptors

Two descriptive variables related to catchment shape and drainage were derived in R by using the catchment outlines, namely the *basin shape index* (BSI) and *drainage density*. The HYD-RESPONSES dataset provides two BSI variants. The first variant is derived based on a ratio between area and basin length (A/L^2) known as form factor (Horton, 1932) and the second variant is based on a ratio between the catchment area and the area of the circle with the smallest radius encircling the entire catchment (A_{catch}/A_{circle}) known as circularity ratio (Miller, 1953). Both indices range from 0 to 1. Both are frequently used (also in combination) as morphometric catchment indicators (see e.g., Das et al., 2022; Pisupati and Ratnakar, 2025). Albeit providing similar information, the form factor is primarily controlled by basin length and hence provides information on catchment elongation, while the circularity ratio is more sensitive to basin shape accounting for complex/irregular shapes resulting in larger areas (for more information on basin shape indices see Das et al., 2022). The drainage density denotes the ratio between the catchment area and the total length of streamflow channels (both natural and stormwater drainage infrastructure; Dingham, 1978; USGS, 2023). The drainage density was calculated by using the *swissTLM3D* hydrography dataset (see Sect. 10 for a download link). Both indices (BSI and drainage density) are frequently used in flood-related studies but may also provide valuable information during low-flow periods as high-intensity precipitation events are a relevant factor for (streamflow) drought recovery (Eekhout et al., 2018; Floriancic et al., 2022; Lee and Ajami, 2023; Matanó et al., 2024; Qiu et al., 2021; Tarasova et al., 2024; Vicente-Serrano et al., 2022; Wu et al., 2022; Xu et al., 2023). Further, also the overlap percentage with the Swiss territory (*swissBOUNDARIES3D*, see Sect. 10 for a download link) is provided for each catchment and can be used to exclude catchments with significant portions outside of Switzerland which goes along with a limited coverage in both hydro-meteorological and catchment descriptor input datasets (see Sect. 3.2 and 3.3) for ca. 12.5 % of catchments (see Sect. 2). Information on karstic sources and sinks is provided as the number of sources and swallow holes per catchment and km^2 .

460 5.3 Time series-based and climatological descriptors

Several indices related to streamflow characteristics (low flow, responsiveness, baseflow and flow stability) are provided in the HYD-RESPONSES dataset. The Q347 (Aschwanden, 1992; Aschwanden and Kan, 1999) is a low flow index used as the basis for water abstraction restrictions in Switzerland and corresponds to the daily flow rate exceeded for 347 days per year. The Q347 was derived from the flow duration curve (FDC) by using the *hydroTSM* R-package (Zambrano-Bigiarini, 2020) and corresponds roughly to the 5th streamflow percentile (95th percentile of 365 days \approx 347, hence Q347). The baseflow index (BFI; Nathan and McMahon, 1990) is a widely used index linked to multiple catchment characteristics such as aquifer type, productivity and soil characteristics. The BFI provides information on the (base-)flow sustained during dry periods (e.g., by subsurface storages; Tallaksen and Van Lanen, 2004; Bloomfield et al., 2021; Van Loon and Laaha, 2015). The BFI was derived using the *baseflow* function of the *lfstat* R-package (Laaha and Koffler, 2022) and is shown in Fig. 7. Stoezle et al. (2020) introduced the delayed-flow index (DFI) which breaks down the BFI into individual hydrograph components. The components include fast, intermediate, slow and base responses and potentially reflect various storage processes contributing to the overall streamflow response (e.g., snowmelt and groundwater). The DFI was derived by using the *delayedflow* R-package (<https://modche.github.io/delayedflow/>; see also Stoezle et al., 2020). The last two indices related to streamflow behaviour are the "flashiness" or R-B-index (Baker et al., 2004) which represents the ratio of the sum of day-to-day streamflow changes divided by the total streamflow and the flow-stability index which relates the mean annual minimum flows (MAM_q) to the mean annual flow (MQ; MAM_q/MQ). The remaining catchment descriptors were derived from the extracted hydro-meteorological time series and/or their respective climatology. Information on average precipitation, temperature, evaporation, snow water equivalent, streamflow, the fraction of precipitation falling as snow and the runoff fraction (Q/P) are provided on yearly scales for identifying broad climatic (i.e., water balance) and physiographic controls on hydrological behavior. Finally, monthly Pardé coefficients (PCs) are provided which indicate the contribution of monthly mean streamflow to the annual mean streamflow.

6 Discussion

6.1 Relevance and Applications

The HYD-RESPONSES dataset addresses fundamental challenges in hydrological drought analyses by compiling and harmonizing multiple data sources into a coherent catchment-scale framework, enabling multi-variable drought analyses in Switzerland. Drought (deficit) indices derived from two high-resolution snow climatologies for Switzerland (SPASS, OSHD) also allow for in-depth quantitative analyses on the contribution of snow processes to cross-seasonal drought propagation in Alpine catchments (Staudinger et al., 2014, 2017; Brunner et al., 2023). A combined use of standardized indices (SPI, SPEI, SMRI at 1–24 month scales) and non-standardized cumulative deficits (CWD, PCWD, CQD) facilitate multi-scale (drought) deficit and catchment response sensitivity assessments and allows for a concurrent anomaly-based and physically interpretable characterization of drought deficits (Raposo et al., 2023; Van Loon, 2015; Wu et al., 2020; Baez-Villanueva et al., 2024; Stocker et al., 2023). By providing time series for many relevant variables for drought monitoring (precipitation, temperature, evaporation,

soil moisture and streamflow; see e.g., WMO and GWP, 2016) at daily temporal resolution, the HYD-RESPONSES dataset may also be used for training machine learning models such as Random Forests (RFs; e.g., Floriancic et al., 2022) or Long Short-Term Memory models (LSTMs; see Kratzert et al., 2018; Lees et al., 2022; Kratzert et al., 2023) which have recently emerged as promising approach for rainfall-runoff modeling (Kratzert et al., 2018, 2019; Lees et al., 2022). Three example applications of the HYD-RESPONSES dataset are illustrated in Sect. A1, A2 and A3 in Appendix A.

Although the dataset was developed for Switzerland, the methodological framework — combining in-situ observations, gridded products, and reanalysis into catchment-scale time series — is transferable, with requirements that scale with data availability. Replication requires four essential components: (1) streamflow observations with defined catchment boundaries, (2) meteorological forcing data (precipitation, temperature), (3) snow information for mountain regions, and (4) static catchment descriptors (e.g., information on soils, geology, topography). While the first component is often limiting, the second component is decisive for the applicability of the dataset on specific use cases. Switzerland can leverage from high-density observational station networks resulting in high-quality spatially gridded hydro-meteorological products (see e.g., MeteoSwiss, 2024). With known biases in mind (especially over complex terrain), ERA5-Land is a viable alternative by providing temporally and physically consistent variables at sufficiently high spatial resolution for comparative catchment studies and machine learning applications aiming for generalizable results in regions where observational networks are less dense (Muñoz-Sabater et al., 2021; Dalla Torre et al., 2024; Scherrer et al., 2023). For local operational drought management or absolute deficit quantification, reliable high-resolution observational products remain however preferable. Several recent developments address observational data limitations, including the Caravan global community dataset (Kratzert et al., 2023), rapidly advancing machine learning-based bias correction methods for downscaling reanalysis products such as ERA5-Land (Menapace et al., 2025; Najafi et al., 2026; Zhang et al., 2025) or advances in developing high-quality remote sensing-based products for soil moisture (e.g. SMAP; see Brocca et al., 2024b; An et al., 2025), snow (e.g., ICESat-2 Besso et al., 2024), evaporation (see e.g., Anderson et al., 2024) and terrestrial water storage (e.g., GRACE-FO; Rodell and Reager, 2023).

6.2 Limitations and cautionary notes

The HYD-RESPONSES time series are provided for product-specific periods, and the spatial coverage is restricted to Swiss territory for most of the higher resolution MeteoSwiss and SLF products (TabsD, TminD, TmaxD, SPASS, SrelD, OSHD) as well as many catchment descriptor input datasets. Full coverage over the entire hydrological Switzerland is only available for ERA5-Land (all variables) and the MeteoSwiss RhiresD product (after 1992; see MeteoSwiss, 2021a). Catchments with significant areas outside of the Swiss national borders —approximately 12.5 % of the catchments (see Sect. 2) — may therefore be considered with caution or used solely for time series based on ERA5-Land variables only. Time series for standardized drought indices are provided only for the transformation variant based on the best-fitting distribution across all catchments to allow for comparison across catchments comparability (see e.g., Staudinger et al., 2014). The best-fitting distribution may however vary across catchments and climates (see e.g., Stagge et al., 2015). The HYD-RESPONSES dataset therefore also provides information on fits, missing values, and flags which can be used to exclude catchments with unsatisfying fitting and transformation properties from analyses. Field- and feature-based catchment descriptors were aggregated at catchment level

via summarization (e.g., karstic sources) or percentage overlaps (see Sect. 5.1). Maximum percentage overlaps with catchment area may however only insufficiently account for spatial differentiation which could enhance the representation of factors most influential to streamflow evolution by accounting for spatial proximity to the stream/river courses (Tarasova et al., 2024; Floriancic et al., 2022).

530

Several known limitations are further related to the datasets used to compile the HYD-RESPONSES data. ERA5-Land is a state-of-the-art reanalysis product provided at a higher spatial resolution than the standard ERA5 reanalysis (Hersbach et al., 2020; Muñoz-Sabater et al., 2021). The higher spatial resolution results in a better depiction of soil moisture, lakes, river discharge estimations, and the orographic enhancement of precipitation (Muñoz-Sabater et al., 2021). ERA5 and ERA5-Land datasets however share most of the parameterizations, as ERA5-Land consists of output from the ECMWF land surface model driven by downscaled and elevation-corrected ERA5 data (Muñoz-Sabater et al., 2021). Despite the advantage of higher spatial resolution over ERA5, a grid resolution of 9 km still has limitations over complex high-altitude terrain. The extracted time series related to snow water equivalent should be used with caution, as snow depth in ERA5-Land is of mixed quality depending on geographical location and altitude (Dalla Torre et al., 2024). Scherrer et al. (2023) showed that ERA5-Land overestimates SWE at high elevations with larger biases in the southern compared to the northern Alps. Higher-resolution datasets such as SPASS (Marty et al., 2025) and OSHD (Mott, 2023; Mott et al., 2023) should hence be preferred over ERA5-Land. Note however that all snow-related datasets have problems in representing small SWE amounts at low altitudes (Scherrer et al., 2023; Michel et al., 2023; Marty et al., 2025). Caution is also required when using the snow-corrected precipitation (water input) time series. The time series corrected by the Δ SWE series consider both snowfall (Δ SWE > 0) and snowmelt (Δ SWE < 0), while the correction based on snowmelt variables only accounts for snowmelt (smlt in ERA5-Land and romc in OSHD; see Table 1 and Tables B1 and B2 and Sect. 4.2.2). Snowmelt-corrected precipitation time series may therefore be of limited use during the main snow accumulation season but can still provide valuable information during the snowmelt season.

Another limitation of the ERA5-Land dataset is the parameterization of subgrid-scale processes and the representation of subsurface storages that affect evapotranspiration (e.g., fixed maximum storage volume assumption; see Muñoz-Sabater et al., 2021). Key processes such as dynamic groundwater–vegetation interactions, irrigation withdrawals, and adaptive rooting strategies are hence not represented and may lead to biases in evapotranspiration responses (Muñoz-Sabater et al., 2021; Dalla Torre et al., 2024; Wood et al., 2025; Stocker et al., 2023). Although ERA5-Land compares more favorably with in situ soil moisture and evapotranspiration observations than previous reanalyses (e.g., ERA5), considerable discrepancies remain, especially in dry summers and in regions with heterogeneous land cover (Scherrer et al., 2022; Fluhrer et al., 2025). Given these limitations, drought indicators based on ERA5-Land evapotranspiration should generally be interpreted with caution. This limitation is further compounded by the fact that the validation of long-term soil moisture and evapotranspiration remains challenging due to the scarcity of consistent observational datasets, particularly at high spatial resolution and over multi-decadal time scales (Hirschi et al., 2020; Yi et al., 2024; Mukherjee et al., 2018). Many state-of-the-art evapotranspiration products are limited in temporal or spatial extent and can be affected by gaps and cloud contamination (e.g., remote sensing-based products; see Yi et al., 2024). ERA5-Land thus remains one of the few datasets providing spatially consistent

560

and continuous long-term evapotranspiration estimates with sufficiently high spatial resolution over Switzerland.

Additional caution is warranted when using HYD-RESPONSES water balance time series (and indicators derived from them) when they were derived by combining ERA5-Land evapotranspiration with (snow-corrected) precipitation from independent data sources (RhiresD, OSHD, and SPASS). While ERA5-Land variables are internally consistent, the combination with independent data sources may lead to systematic biases in absolute deficit estimates. This limits the interpretability of absolute cumulative deficits but does not invalidate the approach for comparative, process-oriented drought analyses across regions and catchments (e.g., drought propagation, catchment response sensitivities). Relative measures of cumulative deficits, their temporal evolution, and their normalization through ratios (e.g., CWD/PCWD) can still provide valuable insights, even when absolute magnitudes are uncertain. In such contexts, relative anomalies, temporal evolution, and spatial patterns are more informative than absolute deficit magnitudes. Studies have further demonstrated coherent representation of major drought events (e.g., drought years 2003 and 2018) across datasets, which supports the usability of combined indicator time series when known limitations are adequately taken into account (Scherrer et al., 2022; Wood et al., 2025). Note that the HYD-RESPONSES dataset also provides complementary water balance and SPEI time series derived from ERA5-Land variables only, providing consistent metrics and opportunity for comparisons among data products. Guidance on the usage and reliability of all HYD-RESPONSES time series products is provided by a classification based on three reliability levels (see Sect. 4 and Table 3). The levels are based on the origin of the underlying data, the extent to which variables rely on (model) assumptions, and the degree of processing applied to derive the hydro-meteorological time series.

580 7 Complementary datasets

Complementary datasets provide a wide range of additional catchment descriptors and hydro-meteorological time series. An overview of datasets and variables is provided in Table 4. The FOEN provides additional geodata related to both surface and groundwater via the Hydrological Service (<https://www.bafu.admin.ch/bafu/de/home/themen/wasser/zustand/karten/geodaten.html>). The datasets include additional catchment descriptors with information on population density, catchment areas covered by forest and agriculture (among others) as well as information on water quality aspects and sewage. The FOEN further operates both a groundwater monitoring network (NAQUA) providing continuous groundwater measurements for selected point locations (BAFU, 2019) and a water quality measurement network (NAWA) providing information on concentration and loads of important dissolved compounds (e.g., pH, electric conductivity, nutrient contents; BAFU, 2023).

The “Catchment Attributes and Meteorology for Large-sample catchment Studies” (CAMELS) datasets aim at providing a consistent set of hydro-meteorological time series and catchment descriptors over a large sample of hydrological catchments on country level (Clerc-Schwarzenbach et al., 2024). The catchments in the Swiss version of the CAMELS data (CAMELS-CH; Höge et al., 2023a) are largely congruent with our dataset. The only exception is station 2646, which is only contained in the HYD-RESPONSES dataset. Note that the HYD-RESPONSES dataset provides only a sample subset of 184 catchments. The

CAMELS-CH dataset provides valuable complementary catchment-level information on glacier changes (based on GLAMOS, 595 for details see Höge et al., 2023a), land use, hydro-geological and hydro-terrestrial information (e.g., the contributions of various grain size categories and bulk-density) as well as anthropogenic disturbances (e.g., hydropower and reservoir capacities). CAMELS-CH further provides modelled time series based on the hydrological model PREVAH (see e.g., Höge et al., 2023a; Viviroli et al., 2009). The CAMELS-CH dataset is freely available from Zenodo (<https://zenodo.org/records/10354485>; Höge et al., 2023b).

600 The CombiPrecip dataset (MeteoSwiss) provides high-resolution (10 minutes, 1×1 km) precipitation fields derived from a combination of radar and station measurement data (Sideris et al., 2014). The CombiPrecip dataset could be a valuable addition for studying drought recovery where extreme precipitation is often considered an important factor (Wu et al., 2022).

The HydCheck project (Streeb et al., 2024) evaluated the influence of (anthropogenic) disturbance factors on streamflow at stations of the National Surface Water Quality (NAWA) Programme (BAFU, 2023). The evaluated NAWA stations are largely 605 (87.5% of the stations) congruent with the HYD-RESPONSES dataset. The HydCheck dataset provides catchment-level information on the magnitudes for all evaluated disturbance categories including water storage and regulation, hydropower, sewage water, constructions, agriculture as well as drinking and groundwater. The overall impact on several hydrological properties including low-, mid- and high-flow regimes as well as short-term effects and hydraulics is provided as categorical information (from "not disturbed" to "strongly disturbed"). For more information see Streeb et al. (2024).

610 As part of the planned Swiss National drought early warning system (DEWS), both a high-resolution remote-sensing based evaporation product (V. Humphrey, pers. comm.) and an automatic soil moisture measurement network are under development at MeteoSwiss, ETH Zurich and WSL and may become a valuable addition in a future.

8 Conclusions

The HYD-RESPONSES dataset contains data for 184 Swiss catchments that cover a variety of streamflow regimes, mean alti- 615 tudes, catchment areas, and anthropogenic influences/disturbances. The catchments cover all biogeographic regions of Switzerland. The HYD-RESPONSES dataset provides daily streamflow data and daily hydro-meteorological time series extracted from gridded data products of MeteoSwiss (TabsD, RhiresD, TmaxD, TminD, SrelD), Meteoswiss and SLF (SPASS), SLF (OSHD) and ECMWF (ERA5-Land). The variables include temperature, precipitation, evaporation, sunshine duration, solar radiation, snowmelt, snow water equivalent, soil moisture, surface runoff, runoff, and streamflow. HYD-RESPONSES further provides 620 derived variables related to streamflow (e.g., M7Q), water balance (e.g., P-E) and snowfall. Additionally, three standardized drought indices (SPI, SPEI, SMRI) for accumulation windows from 1 to 24 months and information on the (non-standardized) cumulative water deficit (CWD), the potential cumulative water deficit (PCWD) and cumulative streamflow deficit (CQD) are provided.

The dataset also provides information on (streamflow) drought events (occurrence and duration). For each catchment, the 625 drought events have been identified based on fixed and on seasonally varying percentile thresholds.

The combination of data sources, the information on hydro-meteorological variables (mainly temperature, precipitation and

Table 4. Datasets compatible and complementary to the HYD-RESPONSES dataset.

Dataset	Short description	Provider
Accompanying catchment information	Includes catchment proportions of forests, agricultural (crop) land, population, built-up area and more	FOEN
Groundwater measurement network (NAQUA)	Groundwater measurements	FOEN
Water quality measurement network (NAWA)	Information on water quality parameters	FOEN
CAMELS-CH (Höge et al., 2023b)	Swiss version of the Catchment Attributes and Meteorology for Large sample catchment Studies (CAMELS) dataset	via Zenodo
MeteoSwiss CombiPrecip (CPC)	High-resolution precipitation fields at ground based on a combination of radar and measurement data	MeteoSwiss
HydCheck (Streeb et al., 2024)	Detailed evaluation of influences and disturbances of the streamflow at NAWA measurement stations	FOEN

snow), the derived indices (water balance, cumulative water deficits, standardized drought indices, climatology and anomalies) allow for a multi-purpose use and various analytical approaches such as time series analysis (e.g., Kratzert et al., 2018; Lees et al., 2022), drought propagation and catchment sensitivity analysis (e.g., based on principal component analysis and clustering; Jehn et al., 2020) and changes in rainfall-runoff relationships during hydrological droughts (e.g., Wu et al., 2021).

The HYD-RESPONSES dataset can easily be combined with complementary datasets such as CAMELS-CH (Höge et al., 2023a) and HydCheck (Streeb et al., 2024). The catchment time series vary in length (subject to station initialization), the hydrological time series are provided for the entire measurement period along with information on data homogeneity (see BAFU (2024) for more details).

635 Limitations exist for catchments extending beyond the Swiss borders. The catchment descriptors were extracted from datasets mainly covering Swiss national territory. The MeteoSwiss-based datasets cover only Switzerland except for RhiresD, which covers the entire hydrological Switzerland from 1992 onward. In summary, the dataset provides a state-of-the-art data basis to study droughts in Switzerland.

9 Code and data availability

640 The HYD-RESPONSES dataset is freely available (CC BY 4.0) from Zenodo (<https://doi.org/10.5281/zenodo.15748821>; von Matt et al., 2026). Regular updates are not planned. An R tutorial on how to use and combine the different data products is provided with the dataset but can also be accessed on GitHub (<https://github.com/codicolus/HYD-RESPONSES>).

As of now, MeteoSwiss gridded spatial analyses products (MeteoSwiss, 2021a, b, c) are not available for free but will be available for free in the course of 2025 (MeteoSwiss, 2025). The preliminary snow climatology for Switzerland (SPASS; see Michel et al., 2023; Marty et al., 2025) was provided directly by MeteoSwiss and is not yet available for public use. The SLF snow climatology (OSHD; Mott, 2023; Mott et al., 2023) was published under the WSL Data Policy and can be downloaded via Envidat (<https://www.envidat.ch/#/metadata/climatological-snow-data-1998-2022-oshd>). The hourly ERA5-Land dataset (Muñoz-Sabater et al., 2021) is accessible via the Copernicus Climate Data Store (CDS) (see <https://cds.climate.copernicus.eu/datasets/reanalysis-era5-land?tab=download>). Daily streamflow time series can be requested via the Hydrological Service of the FOEN via <https://www.bafu.admin.ch/bafu/de/home/themen/wasser/zustand/daten/messwerte-zum-thema-wasser-beziehen.html>. The soil suitability maps (FOAG), the hydrogeological map (FOEN) and the lithological map (Swisstopo) are available from <https://opendata.swiss> or directly via Swisstopo (<https://www.swisstopo.admin.ch/de/geokarten-500-vektor>). Directly available from Swisstopo are also the datasets swissTLM3D Hydrography (<https://www.swisstopo.admin.ch/de/landschaftsmodell-swisstlm3d#swissTLM3D---Download>) and swissBOUNDARIES3D (<https://www.swisstopo.admin.ch/de/landschaftsmodell-swissboundaries3d>). Further available via <https://opendata.swiss> are the Biogeographic regions (<https://opendata.swiss/de/dataset/biogeographische-regionen-der-schweiz-ch>; see also BAFU (Eds.), 2022) and information on karstic springs and swallow holes (also produced by the FOEN; <https://opendata.swiss/de/dataset/quellen-und-schwinden-in-karstgebieten>). Data used for the overview map of the study region (Fig. 1) is available for free from Swisstopo and FOEN. Datasets used include: the digital height model DHM25 (<https://www.swisstopo.admin.ch/de/hoehenmodell-dhm25>) and the general hydrological background map (downloadable via <https://opendata.swiss>; see <https://opendata.swiss/en/dataset/generalisierte-hintergrundkarte-zur-darstellung-hydrologischer-daten>).

The software used to compile the datasets are all open-source and contain the following R-packages available via CRAN: *tidyverse* (<https://cran.r-project.org/web/packages/tidyverse/index.html>; Wickham et al., 2019), *exactextractr* (<https://cran.r-project.org/web/packages/exactextractr/index.html>; Baston, 2023), *sf* (<https://cran.r-project.org/web/packages/sf/index.html>; Pebesma, 2018), *lfstat* (<https://cran.r-project.org/web/packages/lfstat/index.html>; Laaha and Koffler, 2022), *SCI* (<https://cran.r-project.org/web/packages/SCI/index.html>; Gudmundsson and Stagge, 2016; Stagge et al., 2015) and *stars* (<https://cran.r-project.org/web/packages/stars/index.html>; Pebesma and Bivand, 2023).

Available via Github are the R-packages *cwd* (Stocker (2021); available via: <https://github.com/stineb/cwd>), and *delayedflow* (Stoelzle et al. (2020); available via: <https://modche.github.io/delayedflow/>).

Author contributions. CNvM conceptualized the project proposal, acquired funding from the FOEN, performed the formal analysis and drafted the article. OM and BS provided guidance on the methodological aspects. CNvM, OM and BS assisted with writing the paper and revisions.

Competing interests. The contact author has declared that none of the authors has any competing interests.

675 *Acknowledgements.* The HYD-RESPONSES project was funded by the Federal Office for the Environment (FOEN). The preliminary SPASS dataset was kindly provided by Regula Muelchi (MeteoSwiss). We thank Caroline Kan (FOEN) for her help with the catchment selection.

Appendix A: Exemplary use cases

The different data types can be combined to comprehensively analyse hydrological streamflow droughts in response to various hydro-meteorological indicators. This section presents three use cases: catchment regionalization, in-depth event analysis, and
680 composite analysis. A comprehensive R-tutorial on how to read and combine the different data products is provided with the dataset but can also be accessed via Github (<https://github.com/codicolus/HYD-RESPONSES>).

A1 Catchment grouping

For some applications, catchments need to be grouped by similarity, as measured by a set catchment descriptors related to hydro-meteorological, terrestrial characteristics and/or anthropogenic disturbances (e.g., Tarasova et al., 2024). As an example
685 application, we show the distribution of catchment coverage fractions across biogeographic regions for the soil characteristics *soil depth, skeletal content, water logging, permeability, and water storage capacity* (Figure A1).

The percentage coverage distributions reveal notable differences in soil characteristics and their subcategories. Catchments in the Swiss Plateau region are characterized by larger coverages of deep to very deep soils with a mostly poor to medium skeletal content, normal soil permeability and good water storage capacities (see Fig. A1). Alpine catchments, on the other
690 hand, are characterized by shallower soils (especially the Southern Alps) and a higher skeletal content. Soils in the Alps further have almost no water logging and a low water storage capacity. Soils with a (weakly) inhibited permeability or with a very good water storage capacity are infrequent across all biogeographic regions.

Whereas soil characteristics reflect differences in terrestrial catchment characteristics, the streamflow regime types are more indicative of hydro-climatic streamflow generation processes (see Sect. 2, Fig. A2). In Alpine environments, snow- and glacier
695 processes are important contributors to streamflow generation. Hence, both Western and Eastern Central Alps show predominantly glacial and nival streamflow regime types of which 86 % are shared among regions (see Fig. A2a,b). In contrast to the Central Alps, the hydro-climatology of the Southern Alps is more Mediterranean with the Alps often described as "Alpine divide" between the warmer and drier conditions in the South and more temperate Atlantic influences in the North (NCCS, 2025; Haslinger et al., 2019). Despite similar streamflow generating processes, the streamflow regime types in the Southern Alps
700 are differentiated from their counterparts in the Central Alps (*méridional*, see Fig. A2d) and, in contrast to the Central Alps, can also include stronger contributions of pluvial processes. The Northern Pre-Alps show the largest variability of streamflow regime types (Fig. A2c). As transitional region between Alps and lowlands, streamflow regime types also show a large variety of processes contributing to streamflow generation including glacial, nival and pluvial processes. The Jura is a subalpine

mountain range characterized by a strongly karstified geology. The variability of streamflow regime types is the lowest among
705 biogeographic regions and consists mainly of locally specific types (*jurassien*) influenced by a mixture of nival and pluvial
processes (Fig. A2e). The Swiss Plateau region is equivalent to the lowlands and hence is dominated by pluvial streamflow
regime types (Fig. A2f).

Note that whereas catchments smaller than 500 km² allow for a more distinct discrimination in streamflow regime types
and hence streamflow generating processes, catchments with an area larger than 500 km² are influenced by a multitude of
710 streamflow generating and/or storage processes (e.g., groundwater contributions) and are hence provided as *mixed regime*
(*>500 km²*) type (see Sect. 2). The mixed regime type is the most prevalent among catchments (see Fig. 2 and occurs across
all biogeographic regions (Fig. A2) being the most frequent regime type in Western and Eastern Central Alps as well as in the
Northern Pre-Alps.

The catchment grouping to biogeographic regions presented here is again based on maximum overlap of catchment area
715 with the specific biogeographic region (see also Fig. 7a). Biogeographic regions are frequently used for grouping catchments
into groups of similar streamflow (generation) characteristics and provides usable results (see e.g., Brunner et al., 2019b;
Muelchi et al., 2021b; von Matt et al., 2024). In specific cases where a categorization into biogeographic regions may not
be unambiguous (see Sect. 5.1), categorization may be reconsidered by the user via alternative grouping (e.g. directly on
streamflow regime types), alternative categorization approach (other than maximum overlap) or expert judgement. As such the
720 streamflow regime types *nivo-pluvial jurassien* and *pluvial jurassien* could for example be recategorized to the Jura region (see
Fig. A2f).

A2 Detailed Event analysis

The combination of hydro-meteorological indicators, standardized (drought) indices (SPI, SPEI, SMRI), (potential) cumula-
725 tive water and streamflow deficits (CWD, PCWD, CQD) and accompanying climatological anomalies allow for a detailed
analysis of specific (streamflow) drought events. Drought-generating processes vary across catchments depending on hydro-
climatological and terrestrial catchment characteristics, the season as well as on anthropogenic disturbances (e.g., Brunner
et al., 2022; Van Loon and Van Lanen, 2012; Van Loon, 2015; Apurv et al., 2017). Except for glacier melt and groundwa-
ter, the HYD-RESPONSES dataset provides time series for all relevant hydro-meteorological indicators required to analyse
(streamflow) drought generation, drought propagation as well as drought type classification.

730 Figure 6 illustrates time series for the year 2022 of a subset of relevant hydro-meteorological variables for catchment 2034 -
Broye, Payerne, Caserne d'aviation. This catchment is located in the western Swiss Plateau region (highlighted in Fig. A4).
The year 2022 was an exceptional year with unprecedented combined heat and drought conditions over Europe (Tripathy
and Mishra, 2023). The Broye catchment experienced low-flow conditions beyond a 100-year return period (BAFU (Eds.),
2023). In the Broye catchment, the lowest 7-day average streamflow values were observed between July and August (see
735 Fig. 6i) Several streamflow drought events were identified for both yearly fixed (purple shading) and variable (green shading)
threshold definitions (see Fig. 6 (all panels)). The longest events occur during the annual low-flow season for both definitions.
The year 2022 was also one of the warmest years on record with three heatwaves occurring in mid-June, mid-July and in the

beginning of August (Imfeld et al., 2022). During the longest streamflow drought event in July 2022 (see Fig. 6i), evaporation anomalies begin to decline and become negative towards the end of the event (see Fig. 6c). Concurrent strong negative soil
740 moisture anomalies at shallow and deeper levels (see Fig. 6d) suggest that the successively decreasing evaporation anomalies may be related to increasingly depleted soil moisture storages resulting in limited water availability for evaporation. Interactions between (subsurface) storage processes are however complex and also include groundwater–soil moisture interactions (e.g., Orth and Destouni, 2018).

The HYD-RESPONSES dataset further provides information on cumulative (atmospheric) water deficits represented by
745 standardized and non-standardized (drought) indices. For the Broye catchment, the 2022 streamflow drought events identified with the variable threshold (green shading) correlate well with shorter aggregation scales (1- to 3-monthly) SPI and SMRI indices in spring and summer. The correspondence between short-term precipitation deficits and streamflow droughts is, however, not consistent throughout the year. During the variable threshold streamflow droughts in mid-March to April, both SMRI-1 and SMRI-3 reach more negative values than their SPI equivalents, which indicates that lacking snowmelt contributed to the
750 streamflow drought generation (see Fig. 6g,h). Lacking snowmelt as contributing factor is further confirmed by considering the larger and rather persistent negative anomalies in both SWE and snowmelt in the preceding 1 to 3 months (see Fig. 6e,f).

Cumulative deficits in actual (CWD, Fig. 6k) and potential (PCWD, Fig.6l) water balance as well as streamflow (CQD, Fig. 6j) provide complementary information to the SPI, SMRI and SPEI in the form of non-standardized and hence physically interpretable deficit amounts. Cumulative streamflow deficits (CQD) show only two phases without deficit compensation for
755 both drought definitions (Fig.6j). A shorter CQD phase coincides with the drought events in spring (variable threshold) and the shorter drought event in June (fixed threshold), while a longer phase coincides with the remaining shorter and longer streamflow drought phases in July and August before CQD is compensated by September 2022. For both CQD phases, the CQD is larger for streamflow droughts based on a variable threshold definition. Above average precipitation (+130 %; BAFU (Eds.), 2023) was reported in September 2022 and corresponds well with the compensation of CQD and is also reflected in
760 the positive monthly (31d) precipitation anomalies (P anomaly, Fig. 6b). Similar to the longest streamflow drought phases, also the largest cumulative deficits in water balance (CWD) occurred between May–August 2022 (in terms of both absolute deficits and anomalies, see Fig.6k,m). Based on the seasonal climatology of both temperature and evaporation (highest values during summer), larger absolute CWDs are generally expected to occur during the warm season (not shown). Major CWD phases match streamflow drought phases remarkably well, especially for the variable threshold definition with one exception
765 in April. The two longer streamflow drought phases in May–June further show the benefits of considering anomalies in the CWDs. While absolute CWDs were not compensated in between the streamflow droughts, the CWD anomalies indicate that the deficits returned to seasonal norm values (see Fig. 6m). Cumulative deficits in potential water balance (PCWDs, Fig. 6l) are more similar to cumulative streamflow deficits for the variable-threshold definition (CQD, Fig. 6j (blue line)). This reflects the different nature of CWDs and PCWDs. Deficits based on the actual water balance (P-E) are more strongly tied to the actual
770 water availability and hence the individual streamflow (drought) phases (Fig. 6i,k). The potential water balance (P-PET), on the other hand, represents the deficit that would have been accumulated under unlimited water availability. Similar to PCWD,

CQDs reflect the integrated streamflow deficit over time while an actual deficit in terms of low streamflow levels does not necessarily have to exist (anymore).

A3 Composite analysis (catchment response patterns)

775 Composite analysis is a frequently used approach to understand the driving processes of a phenomenon such as droughts (see e.g., Bevacqua et al., 2021; Floriancic et al., 2020; Mahto and Mishra, 2024). By considering the median values of drought indicators across all streamflow drought events in a catchment, typical response patterns may become more evident and may allow for more generalized inferences on typical streamflow drought response patterns e.g., to precipitation deficits accumulated over various aggregation time-scales. Here, we present a composite analysis of median SPI values associated with streamflow
780 droughts defined by the monthly 15th-percentiles of the streamflow which corresponds to the highest of the low-flow percentile used for the Swiss national drought platform (see BAFU, 2025).

Note that streamflow drought characteristics and drought propagation processes may differ among catchments depending on hydro-meteorological climatologies, geological and terrestrial characteristics (e.g., aquifer, rock type, (soil) water storage capacity), seasonality of and differences in contributing streamflow (drought) generating processes and human disturbances (e.g.,
785 Van Loon and Laaha, 2015; Floriancic et al., 2022; Jehn et al., 2020; Apurv and Cai, 2020; Savelli et al., 2022; Haile et al., 2020; Brunner et al., 2022, 2021, 2023; Tjrdeman et al., 2022; de Jager et al., 2022). We therefore separate the streamflow droughts and catchments by seasons winter (DJF, December–February), spring (MAM, March–May), summer (JJA, June–August) and autumn (SON, September–November) and by streamflow regime types. Six streamflow regime types are selected to capture a variety in dominant streamflow (drought) generating processes. These include glacial (*a-glaciaire*, *nivo-glaciaire*),
790 nival (*nival alpin*, *nival méridional*) and pluvial (*pluvial jurassien*, *pluvial supérieur*) processes. The importance of precipitation deficits across scales is assessed using SPIs (SPI-1 to SPI-24). Streamflow drought events are only considered for the longest common homogeneous period across catchments (1991–2022). The selection is further restricted to catchments with at least 10 streamflow drought events in each season (over the entire time series length) with a minimum duration of at least 10 days to enhance robustness and exclude minor droughts.

795 Median SPI values are mostly negative across all aggregation time-scales indicating that precipitation conditions co-occurring with streamflow droughts tend to be drier than normal. Several streamflow regimetype-specific response patterns are evident and change across seasons along with contributing streamflow (drought) generating processes.

Glacier melt is the dominant factor for the *a-glaciaire* regime type (Fig A3a–d). Streamflow levels are typically lowest in winter (January–March) as a result of precipitation falling as snow (intermediate storage) and highest in summer due to large
800 contributions of glacier melt (Aschwanden and Weingartner, 1985; Weingartner and Schwanbeck, 2020; Muelchi et al., 2021b). Streamflow droughts of strongly glaciated catchments are not associated with moderate drought conditions at any SPI scale. In glacial and nival catchments a shift towards short-term precipitation deficits (SPI-1 to SPI-6) being associated with droughts is present across seasons and drought-generating processes. The transition towards shorter deficit scales emerges in summer for nival regime types (Fig. A3g,k) and in autumn for glacial regime types (Fig. A3d). In pluvial and transitional regime types
805 short-term precipitation deficits (mostly 1- to 3 months) are relevant throughout the year (Fig. A3q–x). Seasonal shifts are also

observed for pluvial and transitional regime types with mid- and long-term precipitation deficits becoming more relevant in summer and autumn (Fig. A3t,w-x).

In addition to 3-monthly precipitation deficits, also mid- and long-term deficits become relevant in summer and autumn for (nivo-pluvial) catchments in the Jura region and catchments of the regime type *pluvial inférieur* (Fig. A3s,t). Compound
810 moderate droughts are mainly observed for sub-yearly (1- to 9-monthly) scales with most extreme conditions on a 6-monthly scale in the Jura region (especially for nivo-pluvial catchments) and on a (6- to) 9-monthly scale for catchments of the regime type *pluvial inférieur*. In southern Switzerland, precipitation deficits tend to be relevant on longer scales compared to similar regime types north of the Alps (Fig. A3 m-p). In contrast to nival catchments north of the Alps (*nival alpin*, Fig. A3i-l),
815 droughts in the nival catchments south of the Alps (*nival méridional*, Fig. A3m-p) are associated with substantial precipitation deficits at longer aggregation times (9-24 months). The deficits occur in winter and in summer, but conditions are more extreme in summer ($SPI \approx -1.5$) on scales longer than 15 months. Further, also 3-monthly precipitation deficits appear to be relevant for streamflow (drought) generation in summer (moderate drought conditions). In spring and autumn, mid- to short-term accumulation scales are more relevant (Fig. A3). Interpretations of the differences between the south and north sides of the Alps should, however, be considered with caution due to the small catchment sample sizes and the spatial proximity of
820 the two *nival méridional* catchments. The observed response patterns may therefore not be representative of nival catchments south of the Alps in general.

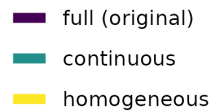
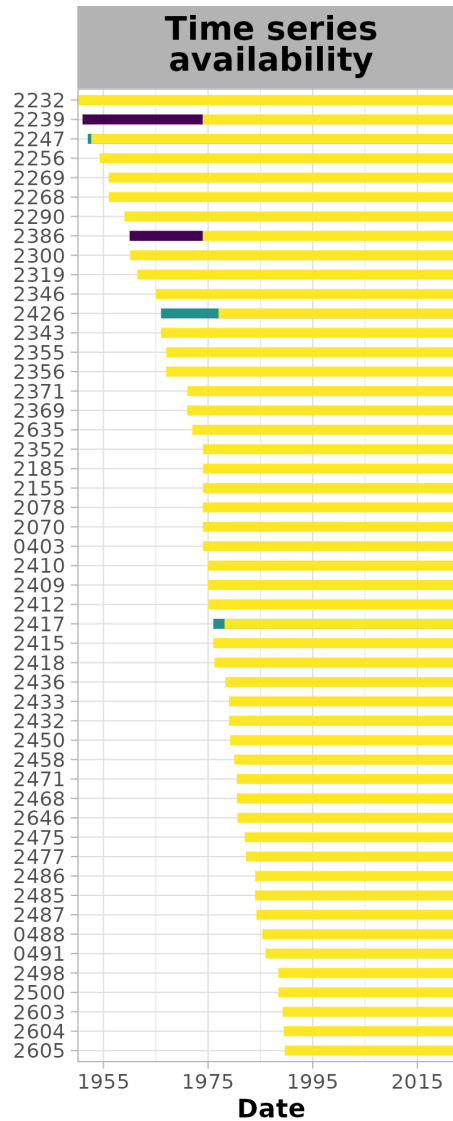


Figure 3. Streamflow time series availability for 50 example catchments. The colours indicate the periods covered by availability type. Full is equivalent to the original time series provided by the FOEN. Continuous denotes the gap-checked time series and the homogeneous period accounts for homogeneity (starting at a breakpoint). In the case of overlapping periods, only the most important period type for analysis (e.g., homogeneous) is displayed. The importance of the periods for analysis is defined as follows: *homogeneous* is more important than *continuous* is more important than *full (original)*.

Evaluation of Standardized Indices

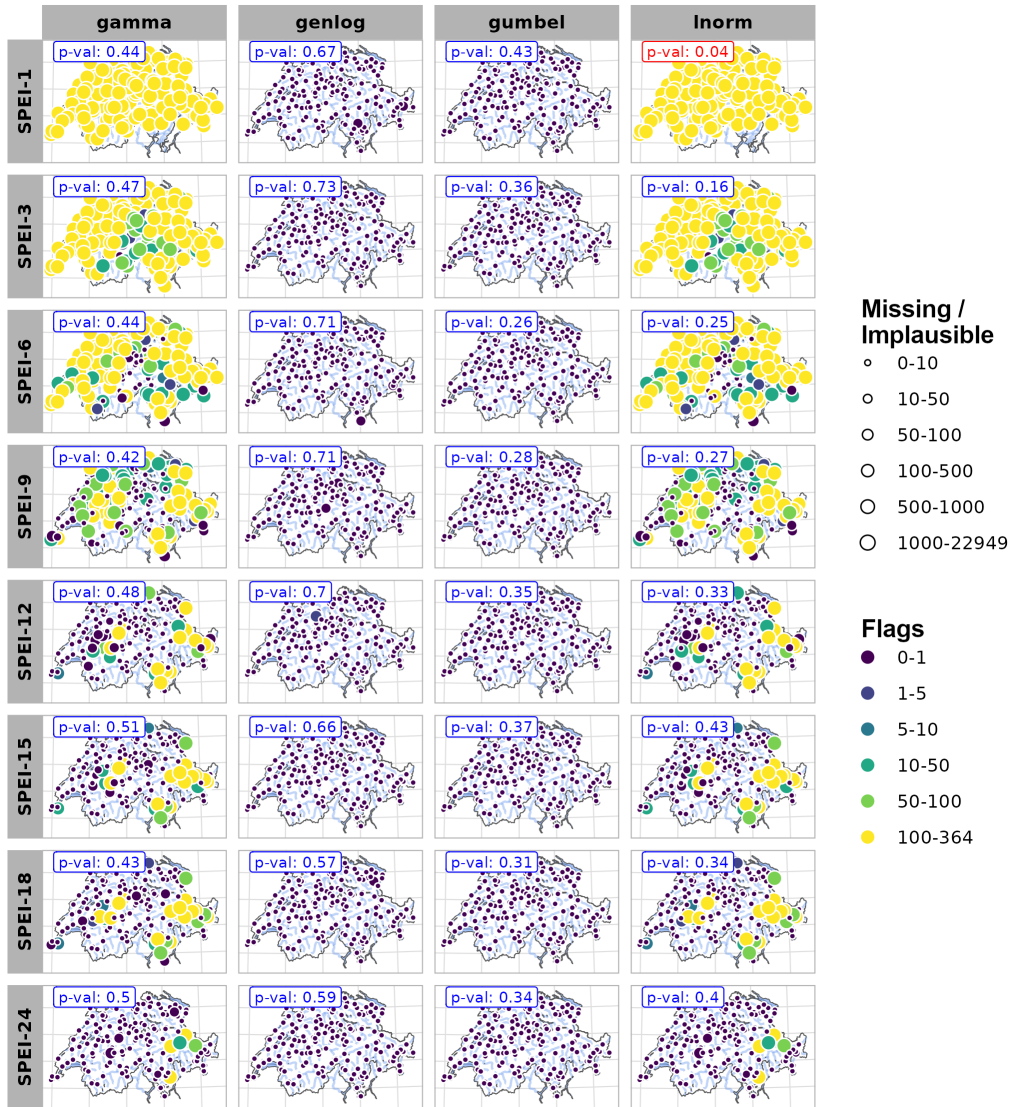


Figure 4. Evaluation statistics for the transformation of standardized (drought) indices. Information on the normality tests (p -values), flags and implausible/missing values ($\text{SPEI} \notin [-3,3]$) for four example candidate distributions for the Standardized Precipitation and Evaporation Index (SPEI; Vicente-Serrano et al., 2010). The circle size indicates the number of missing and implausible values. Colours show the number of flags (= convergence issues) returned by the fitting function of the *SCI* R-package (Stagge et al., 2015; Gudmundsson and Stagge, 2016) for all days of the year (DOY). The maximum number of flags is equivalent to 366. Median p -values of the Shapiro-Wilk normality test (Shapiro and Wilk, 1965) were calculated by considering all catchments and are coloured in red in case of rejection ($p < 0.05$). The final HYD-RESPONSES dataset only provides SPEIs fitted by the *genlog*-distribution (best choice based on the evaluation criteria).

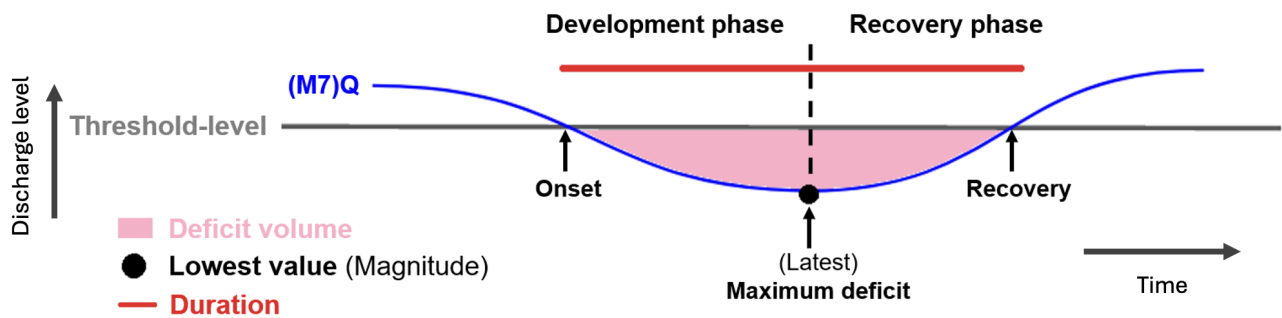


Figure 5. Schematic depiction of the event definition and phase subdivision. The extracted (streamflow) drought phases are characterized by duration, event start (onset), the latest date of the maximum streamflow deficit (anomaly), and event recovery. Additional characteristics are the drought intensity (deficit volume or accumulated deficit) and severity/magnitude (maximum streamflow deficit). The computation of other characteristics is left to the user.

Drought 2022 – Example 2034 - Broye (Payerne, Caserne d'aviation)

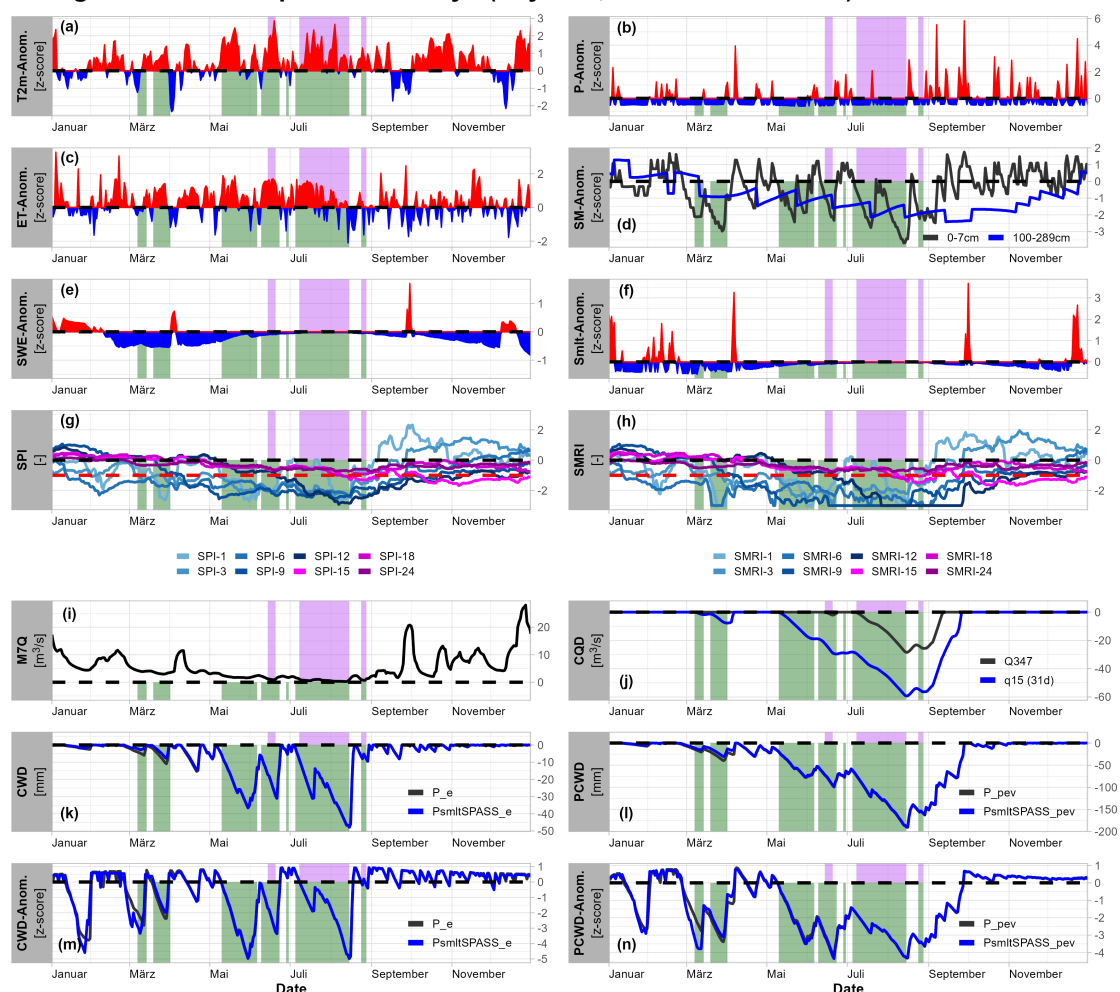


Figure 6. Hydro-meteorological time series for the Swiss Plateau catchment 2034 - Broye, Payerne (Caserne d'aviation) for the year 2022. Color shadings in all panels highlight streamflow drought events for two definitions: yearly Q347 (pink, fixed threshold approach) and a moving monthly 15th percentile threshold (green, variable threshold approach). (a) Moving monthly anomalies of the 2 m-temperature (T2m), positive anomalies are shown in red and negative anomalies in blue. (b) Moving monthly anomalies of the precipitation (P, RhiresD) (c) Moving monthly anomalies of the evaporation (ET, ERA5-land). (d) Moving monthly anomalies of the soil moisture volume (ESM ERA5-land), soil moisture anomalies are depicted for a near-surface SM-level (black, 0–7 cm) and the deepest level (blue, 100–289 cm) available from ERA5-Land. (e) Moving monthly anomalies of the snow water equivalent (SWE SPASS). (f) Moving monthly anomalies of the snowmelt (smlt, SPASS). (g) SPI colored by aggregation scales from 1- to 24-months. (h) SMRI colored by aggregation scales from 1- to 24-months. (i) Seven day average streamflow (M7Q) on which streamflow drought events were identified. (j) The CQD time series shows the corresponding accumulated M7Q-deficits for both the fixed threshold approach (black) and the variable threshold approach (blue). (k) Absolute cumulative water deficit (CWD). (l) Potential cumulative water deficit (PCWD). (m) Monthly anomalies of the CWD (CWD anomaly). (n) Monthly anomalies of the PCWD. Time series of the cumulative water deficits for both absolute values and monthly anomalies are shown for both standard (black, P–E (P_e) and P–E+ΔSWE (P_{smlt}SPASS_e)) and snowmelt-corrected (blue, P–E+ΔSWE (P_{smlt}SPASS_{pev})) variants. The same is shown for potential cumulative water deficits which are based on the potential water balance (P–PET (P_{pev}) and P–PET+ΔSWE (P_{smlt}SPASS_{pev})).

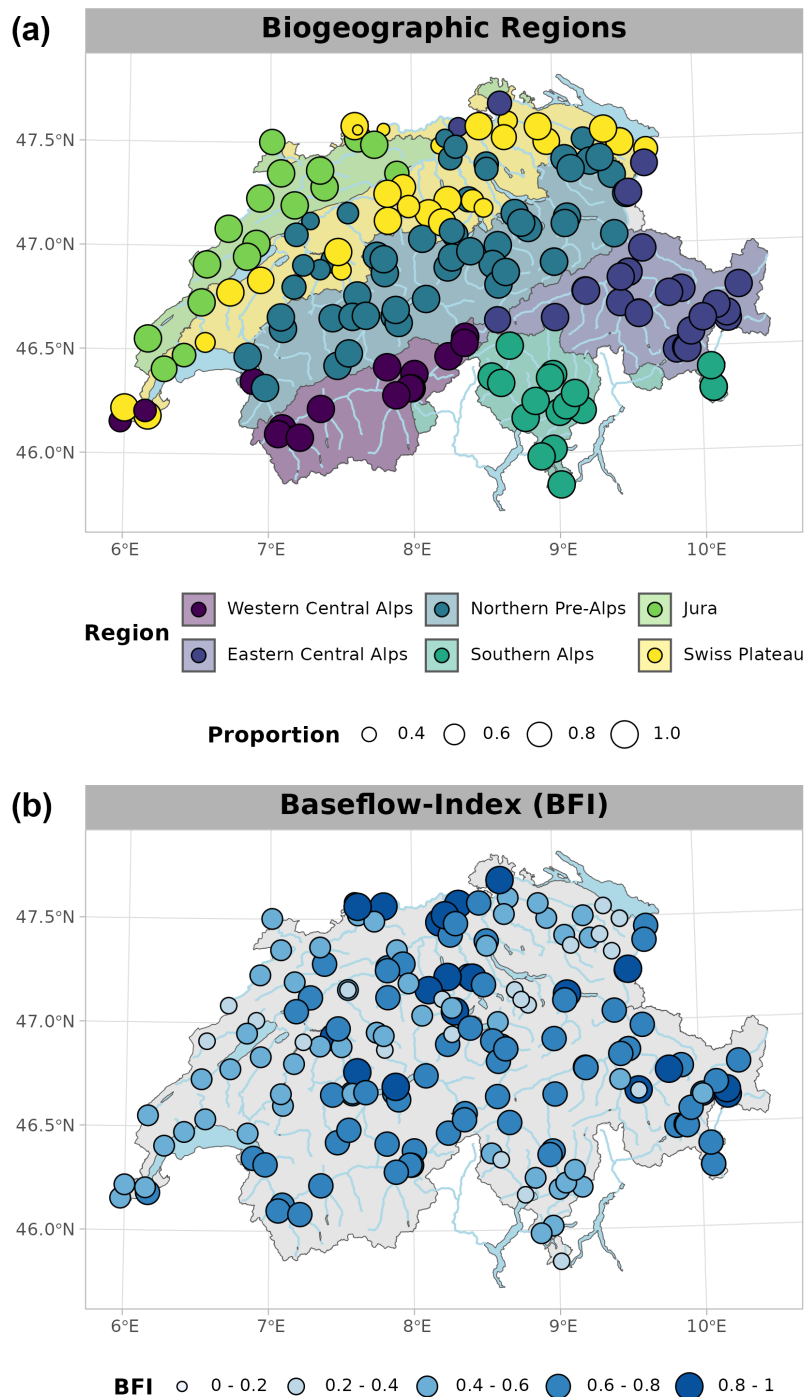


Figure 7. Catchment descriptors (examples). **(a)** Dominant (largest overlap percentage with the catchment area) biogeographic region (colours). Point sizes indicate the catchment area proportion covered by the dominant biogeographic region. **(b)** Baseflow-Index (BFI, Nathan and McMahon, 1990) for each catchment derived from the daily streamflow time series.

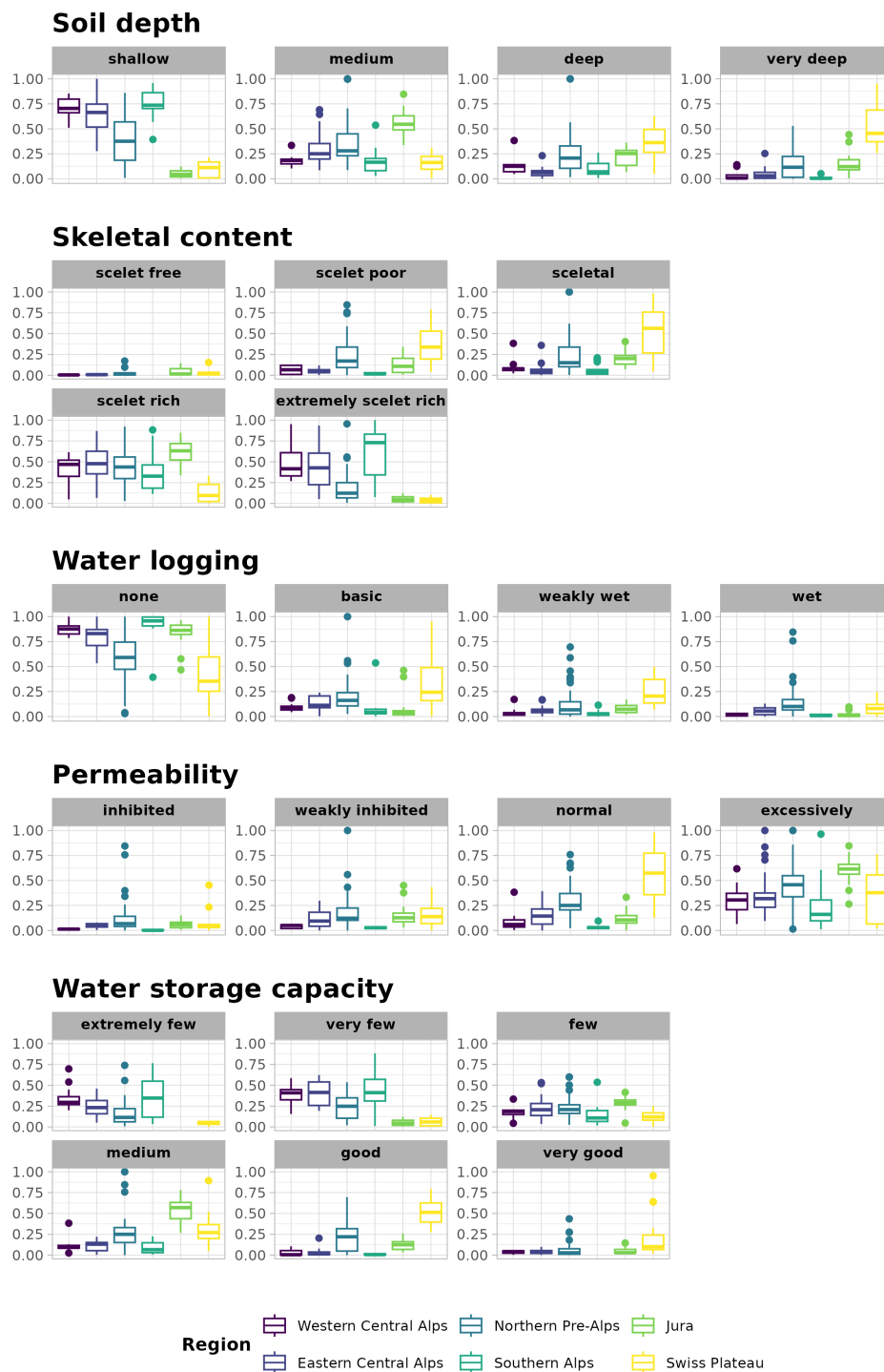


Figure A1. Catchment coverage fractions for all (sub-)categories of the soil characteristics: soil depth, skeletal content, water logging, soil permeability, and water storage capacity across regionalized catchment groups derived from the biogeographic regions of Switzerland (colours, see also Fig. 7a).

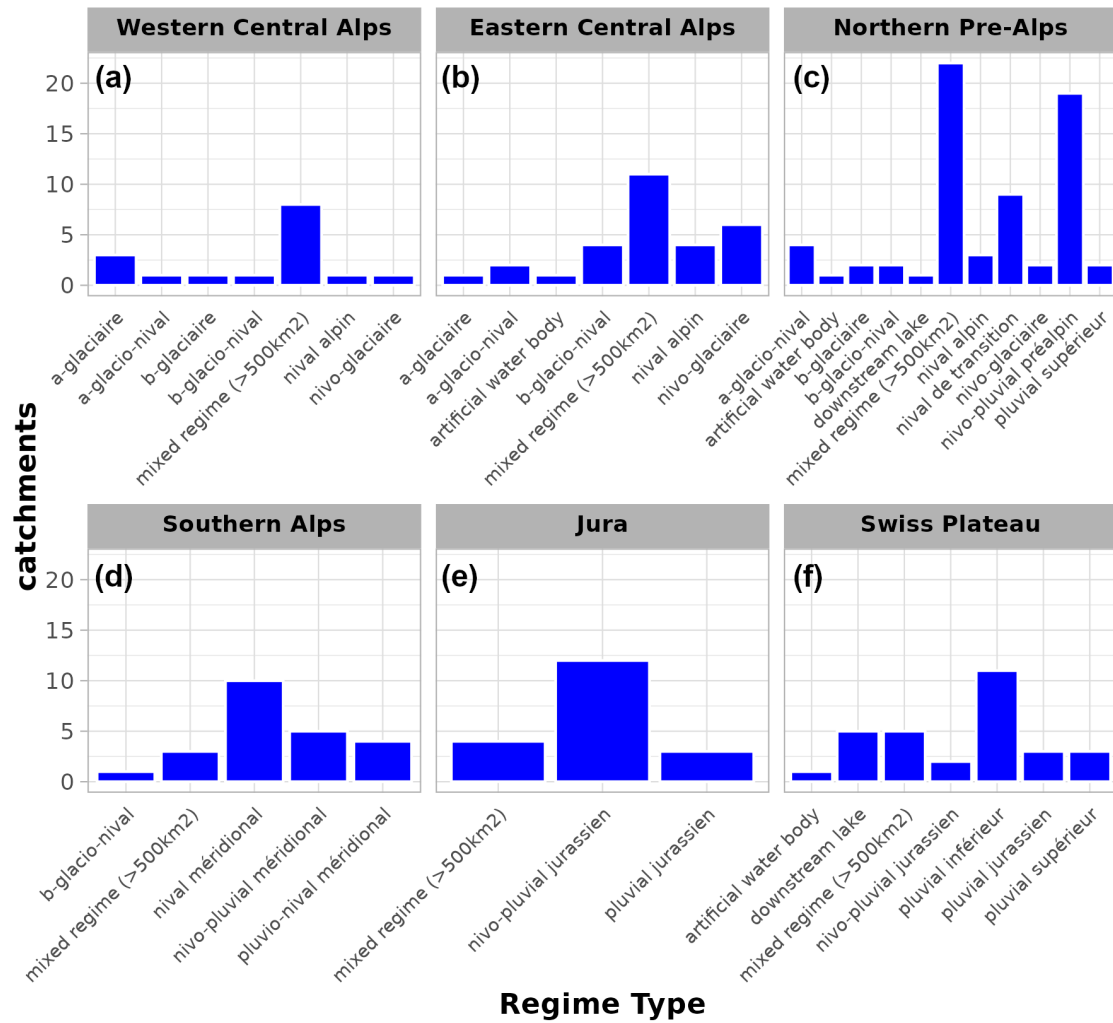


Figure A2. Streamflow regime type incidence among catchments grouped by the biogeographic regions of Switzerland (Western Central Alps, Eastern Central Alps, Northern Pre-Alps, Southern Alps, Jura and Swiss Plateau region; see Sect. 3.3 and also Fig. 7). The streamflow regime type classification was provided by the FOEN. The Y-axis shows the number of catchments associated with each category.

Median SPI-values during hydrological events

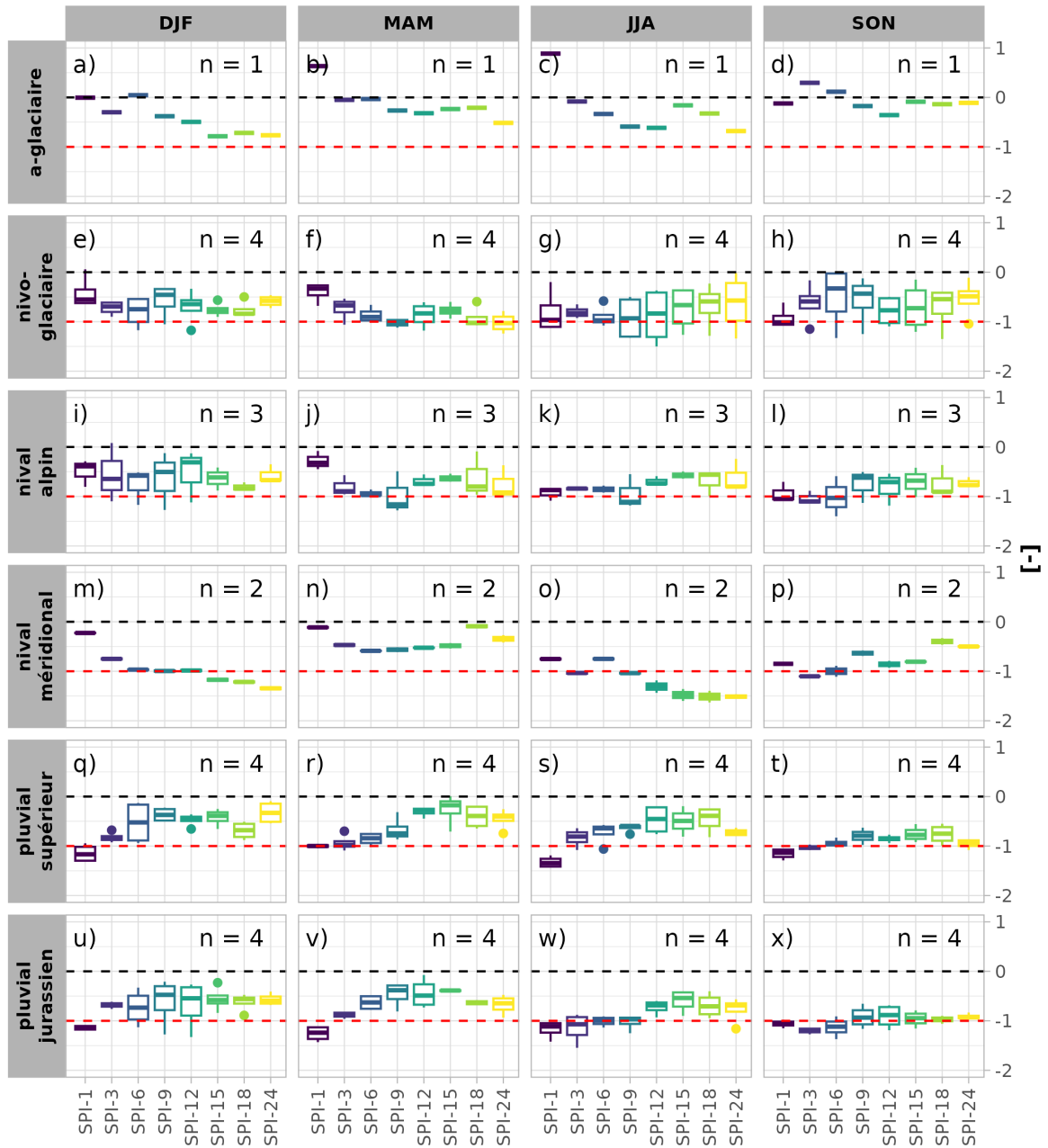


Figure A3. Median SPI values during hydrological drought conditions for all events of all catchments for six selected streamflow regime types across the four seasons winter (DJF), spring (MAM), summer (JJA) and autumn (SON). The streamflow regime types were selected to represent catchments with (dominant) glacial (a-glaciaire, nivo-glaciaire), snow (nival alpin, nival méridional) and pluvial processes (pluvial jurassien, pluvial supérieur) and spatial diversity. Hydrological drought events were defined by a moving monthly (31d) 15th-percentile (variable) threshold. Boxplots are coloured according to SPI aggregation time scales (1- to 24-months). Moderate drought conditions are indicated by the red dashed lines, the black dashed line indicates 0. "n=" refers to the number of catchments with a specific streamflow regime type.

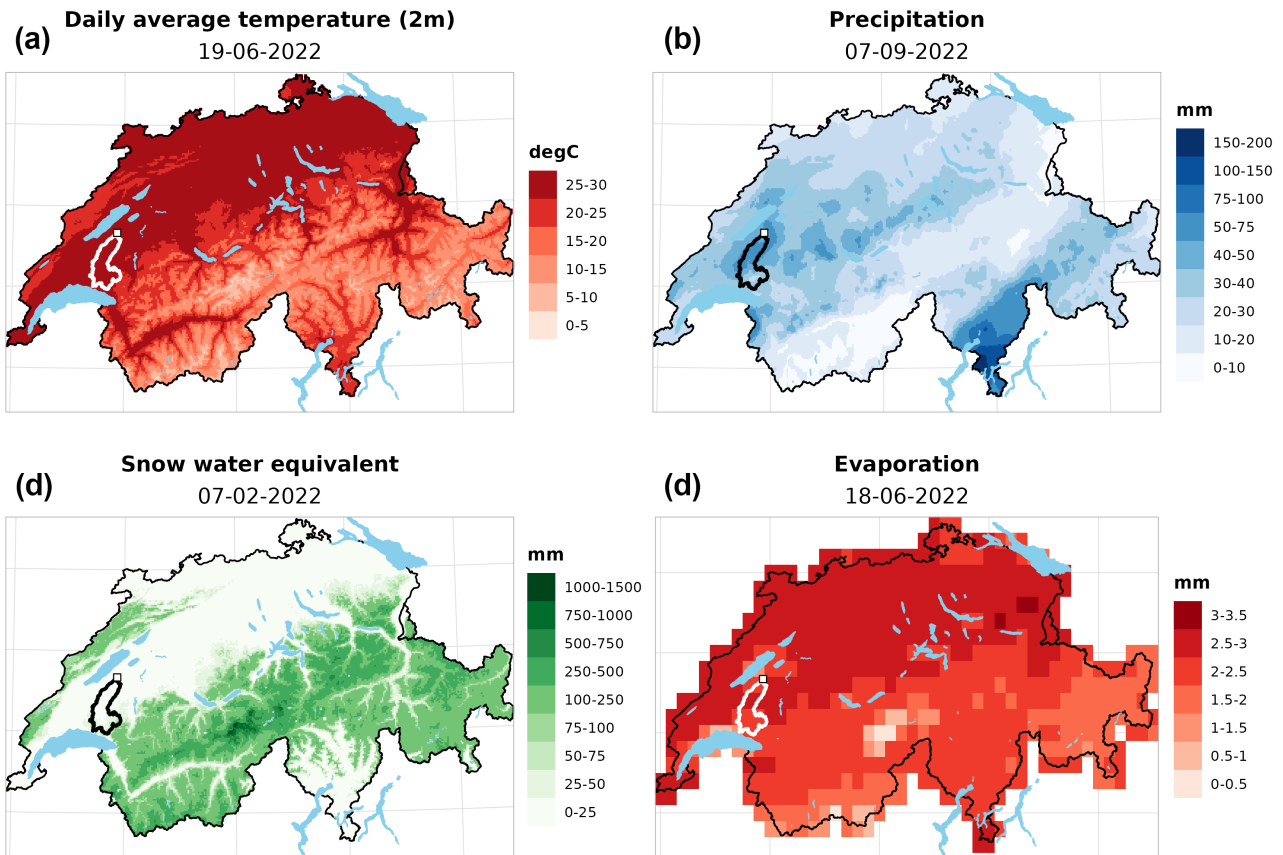


Figure A4. Overview of the spatial raster products used to extract daily time series. **(a)** Mean daily temperature (TabsD, MeteoSwiss), **(b)** Daily precipitation sun (RhiresD, MeteoSwiss), **(c)** Daily snow water equivalent of the Swiss snow climatology (SPASS) (SWE, MeteoSwiss & SLF), **(d)** Daily evaporation sum (aggregated from hourly ERA5-Land data, ECMWF). Note that the second snow climatology product (OSHD) is not shown. Contours in white/black show catchment 2034 - *Broye, Payerne, Casernde d'aviation* for the day with the highest observed catchment average values for each specific product for the year 2022. White squares show the catchment outlet where daily streamflow is measured. Extracted and derived time series over the year 2022 are shown for the same catchment in Figure 6.

Appendix B: Tables

Table B1. Glossary of extracted time series variables, their description and units.

Dataset	Variables	Variables (fullname)	Units	Producer
Spatial Climate Analyses	TabsD	Daily 2 m mean temperature	°C	MeteoSwiss
	RhiresD	Daily precipitation sums	mm	
	TminD	Daily 2 m minimum temperature	°C	
	TmaxD	Daily 2 m maximum temperature	°C	
	SrelD	Daily sunshine duration	%	
Snow Climatology for Switzerland (SPASS)	SWECLQMD	Daily snow water equivalent	mm	MeteoSwiss & SLF
Climatological snow data since 1998 (OSHD)	swee	Daily snow water equivalent	mm	SLF
	romc	Daily snowmelt-contribution to runoff	mm	
ERA5-Land	tp	Total precipitation	mm	ECMWF
	t2m	Average 2 m temperature	°C	
	e	Total evaporation	mm	
	pev	Total potential evaporation	mm	
	smlt	Snowmelt	mm	
	sd	Snow water equivalent	mm	
	ssr	Total solar radiation	MJ/m ²	
	ro	Runoff	mm	
	sro	Surface runoff	mm	
	swv11	Soil water volume level 1 (0–7cm)	mm	
	swv12	Soil water volume level 2 (7–28cm)	mm	
swv13	Soil water volume level 3 (28–100cm)	mm		
swv14	Soil water volume level 4 (100–289cm)	mm		
Streamflow time series	Q	Daily mean streamflow	m ³ /s	FOEN

Table B2. Information on the underlying processing and reliability of basic and derived time series variables.

	Type	Level	Data source	Processing	Temporal resolution	Modeling component	Variables
	Streamflow	L1	Streamflow measurements (Q-Meas.)	–	daily mean	–	Q
	Precipitation	L2	Spatial climate analyses (SCA)	catchment average	daily total (sum)	–	RhiresD
	Sunshine Duration	L2		catchment average	daily relative (%)	–	SrelD
	Temperature	L2		catchment average	daily mean	–	TabsD, TmaxD, TminD
Sect. 4.1	Snow	L2	SPASS	catchment average	daily mean	yes	SWECLQMD
	Snow	L2	OSHD	catchment average	daily mean	yes	swee
		L2		catchment average	daily total (sum)	yes	romc
	Various	L2	ERA5-Land	catchment average, daily mean	daily mean	–	t2m
		L2		catchment average, daily mean	daily mean	strong	pev, sd, ssr, swvl11, swvl2, swvl3, swvl4
		L2		catchment average, daily total (sum)	daily total (sum)	–	tp
		L2		catchment average, daily total (sum)	daily total (sum)	strong	ro, smlt, sro, e
	Streamflow	L1	Q-Meas.	7-day average	daily	–	M7Q
		L3	ERA5-Land	(centered)		strong	ro7Q
	Snow-related	L2	SCA, OSHD	P + Snowmelt	daily	yes	P_SMLT_OSHDromc
		L2	SCA, OSHD	P + Δ SWE	daily	yes	P_SMLT_OSHDswe
		L2	SCA, SPASS	P + Δ SWE	daily	yes	P_SMLT_SPASS
		L2	OSHD	Δ SWE	daily	yes	SWE_diff_OSHD
		L2	SPASS	Δ SWE	daily	yes	SWE_diff_SPASS
		L2	OSHD	Δ SWE > 0	daily	yes	SWE_posdiff_OSHD
		L2	SPASS	Δ SWE > 0	daily	yes	SWE_posdiff_SPASS
Sect. 4.2		L3	ERA5-Land	P + Snowmelt	daily	strong	tp_smlt
	Water balance	L3	SCA, ERA5-Land	P - E	daily	strong	P_e
		L3	SCA, ERA5-Land	P - PET	daily	strong	P_pev
		L3	SCA, OSHD, ERA5-Land	P + Snowmelt - E	daily	strong	PsmltOSHDromc_e
		L3	SCA, OSHD, ERA5-Land	P + Snowmelt - PET	daily	strong	PsmltOSHDromc_pev
		L3	SCA, OSHD, ERA5-Land	P + Δ SWE - E	daily	strong	PsmltOSHDswe_e
		L3	SCA, OSHD, ERA5-Land	P + Δ SWE - PET	daily	strong	PsmltOSHDswe_pev
		L3	SCA, SPASS, ERA5-Land	P + Δ SWE - E	daily	strong	PsmltSPASS_e
		L3	SCA, SPASS, ERA5-Land	P + Δ SWE - PET	daily	strong	PsmltSPASS_pev
		L3	ERA5-Land	P - E	daily	strong	tp_e
		L3	ERA5-Land	P - PET	daily	strong	tp_pev
		L3	ERA5-Land	P + Snowmelt - E	daily	strong	tpsmlt_e
		L3	ERA5-Land	P + Snowmelt - PET	daily	strong	tpsmlt_pev

Table B3. Information on the underlying processing and reliability of standardized (drought) indices and cumulative deficit time series.

	Type	Level	Data source	Processing	Temporal resolution	Distributions	Index Aggregation (months)	Modeling component	Variables
	SPI	L3	SCA	fitted transformation	daily	gamma	1 - 24	yes	RhiresD
		L3	ERA5-Land	fitted transformation	daily	gamma	1 - 24	yes	tp
Sect. 4.4	SPEI	L3	SCA, ERA5-Land	fitted transformation	daily	genlog	1 - 24	strong	P_peg
		L3	ERA5-Land	fitted transformation	daily	genlog	1 - 24	strong	tp_peg
	SMRI	L3	SCA, SPASS	fitted transformation	daily	genlog	1 - 24	yes	P_SMLT_SPASS
		L3	SCA, OSHD	fitted transformation	daily	Inorm	1 - 24	yes	P_SMLT_OSHDromc
		L3	SCA, OSHD	fitted transformation	daily	Inorm	1 - 24	yes	P_SMLT_OSHDswe
		L3	ERA5-Land	fitted transformation	daily	Inorm	1 - 24	strong	tp_smlt
	Type	Level	Data source	Processing	Temporal resolution	Variants	Threshold-level	Modeling component	Variables
Sect. 4.3	CWD	L3	SCA, ERA5-Land	cumulative sum of negative threshold deviations	daily	multi-year,yearly	P - E < 0	strong	P_e
		L3	SCA, OSHD, ERA5-Land		daily	multi-year,yearly	P - E < 0	strong	P_smltOSHDromc_e
		L3	SCA, OSHD, ERA5-Land		daily	multi-year,yearly	P - E < 0	strong	P_smltOSHDswe_e
		L3	SCA, SPASS, ERA5-Land		daily	multi-year,yearly	P - E < 0	strong	P_smltSPASS_e
		L3	ERA5-Land		daily	multi-year,yearly	P - E < 0	strong	tp_e
		L3	ERA5-Land		daily	multi-year,yearly	P - E < 0	strong	tp_smlt_e
	PCWD	L3	SCA, ERA5-Land	cumulative sum of negative threshold deviations	daily	multi-year,yearly	P - PET < 0	strong	P_peg
		L3	SCA, OSHD, ERA5-Land		daily	multi-year,yearly	P - PET < 0	strong	P_smltOSHDromc_peg
		L3	SCA, OSHD, ERA5-Land		daily	multi-year,yearly	P - PET < 0	strong	P_smltOSHDswe_peg
		L3	SCA, SPASS, ERA5-Land		daily	multi-year,yearly	P - PET < 0	strong	P_smltSPASS_peg
		L3	ERA5-Land		daily	multi-year,yearly	P - PET < 0	strong	tp_peg
		L3	ERA5-Land		daily	multi-year,yearly	P - PET < 0	strong	tp_smlt_peg
Sect. 4.6	CQD	L2	Q-Meas.	cumulative sum of negative threshold deviations	daily	multi-year,yearly	monthly/seasonal: 2 nd , 5 th , 10 th , 15 th , 25 th , 50 th (median), mean yearly: Q347	-	M7Q

Table B4. Information on the underlying processing of the climatology and anomaly time series.

	Type	Level	Processing	Temporal resolution	Variant	Statistics	Window / Anomaly-Scale	Variables
	climatology	L2	statistical summary	monthly seasonal extended season yearly	regular	min, q05, q25, med, mean, q75, q95, max, sd, sum	–	Sect. 4.1
	climatology	L2–L3	statistical summary	monthly seasonal extended season yearly	regular	min, q05, q25, med, mean, q75, q95, max, sd, sum	–	Sect. 4.2
	climatology	L2–L3	statistical summary	monthly seasonal extended season yearly	regular	min, q05, q25, med, mean, q75, q95, max, sd, sum	–	Sect. 4.3
	climatology	L2	statistical summary	monthly seasonal extended season yearly	regular	min, q05, q25, med, mean, q75, q95, max, sd, sum	–	Sect. 4.6
Sect. 4.5	climatology	L2	statistical summary	daily	window	min, q05, q25, med, mean, q75, q95, max, sd, sum	no window (daily) 31 days (monthly) 91 days (seasonal)	Sect. 4.1
	climatology	L2–L3	statistical summary	daily	window	min, q05, q25, med, mean, q75, q95, max, sd, sum	no window (daily) 31 days (monthly) 91 days (seasonal)	Sect. 4.2
	climatology	L2–L3	statistical summary	daily	window	min, q05, q25, med, mean, q75, q95, max, sd, sum	no window (daily) 31 days (monthly) 91 days (seasonal)	Sect. 4.3
	climatology	L2	statistical summary	daily	window	min, q05, q25, med, mean, q75, q95, max, sd, sum	no window (daily) 31 days (monthly) 91 days (seasonal)	Sect. 4.6
	anomalies	L2	z-scores	daily	window	(value - mean) / sd	no window (daily) 31 days (monthly) 91 days (seasonal)	Sect. 4.1
	anomalies	L2–L3	z-scores	daily	window	(value - mean) / sd	no window (daily) 31 days (monthly) 91 days (seasonal)	Sect. 4.2
	anomalies	L2–L3	z-scores	daily	window	(value - mean) / sd	no window (daily) 31 days (monthly)	Sect. 4.3

Table B5. Information on the underlying processing and reliability of event time series.

	Type	Level	Data source	Processing	Temporal resolution	Threshold-level	Variables
	Cumulative water deficits	L3	Sect. 4.3	deficit > 0	daily	–	Sect. 4.3
	Cumulative streamflow deficits	L2	Sect. 4.6	deficit > 0	daily	–	Sect. 4.6
Sect. 4.7	Streamflow droughts	L2	FOEN	M7Q < threshold-level	daily	monthly/seasonal: 2 nd , 5 th , 10 th , 15 th , 25 th , 50 th (median), mean yearly: Q347	Sect. 4.7

Table B6. Characteristics of all 184 catchments in the HYD-RESPONSES dataset (Part 1/5).

Catchment	Water name	Place	Lon / Lat EPSG:21781	Glaciation %	Area km ²	Avg. Height m asl	Regime Type	Yearly Avg. T °C	Yearly P mm	Yearly E mm	Yearly Q mm
0070	Emme	Emmenmatt	623610 / 200420	0.0	443.00	1065	nivo-pluvial préalpin	6.94	1539.26	300.29	856.45
0078	Poschiavino	Le Presse	803490 / 130520	4.0	168.00	2162	nival méridional	1.58	1324.78	175.84	1078.26
0155	Emme	Wiler, Limpachmündung	608220 / 223240	0.0	937.00	858	mixed regime (> 500km ²)	7.80	1356.58	313.03	623.66
0185	Plessur	Chur	757975 / 191925	0.0	264.00	1868	nival alpin	3.42	1179.00	194.41	915.28
0308	Goldach	Goldach, Bleiche	753190 / 261590	0.0	51.10	827	pluvial supérieur	8.33	1423.14	317.59	889.48
0352	Linth	Linthal, Ausgleichsbecken KLL	718285 / 197310	9.4	147.00	2085	a-glacio-nival	1.83	1874.45	169.98	2422.14
0403	Inn	Cinuos-chel	797700 / 168170	5.2	733.00	2456	mixed regime (> 500km ²)	-0.66	1007.10	146.31	1007.68
0488	Simme	Latterbach	610680 / 167840	1.5	563.00	1594	nival de transition	4.79	1506.56	225.96	1108.96
0491	Schächen	Bürglen, Galgenwäldli	692480 / 191800	1.5	108.00	1728	nivo-glaciaire	3.55	1854.00	188.20	1646.44
2009	Rhône	Porte du Seex	557660 / 133280	11.0	5238.00	2127	mixed regime (> 500km ²)	1.96	1292.71	148.24	1116.86
2011	Rhône	Sion	593770 / 118630	14.2	3372.00	2291	mixed regime (> 500km ²)	1.00	1240.59	127.84	966.98
2016	Aare	Brugg	657000 / 259360	1.5	11681.00	1000	mixed regime (> 500km ²)	7.34	1317.32	291.55	833.95
2018	Reuss	Mellingen	662830 / 252580	1.8	3386.00	1259	mixed regime (> 500km ²)	5.98	1592.79	239.54	1300.70
2019	Aare	Brienzwiler	649930 / 177380	15.5	555.00	2135	mixed regime (> 500km ²)	1.41	1842.89	123.14	2077.41
2020	Ticino	Bellinzona	721245 / 117025	0.2	1517.00	1679	mixed regime (> 500km ²)	4.27	1658.40	209.25	1339.14
2024	Rhône	Branson	573150 / 108300	13.0	3728.00	2235	mixed regime (> 500km ²)	1.35	1249.40	133.83	1166.41
2029	Aare	Brigg, Aegerten	588220 / 219020	2.1	8249.00	1142	mixed regime (> 500km ²)	6.73	1366.01	276.35	908.00
2030	Aare	Thun	613230 / 179280	6.9	2459.00	1746	mixed regime (> 500km ²)	3.72	1604.05	176.90	1438.59
2033	Vorderrhein	Ilanz	735000 / 182030	1.8	774.00	2030	mixed regime (> 500km ²)	2.28	1534.35	157.08	1340.76
2034	Broye	Payeme, Caserne d'aviation	561660 / 187320	0.0	416.00	715	pluvial inférieur	9.19	1186.40	322.34	564.59
2044	Thur	Andelfingen	693510 / 272500	0.0	1702.00	770	mixed regime (> 500km ²)	8.25	1392.81	333.74	857.45
2053	Dranee	Marrigny, Pont de Rossettan	570930 / 105200	11.3	676.00	2250	mixed regime (> 500km ²)	1.40	1269.62	138.70	462.70
2056	Reuss	Secdorf	690085 / 193210	6.4	833.00	2013	mixed regime (> 500km ²)	1.96	1681.87	150.85	1624.38
2063	Aare	Murgenthal	629530 / 235090	1.7	10059.00	1066	mixed regime (> 500km ²)	7.04	1346.17	284.49	888.26
2070	Emme	Emmenmatt, nur Hauptstation	623610 / 200420	0.0	443.00	1065	nivo-pluvial préalpin	6.94	1539.26	300.29	835.36
2078	Poschiavino	Le Presse, stazione principale	803490 / 130520	4.0	168.00	2162	nival méridional	1.58	1324.78	175.84	1064.96
2084	Muota	Ingenbohl	688230 / 206140	0.0	317.00	1363	nival de transition	5.45	1958.67	237.00	1915.23
2085	Aare	Hagneck	580680 / 211650	3.4	5112.00	1368	mixed regime (> 500km ²)	5.61	1452.15	237.22	1068.53
2086	Brenno	Loderio	717770 / 137270	0.3	400.00	1815	nival méridional	3.68	1618.84	185.01	342.59
2087	Reuss	Andermatt	688120 / 166320	2.9	190.00	2284	b-glacio-nival	0.59	1709.03	116.01	1167.49
2091	Rhein	Rheinfelden, Messstation	627190 / 267840	0.8	34524.00	1068	mixed regime (> 500km ²)	6.68	1351.54	281.92	935.92
2099	Limmat	Zürich, Unterhard	682055 / 249430	0.8	2174.00	1194	mixed regime (> 500km ²)	6.28	1719.03	264.98	1353.24
2102	Sarner Aa	Sarnen	661460 / 194220	0.0	269.00	1281	downstream lake	5.99	1648.90	224.99	1167.84
2104	Linth	Weesen, Bäsche	725160 / 221380	1.6	1062.00	1584	mixed regime (> 500km ²)	4.39	1785.64	221.45	1538.41
2105	Inn	St. Moritzbad	783910 / 150960	3.8	155.00	2399	b-glacio-nival	-0.33	1055.10	161.39	1145.54
2106	Birs	Münchenstein, Hofmatt	613570 / 263080	0.0	887.00	728	mixed regime (> 500km ²)	8.53	1206.82	335.73	545.50
2109	Lätschine	Gsteig	633130 / 168200	13.5	381.00	2050	a-glacio-nival	2.11	1780.73	119.63	1580.50
2110	Reuss	Mühlau, Hünenberg	672520 / 230600	2.2	2902.00	1371	mixed regime (> 500km ²)	5.42	1641.78	226.17	1399.39
2112	Sitter	Appenzell	749040 / 244220	0.1	74.40	1256	nival de transition	6.22	1896.65	345.94	1421.58
2117	Dranee de Bagnes	Le Châble, Villette	582550 / 103270	22.1	254.00	2609	b-glaciaire	-0.59	1274.15	118.82	254.59
2119	Sarine	Fribourg	579420 / 183670	0.2	1271.00	1247	mixed regime (> 500km ²)	6.35	1420.49	276.29	975.93
2122	Birse	Moutier, La Charrue	595740 / 237010	0.0	186.00	921	nivo-pluvial jurassien	7.49	1371.76	333.62	520.67

T = Temperature, P = Precipitation, E = Evaporation, Q = Streamflow/Runoff

Table B7. Characteristics of all 184 catchments in the HYD-RESPONSES dataset (Part 2/5).

Catchment	Water name	Place	Lon / Lat EPSC:21781	Glaciation %	Area km ²	Avg. Height m asl	Regime Type	Yearly Avg. T °C	Yearly P mm	Yearly E mm	Yearly Q mm
2125	Lorze	Frauenthal	674715 / 229845	0.0	262.00	678	downstream lake	8.91	1427.56	309.43	911.18
2126	Murg	Wängi	714105 / 261720	0.0	80.20	652	pluvial inférieur	8.72	1282.82	340.64	693.21
2132	Töss	Nefenbach	691460 / 263820	0.0	343.00	658	pluvial inférieur	8.89	1331.52	339.46	701.10
2135	Aare	Bern, Schönau	600710 / 198000	5.8	2941.00	1596	mixed regime (>500km ²)	4.43	1542.51	196.01	1317.74
2139	Rheinaler Binnenkanal	St. Margrethen	767160 / 257780	0.0	175.00	710	artificial waterbody	9.01	1451.16	310.08	2038.65
2141	Albula	Tiefencastel	763420 / 170145	0.5	529.00	2128	mixed regime (>500km ²)	1.53	1018.61	159.38	904.27
2143	Rhein	Rekingen	667060 / 269230	0.2	14767.00	1131	mixed regime (>500km ²)	5.83	1296.20	276.20	945.75
2150	Landquart	Felsenbach	765365 / 204910	0.7	614.00	1797	mixed regime (>500km ²)	3.34	1289.45	188.82	1203.19
2151	Simme	Oberwil	600060 / 167090	2.4	344.00	1641	nival de transition	4.52	1536.17	215.10	1084.54
2152	Reuss	Luzern, Geissmattribücke	665330 / 211800	2.8	2254.00	1504	mixed regime (>500km ²)	4.72	1683.08	207.59	1526.87
2155	Emme	Wiler, Limpachmündung, nur Hauptstation	608220 / 223240	0.0	924.00	863	mixed regime (>500km ²)	7.80	1356.58	313.03	316.15
2159	Gürbe	Belp, Mülimatt	604810 / 192680	0.0	116.00	846	pluvial supérieur	8.05	1236.50	298.87	715.53
2160	Sarine	Broc, Château d'en bas	573520 / 161345	0.3	636.00	1500	mixed regime (>500km ²)	5.12	1500.63	248.29	1014.01
2161	Massa	Blatten bei Naters	643700 / 137290	56.5	196.00	2937	a-glaciaire	-2.89	2036.03	45.98	2433.50
2167	Tresa	Ponte Tresa, Rocchetta	709580 / 92145	0.0	609.00	803	mixed regime (>500km ²)	9.59	1789.28	351.80	1107.04
2170	Arve	Genève, Bout du Monde	501220 / 115120	5.1	1973.00	1370	mixed regime (>500km ²)	5.65	1505.42	249.36	1153.49
2174	Rhône	Chancy, Aux Ripes	486600 / 112340	6.6	10308.00	1569	mixed regime (>500km ²)	4.32	1324.91	216.70	1027.76
2176	Sihl	Zürich, Sihlhölzli	682145 / 246890	0.0	343.00	1045	nivo-pluvial préalpin	6.97	1787.58	294.48	621.39
2179	Sense	Thorishaus, Sense matt	593550 / 193020	0.0	351.00	1071	nivo-pluvial préalpin	7.22	1404.55	306.68	756.67
2181	Thur	Halden	733560 / 263180	0.0	1085.00	908	mixed regime (>500km ²)	7.61	1585.63	329.74	1082.92
2185	Plessur	Chur, nur Hauptstation	757975 / 191925	0.0	264.00	1868	nival alpin	3.42	1179.00	194.41	693.27
2187	Werdenberger Binnenkanal	Salz	756795 / 234005	0.0	185.00	1003	artificial waterbody	7.74	1547.48	279.64	1344.65
2199	Wiese	Basel	611800 / 269700	0.0	442.00	720	pluvial jurassien	10.67	1508.42	342.75	800.00
2200	Weisse Lütchine	Zweilütschinen	635310 / 164550	13.1	165.00	2165	a-glacio-nival	1.58	1767.24	112.23	1531.27
2202	Ergolz	Liestal	622270 / 259750	0.0	261.00	588	pluvial jurassien	9.55	1076.57	341.74	436.87
2203	Grande Eau	Aigle	563975 / 129825	0.8	132.00	1562	nival de transition	4.96	1617.15	240.72	1082.21
2205	Aare	Untersiggenthal, Stilli	659970 / 263180	1.4	17553.00	1064	mixed regime (>500km ²)	6.99	1416.13	279.19	984.66
2206	Melera	Melera (Vallée Morobbia)	726988 / 114670	0.0	1.07	1423	nivo-pluvial méridional	5.88	1712.31	290.07	1297523.71
2210	Doubs	Ocourt	572530 / 244460	0.0	1275.00	952	mixed regime (>500km ²)	7.10	1499.13	346.76	790.06
2215	Saane	Laupen	584440 / 195300	0.1	1862.00	1137	mixed regime (>500km ²)	6.87	1373.00	288.00	866.85
2219	Simme	Oberried / Lenk	602630 / 141660	22.6	34.80	2347	b-glaciaire	0.92	1779.85	171.95	2130.36
2232	Allenbach	Adelboden	608710 / 148300	0.0	28.80	1863	nival alpin	3.64	1557.08	174.36	1332.39
2239	Spöl	Punt dal Gall	811020 / 167920	0.3	295.00	2389	nivo-glaciaire	-0.61	940.86	152.75	105.09
2243	Limmatt	Baden, Limmattpromenade	665640 / 258690	0.7	2394.00	1131	mixed regime (>500km ²)	6.59	1662.82	272.41	1311.73
2244	Krummbach	Klusmatten	644500 / 119420	0.4	19.40	2271	nival méridional	1.35	1342.63	166.60	1232.18
2247	Doubs	Sortie du lac des Bremets	544560 / 214880	0.0	867.00	977	mixed regime (>500km ²)	6.41	1548.43	350.16	635.02
2251	Rotenbach	Plaffeien, Schwyberg	587980 / 170590	0.0	1.69	1455	nival de transition	5.70	1688.19	296.97	1427822.37
2252	Schwendlbach	Plaffeien, Schwyberg	588340 / 171015	0.0	1.38	1439	nival de transition	5.76	1662.14	296.97	832954.23
2256	Rosgebach	Pontresina	788810 / 151690	21.7	66.50	2704	a-glaciaire	-1.75	1137.41	119.24	1398.90
2262	Berninabach	Pontresina	789440 / 151320	14.4	107.00	2615	a-glacio-nival	-1.18	1203.87	131.81	1411.84
2263	Chamuerabach	La Punt-Chamues-ch	791430 / 160600	0.1	73.40	2548	nivo-glaciaire	-1.10	1011.37	145.82	930.92
2265	Inn	Taras	816800 / 185910	3.0	1581.00	2384	mixed regime (>500km ²)	-0.37	992.18	147.59	383.43
2268	Rhone	Gletsch	670810 / 157200	41.8	39.40	2710	a-glaciaire	-1.75	1937.62	75.90	2342.03
2269	Lonza	Blatten	629130 / 140910	24.7	77.40	2624	a-glaciaire	-1.28	1566.54	86.75	1924.12
2276	Grosstalbach	Isenthal	685500 / 196050	6.7	43.90	1819	nival alpin	3.28	1731.55	227.73	1270.99

T = Temperature, P = Precipitation, E = Evaporation, Q = Streamflow/Runoff

Table B8. Characteristics of all 184 catchments in the HYD-RESPONSES dataset (Part 3/5).

Catchment	Water name	Place	Lon / Lat EPSG:21781	Glaciation %	Area km ²	Avg. Height m asl	Regime Type	Yearly Avg. T °C	Yearly P mm	Yearly E mm	Yearly Q mm
2282	Sperbelgraben	Wisen, Kurzeneitlalp	630725 / 207270	0.0	0.56	1070	nivo-pluvial préalpin	7.06	1631.78	342.53	8833404.51
2283	Rappengraben	Wisen, Riedbad	634340 / 207350	0.0	0.60	1142	nivo-pluvial préalpin	6.87	1656.81	355.40	10647734.56
2288	Rhein	Neuhausen, Flurlingerbrücke	689145 / 281975	0.3	11930.00	1239	mixed regime (>500km ²)	4.59	1295.50	261.93	960.66
2289	Rhein	Basel, Rheinhalle	613400 / 267650	0.8	35878.00	1052	mixed regime (>500km ²)	6.78	1343.83	284.04	919.47
2290	Areuse	St-Sulpice	532980 / 195880	0.0	104.00	1110	nivo-pluvial Jurassien	5.67	1500.18	344.81	1408.21
2299	Alpbach	Ersfeld, Bodenberg	688560 / 185120	19.7	20.70	2205	b-glaciaire	1.07	1669.66	171.48	2406.18
2300	Minster	Euthal, Riti	704425 / 215310	0.0	59.10	1352	nival de transition	5.53	2115.46	259.83	1639.61
2303	Thur	Jonschwil, Mühlau	723675 / 252720	0.0	493.00	1021	nivo-pluvial préalpin	6.93	1757.19	320.59	1285.82
2304	Ova dal Fuorn	Zomez, Punt la Drossa	810560 / 170790	0.0	55.30	2327	nival alpin	-0.46	937.69	150.89	586.32
2305	Glatt	Heisau, Zellersmühle	737270 / 251290	0.0	16.70	829	pluvial supérieur	8.18	1491.95	329.49	1063.60
2307	Suze	Sonceboz	579810 / 227350	0.0	127.00	1036	nivo-pluvial Jurassien	6.97	1332.88	340.21	1008.10
2308	Goldach	Goldach, Bleiche, nur Hauptstation	753190 / 261590	0.0	50.40	832	pluvial supérieur	8.33	1423.14	317.59	853.11
2312	Aach	Salmisach, Hungerbühl	744410 / 268400	0.0	47.40	467	pluvial inférieur	9.68	1019.41	335.09	488.00
2319	Ova da Cluozza	Zomez	804930 / 174830	0.0	27.00	2371	nivo-glaciaire	-0.47	919.61	150.80	888.70
2321	Cassarate	Pregassona	718010 / 97380	0.0	75.80	987	pluvio-nival méridional	8.52	1900.06	330.75	983.33
2327	Dischmabach	Davos, Kriegsmatte	786220 / 183370	0.7	42.90	2376	b-glacio-nival	0.15	1015.77	147.17	1242.21
2342	Salfina	Brig	642220 / 129630	2.5	76.50	2014	nivo-glaciaire	2.53	1165.38	167.60	948.67
2343	Langete	Huttwil, Häberenhud	629560 / 219135	0.0	59.90	760	pluvial inférieur	8.14	1276.02	329.38	618.66
2346	Rhone	Brig	641340 / 129700	19.2	906.00	2339	mixed regime (>500km ²)	0.31	1630.34	103.68	1481.12
2347	Riale di Roggiasca	Roveredo, Bacino di compenso	733545 / 118160	0.0	8.12	1702	nivo-pluvial méridional	4.11	1684.56	288.12	1869.20
2349	Breggia	Chiasso, Ponte di Polenta	722315 / 78320	0.0	47.10	933	pluvio-nival méridional	8.58	1726.83	382.64	712.61
2351	Vispa	Visp	634050 / 125900	23.1	786.00	2648	mixed regime (>500km ²)	-0.92	1125.42	116.03	684.02
2352	Linth	Linthal, Ausgleichsbecken KLL., nur Haupt	718285 / 197310	9.4	147.00	2085	a-glacio-nival	1.83	1874.45	169.98	925.43
2355	Landwasser	Davos, Frauenkirch	779640 / 181200	0.3	184.00	2224	nivo-glaciaire	0.97	1063.29	151.03	926.33
2356	Riale di Calneggia	Cavigorno, Pontit	684970 / 135960	0.0	23.90	2003	nival méridional	3.08	1868.56	188.46	1922.63
2364	Ticino	Protta	694610 / 152450	0.3	159.00	2071	nival méridional	2.16	1803.44	136.09	413.29
2366	Poschiavino	La Rôsa	802120 / 142010	0.0	14.10	2285	nival méridional	0.86	1398.05	162.22	1189.26
2368	Muggia	Locarno, Soldano	703100 / 113860	0.3	927.00	1530	mixed regime (>500km ²)	5.63	1946.42	245.77	783.83
2369	Mentue	Yvonand, La Mauguettaz	545440 / 180875	0.0	105.00	675	pluvial Jurassien	9.35	1081.13	328.32	457.37
2370	Doubs	Le Noirmont, La Goule	561430 / 231050	0.0	1047.00	977	mixed regime (>500km ²)	6.69	1534.75	348.30	795.29
2371	Orbe	Le Chent, Frontière	501445 / 156305	0.0	45.90	1235	nivo-pluvial Jurassien	6.42	1901.34	337.96	615.79
2372	Linth	Mollis, Linthbrücke	723985 / 217965	2.9	600.00	1743	mixed regime (>500km ²)	3.49	1848.95	197.67	1687.89
2374	Necker	Mogelsberg, Aachsäge	727110 / 247290	0.0	88.10	956	nivo-pluvial préalpin	7.27	1718.29	338.15	1142.38
2378	Orbe	Orbe, Le Chalet	530080 / 175560	0.0	343.00	1139	nivo-pluvial Jurassien	6.73	1692.73	341.81	1016.62
2386	Murg	Frauentfeld	709540 / 269660	0.0	213.00	597	pluvial inférieur	8.98	1178.35	343.21	567.47
2387	Hinterhein	Fürstenuar	753570 / 175730	0.6	1577.00	2127	mixed regime (>500km ²)	1.47	1147.93	165.74	767.37
2403	Inn	Cinuos-chel, nur Hauptstation	797700 / 168170	5.2	733.00	2456	mixed regime (>500km ²)	-0.66	1007.10	146.31	212.71
2409	Emme	Eggwil, Heidbüel	627910 / 191180	0.0	124.00	1281	nivo-pluvial préalpin	6.10	1604.24	270.21	1061.40
2410	Liechtensteiner Binnenkanal	Ruggell	757750 / 234590	0.0	116.00	853	artificial waterbody	8.58	1286.29	264.96	1321.13
2412	Sionge	Vuippens, Château	572420 / 167540	0.0	43.40	865	nivo-pluvial préalpin	8.10	1298.00	302.73	802.84
2414	Rietholzbach	Mosnang, Rietholz	718840 / 248440	0.0	3.19	794	pluvial supérieur	8.13	1476.78	336.69	1006909.39
2415	Glatt	Rheinsfelden	678040 / 269720	0.0	417.00	503	downstream lake	9.70	1165.36	340.63	590.10
2416	Aabach	Hitzkirch, Richensee	661390 / 230220	0.0	73.30	581	downstream lake	9.46	1163.00	317.37	535.90
2417	Suhre	Oberkirch	651320 / 223140	0.0	75.60	583	downstream lake	9.39	1139.68	312.72	510.78
2418	Julia	Tiefencastel	765570 / 169910	0.2	325.00	2196	nivo-glaciaire	1.10	1058.77	161.39	97.09
2419	Rhone	Reckingen	661910 / 146780	11.8	214.00	2305	a-glacio-nival	0.30	1814.00	105.51	1424.61
2420	Moesa	Lumino, Sassello	724765 / 120360	0.1	472.00	1667	nivo-pluvial méridional	3.98	1619.63	234.73	1339.42

T = Temperature, P = Precipitation, E = Evaporation, Q = Streamflow/Runoff

Table B9. Characteristics of all 184 catchments in the HYD-RESPONSES dataset (Part 4/5).

Catchment	Water name	Place	Lon / Lat EPSG:21781	Glaciation %	Area km ²	Avg. Height m asl	Regime Type	Yearly Avg. T °C	Yearly P mm	Yearly E mm	Yearly Q mm
2426	Seez	Mels	750410/212510	0.1	106.00	1803	nival alpin	3.55	1578.39	217.42	640.88
2430	Rein da Sumvltg	Sumvltg, Encardens	718810/167690	1.7	21.80	2457	b-glacio-nival	-0.15	1581.92	160.82	2183.90
2432	Venoge	Ecublens, Les Bois	532040/154160	0.0	228.00	686	nivo-pluvial jurassien	9.62	1148.17	332.99	539.44
2433	Aubonne	Allaman, Le Coulet	520720/147410	0.0	105.00	952	nivo-pluvial jurassien	8.21	1444.62	340.37	1587.98
2434	Dünern	Oltén, Hammermühle	634330/244480	0.0	234.00	711	pluvial jurassien	8.50	1210.83	334.79	437.11
2436	Chli Schliere	Alpnach, Chlitch Erti	663800/199570	0.0	21.60	1345	nivo-pluvial préalpin	5.96	1876.39	271.62	966.44
2437	Parimbot	Ecublens, Eschiens	552060/161650	0.0	6.92	716	pluvial jurassien	9.50	1182.10	311.77	717260.34
2450	Wigger	Zofingen	637580/237080	0.0	366.00	656	pluvial inférieur	8.80	1182.26	328.47	461.60
2457	Aare	Ringenberg, Goldswil	633730/171510	12.1	1138.00	1951	mixed regime (>500km ²)	2.47	1761.77	138.78	1715.63
2458	Seyon	Valangin	559370/206810	0.0	112.00	978	nivo-pluvial jurassien	7.54	1292.29	350.00	214.91
2461	Magliasina	Magliaso, Ponte	711620/93290	0.0	34.40	926	pluvio-nival méridional	8.91	1938.53	357.01	1117.90
2468	Sitter	St. Gallen, Bruggen/Au	742540/253230	0.0	261.00	1042	nivo-pluvial préalpin	7.22	1722.67	343.20	1208.91
2471	Murg	Murgenthal, Walliswil	629340/233555	0.0	183.00	653	pluvial inférieur	8.60	1191.59	333.34	556.21
2473	Rhein	Diepoldsau, Rietbrücke	766280/250360	0.6	6299.00	1771	mixed regime (>500km ²)	3.17	1327.19	193.52	1163.69
2474	Calanca	Buseno	729440/127180	0.2	121.00	1931	nival méridional	2.65	1673.78	227.69	1113.07
2475	Maggia	Bignasco, Ponte nuovo	690040/132550	0.9	316.00	1879	nival méridional	3.67	1939.62	187.23	415.67
2477	Lotze	Zug, Letzi	680600/226070	0.0	100.00	818	downstream lake	8.15	1560.20	295.43	925.59
2478	Birse	Soyhières, Bois du Treuil	596780/249070	0.0	569.00	805	nivo-pluvial jurassien	8.06	1265.37	334.76	580.60
2480	Areuse	Boudry	554350/199940	0.0	378.00	1077	nivo-pluvial jurassien	6.27	1464.77	347.62	906.66
2481	Engelberger Aa	Buochs, Flugplatz	673555/202870	2.5	228.00	1609	b-glacio-nival	4.30	1693.58	196.94	1705.73
2485	Allaine	Boncourt, Frontière	567830/261200	0.0	212.00	562	pluvial jurassien	9.54	1108.82	343.10	464.95
2486	Veveyse	Vevey, Copet	554675/146565	0.0	64.50	1098	nivo-pluvial préalpin	7.37	1497.99	307.89	955.88
2487	Kleine Emme	Werthenstein, Chappelboden	647870/209510	0.0	311.00	1167	nivo-pluvial préalpin	6.61	1695.60	279.00	1095.28
2488	Simme	Latterbach	610680/167840	1.5	563.00	1594	nival de transition	4.79	1506.56	225.96	342.76
2490	Allondon	Dardagny, Les Granges	488880/119460	0.0	119.00	760	nivo-pluvial jurassien	10.64	1372.60	326.46	854.70
2491	Schächen	Bürglen, Galgenwäldli, nur Hauptstation	692480/191800	1.5	108.00	1728	nivo-glaciaire	3.55	1854.00	188.20	1397.24
2493	Promenthouse	Gland, Route Suisse	510080/140080	0.0	120.00	1027	nivo-pluvial jurassien	7.73	1577.83	338.92	430.80
2494	Ticino	Pollegio, Campagna	716120/135330	0.2	444.00	1796	nival méridional	3.85	1710.59	173.72	1438.77
2497	Luthem	Nebikon	640560/226740	0.0	105.00	749	pluvial inférieur	8.31	1268.69	334.87	429.99
2498	Glener	Castrisch	735330/181790	1.1	381.00	2022	nivo-glaciaire	2.11	1307.02	168.97	734.66
2500	Worble	Ittigen	603005/202455	0.0	67.10	666	pluvial inférieur	8.72	1174.24	317.69	475.10
2602	Rhein	Domat/Ems	753890/189370	0.9	3229.00	2013	mixed regime (>500km ²)	2.19	1277.76	168.28	1122.84
2603	Ilfis	Langnau	627320/198600	0.0	187.00	1039	nivo-pluvial préalpin	7.05	1619.21	318.70	882.14
2604	Biber	Biberbrugg	697240/223280	0.0	31.90	1003	nivo-pluvial préalpin	7.00	1789.15	287.37	1085.77
2605	Verzasca	Lavertezzo, Campiöi	708420/122920	0.0	185.00	1651	nivo-pluvial méridional	5.11	2013.18	260.43	1846.37
2606	Rhône	Genève, Halle de l'Île	499890/117850	7.2	8000.00	1658	mixed regime (>500km ²)	4.08	1286.36	204.12	996.79
2607	Goneri	Oberwald	670467/153932	4.0	38.50	2383	b-glacio-nival	0.07	1976.16	121.82	2011.50
2608	Sellenbodenbach	Neuenkirch	658530/218290	0.0	10.40	608	pluvial inférieur	9.33	1193.97	305.25	637.12

T = Temperature, P = Precipitation, E = Evaporation, Q = Streamflow/Runoff

Table B10. Characteristics of all 184 catchments in the HYD-RESPONSES dataset (Part 5/5).

Catchment	Water name	Place	Lon / Lat EPSG:21781	Glaciation %	Area km ²	Avg. Height m asl	Regime Type	Yearly Avg. T °C	Yearly P mm	Yearly E mm	Yearly Q mm
2609	Alp	Einsiedeln	698640 / 223020	0.0	46.70	1157	nivo-pluvial préalpin	6.35	1939.89	279.80	1459.07
2610	Scheulte	Vicques	599485 / 244150	0.0	72.70	792	nivo-pluvial jurassien	8.20	1260.81	333.18	635.64
2612	Riale di Pincascia	Lavertezzo	708060 / 123950	0.0	44.50	1705	nivo-pluvial méridional	4.89	1978.57	277.65	1911.93
2617	Rom	Müstair	830800 / 168700	0.0	128.00	2184	nival alpin	1.03	844.68	158.63	577.25
2620	Mera	Soglio	760770 / 133450	7.4	177.00	2173	b-glacio-nival	0.95	1333.42	191.09	361.81
2629	Vedeggio	Agno, stazione principale	714110 / 95680	0.0	99.90	921	pluvio-nival méridional	8.87	1904.96	334.27	656.21
2630	Sionne	Sion	594400 / 119900	0.0	27.60	1577	nival alpin	5.35	1355.03	186.55	224.58
2631	Hinterrhein	Hinterrhein, Schiessplatz	733706 / 153945	9.1	41.50	2430	a-glacio-nival	-0.38	1704.08	164.40	799.71
2634	Kleine Emme	Emmen	663700 / 213630	0.0	478.00	1054	nivo-pluvial préalpin	7.15	1610.61	284.17	994.18
2635	Grossbach	Einsiedeln, Gross	700710 / 218125	0.0	8.95	1283	nivo-pluvial préalpin	5.90	1952.69	299.45	1387.71
2640	Some	Delémont, Pré-Guillaume	593380 / 245940	0.0	214.00	779	nivo-pluvial jurassien	8.20	1233.60	335.80	603.72
2646	Kander	Emdthal	617790 / 168400	5.1	487.00	1860	b-glacio-nival	3.38	1486.71	167.85	1305.44

T = Temperature, P = Precipitation, E = Evaporation, Q = Streamflow/Runoff

References

- An, H., Ouyang, C., and Chen, X.: Real-time estimation of SMAP soil moisture in mountainous areas and its impact on rainfall-runoff simulation, *Journal of Hydrology*, 660, 133 487, <https://doi.org/10.1016/j.jhydrol.2025.133487>, 2025.
- Anderson, M. C., Kustas, W. P., Norman, J. M., Diak, G. T., Hain, C. R., Gao, F., Yang, Y., Knipper, K. R., Xue, J., Yang, Y., Crow, W. T., Holmes, T. R. H., Nieto, H., Guzinski, R., Otkin, J. A., Mecikalski, J. R., Cammalleri, C., Torres-Rua, A. T., Zhan, X., Fang, L., Colaizzi, P. D., and Agam, N.: A brief history of the thermal IR-based Two-Source Energy Balance (TSEB) model – diagnosing evapotranspiration from plant to global scales, *Agricultural and Forest Meteorology*, 350, 109 951, <https://doi.org/10.1016/j.agrformet.2024.109951>, 2024.
- Apurv, T. and Cai, X.: Drought Propagation in Contiguous U.S. Watersheds: A Process-Based Understanding of the Role of Climate and Watershed Properties, *Water Resources Research*, 56, e2020WR027 755, <https://doi.org/10.1029/2020WR027755>, <https://onlinelibrary.wiley.com/doi/pdf/10.1029/2020WR027755>, 2020.
- Apurv, T., Sivapalan, M., and Cai, X.: Understanding the Role of Climate Characteristics in Drought Propagation, *Water Resources Research*, 53, 9304–9329, <https://doi.org/10.1002/2017WR021445>, [eprint: https://onlinelibrary.wiley.com/doi/pdf/10.1002/2017WR021445](https://onlinelibrary.wiley.com/doi/pdf/10.1002/2017WR021445), 2017.
- Aschwanden, H.: Die Niedrigwasserabflussmenge Q347 – Bestimmung und Abschätzung in alpinen schweizerischen Einzugsgebieten., Tech. Rep. 18, Bern, 1992.
- Aschwanden, H. and Kan, C.: Die Abflussmenge Q347 – eine Standortbestimmung., Tech. Rep. 27, Bern, 1999.
- Aschwanden, H. and Weingartner, R.: Die Abflussregimes der Schweiz., Tech. Rep. 65, Geographisches Institut der Universität Bern (GIUB), Bern, <https://boris.unibe.ch/133660/>, 1985.
- Avanzi, F., Munerol, F., Milelli, M., Gabellani, S., Massari, C., Giroto, M., Cremonese, E., Galvagno, M., Bruno, G., Morra di Cella, U., Rossi, L., Altamura, M., and Ferraris, L.: Winter snow deficit was a harbinger of summer 2022 socio-hydrologic drought in the Po Basin, Italy, *Commun Earth Environ*, 5, 1–12, <https://doi.org/10.1038/s43247-024-01222-z>, publisher: Nature Publishing Group, 2024.
- Bachmair, S., Stahl, K., Collins, K., Hannaford, J., Acreman, M., Svoboda, M., Knutson, C., Smith, K. H., Wall, N., Fuchs, B., Crossman, N. D., and Overton, I. C.: Drought indicators revisited: the need for a wider consideration of environment and society, *WIREs Water*, 3, 516–536, <https://doi.org/10.1002/wat2.1154>, [eprint: https://onlinelibrary.wiley.com/doi/pdf/10.1002/wat2.1154](https://onlinelibrary.wiley.com/doi/pdf/10.1002/wat2.1154), 2016.
- Bachmair, S., Tanguy, M., Hannaford, J., and Stahl, K.: How well do meteorological indicators represent agricultural and forest drought across Europe?, *Environ. Res. Lett.*, 13, 034 042, <https://doi.org/10.1088/1748-9326/aaafda>, publisher: IOP Publishing, 2018.
- Baez-Villanueva, O. M., Zambrano-Bigiarini, M., Miralles, D. G., Beck, H. E., Siegmund, J. F., Alvarez-Garreton, C., Verbist, K., Garreaud, R., Boisier, J. P., and Galleguillos, M.: On the timescale of drought indices for monitoring streamflow drought considering catchment hydrological regimes, *Hydrology and Earth System Sciences*, 28, 1415–1439, <https://doi.org/10.5194/hess-28-1415-2024>, publisher: Copernicus GmbH, 2024.
- BAFU: Hitze und Trockenheit im Sommer 2015. Auswirkungen auf Mensch und Umwelt. Bundesamt für Umwelt BAFU, Bern. Umwelt-Zustand Nr. 1629: 108 S., Tech. rep., 2016.
- BAFU: Nationale Grundwasserbeobachtung NAQUA, <https://www.bafu.admin.ch/bafu/de/home/themen/thema-wasser/wasser-fachinformationen/zustand-der-gewaesser/zustand-des-grundwassers/nationale-grundwasserbeobachtung-naqua.html>, 2019.
- BAFU: Trockenheit: Bundesrat will nationales System zur Früherkennung und Warnung, <https://www.bafu.admin.ch/bafu/de/home/dokumentation/medienmitteilungen/anzeige-nsb-unter-medienmitteilungen.msg-id-88854.html>, 2022.
- BAFU: Nationale Beobachtung Oberflächengewässerqualität (NAWA), <https://www.bafu.admin.ch/bafu/de/home/themen/thema-wasser/wasser-daten-indikatoren-und-karten/wasser-messnetze/nationale-beobachtung-oberflaechengewaesserqualitaet-nawa.html>, 2023.

- 860 BAFU: Stationsbericht Niedrigwasserstatistik - Leitfaden, <https://www.bafu.admin.ch/dam/bafu/de/dokumente/hydrologie/fachinfo-daten/leitfaden-stationsberichte-niedrigwasserstatistik-bafu.pdf.download.pdf/leitfaden-stationsberichte-niedrigwasserstatistik-bafu.pdf>, 2024.
- BAFU: Der kombinierte Trockenheitsindex - Nationale Trockenheitsplattform, <https://www.trockenheit.admin.ch/de/trockenheit/trockenheitsindex>, 2025.
- BAFU (Eds.): Auswirkungen des Klimawandels auf die Schweizer Gewässer. Hydrologie, Gewässerökologie und Wasserwirtschaft. Bundesamt für Umwelt BAFU, Bern. Umwelt-Wissen Nr. 2101: 134 S., Tech. rep., 2021.
- 865 BAFU (Eds.): Die biogeographischen Regionen der Schweiz. 1. aktualisierte Auflage 2022. Erstausgabe 2001. Bundesamt für Umwelt, Bern, Umwelt-Wissen Nr. 2214: p.28, Tech. rep., Bundesamt für Umwelt, https://www.bafu.admin.ch/dam/bafu/de/dokumente/landschaft/uw-umwelt-wissen/die_biogeographischenregionenderschweiz.pdf.download.pdf/die_biogeographischenregionenderschweiz.pdf, 2022.
- BAFU (Eds.): Hydrologisches Jahrbuch der Schweiz 2022. Abfluss, Wasserstand und Wasserqualität der Schweizer Gewässer.,
- 870 Tech. rep., Bundesamt für Umwelt, Ittigen, Bern, https://www.bafu.admin.ch/dam/bafu/de/dokumente/hydrologie/uz-umwelt-zustand/hydrologisches-jahrbuch-2022.pdf.download.pdf/de_BAFU_UZ_2215_Hydrologisches_Jahrbuch_2022_bf.pdf, 2023.
- BAFU et al. (Eds.): Hitze und Trockenheit im Sommer 2018. Auswirkungen auf Mensch und Umwelt. Bundesamt für Umwelt, Bern. Umwelt-Zustand Nr. 1909: 91 S., Tech. rep., 2019.
- Bai, J. and Perron, P.: Estimating and Testing Linear Models with Multiple Structural Changes, *Econometrica*, 66, 47–78,
- 875 <https://doi.org/10.2307/2998540>, publisher: [Wiley, Econometric Society], 1998.
- Baker, D. B., Richards, R. P., Loftus, T. T., and Kramer, J. W.: A New Flashiness Index: Characteristics and Applications to Midwestern Rivers and Streams, *JAWRA Journal of the American Water Resources Association*, 40, 503–522, <https://doi.org/10.1111/j.1752-1688.2004.tb01046.x>, <https://onlinelibrary.wiley.com/doi/pdf/10.1111/j.1752-1688.2004.tb01046.x>, 2004.
- Barker, L. J., Hannaford, J., Chiverton, A., and Svensson, C.: From meteorological to hydrological drought using standardised indicators, *Hydrology and Earth System Sciences*, 20, 2483–2505, <https://doi.org/10.5194/hess-20-2483-2016>, publisher: Copernicus GmbH, 2016.
- 880 Baston, D.: exactextractr: Fast Extraction from Raster Datasets using Polygons. R package version 0.10.0, <https://cran.r-project.org/web/packages/exactextractr/index.html>, 2023.
- Besso, H., Shean, D., and Lundquist, J. D.: Mountain snow depth retrievals from customized processing of ICESat-2 satellite laser altimetry, *Remote Sensing of Environment*, 300, 113 843, <https://doi.org/10.1016/j.rse.2023.113843>, 2024.
- 885 Bevacqua, E., De Michele, C., Manning, C., Couason, A., Ribeiro, A. F. S., Ramos, A. M., Vignotto, E., Bastos, A., Blesić, S., Durante, F., Hillier, J., Oliveira, S. C., Pinto, J. G., Ragno, E., Rivoire, P., Saunders, K., van der Wiel, K., Wu, W., Zhang, T., and Zscheischler, J.: Guidelines for Studying Diverse Types of Compound Weather and Climate Events, *Earth's Future*, 9, e2021EF002 340, <https://doi.org/10.1029/2021EF002340>, <https://onlinelibrary.wiley.com/doi/pdf/10.1029/2021EF002340>, 2021.
- Biegel, S., Schindler, K., and Stocker, B. D.: Unrecognised water limitation is a main source of uncertainty for models of terrestrial photosynthesis, *Biogeosciences*, 22, 7455–7481, <https://doi.org/10.5194/bg-22-7455-2025>, publisher: Copernicus GmbH, 2025.
- 890 Bloomfield, J. P., Gong, M., Marchant, B. P., Coxon, G., and Addor, N.: How is Baseflow Index (BFI) impacted by water resource management practices?, *Hydrology and Earth System Sciences*, 25, 5355–5379, <https://doi.org/10.5194/hess-25-5355-2021>, publisher: Copernicus GmbH, 2021.
- BLW, B. f. L.: Bodeneignungskarte der Schweiz, <https://www.blw.admin.ch/blw/de/home/politik/datenmanagement/geografisches-informationssystem-gis/bodeneignungskarte.html>, 2022.
- 895 Brocca, L., Barbetta, S., Camici, S., Ciabatta, L., Dari, J., Filippucci, P., Massari, C., Modanesi, S., Tarpanelli, A., Bonaccorsi, B., Mosaffa, H., Wagner, W., Vreugdenhil, M., Quast, R., Alfieri, L., Gabellani, S., Avanzi, F., Rains, D., Miralles, D. G., Mantovani, S., Briese, C.,

- Domeneghetti, A., Jacob, A., Castelli, M., Camps-Valls, G., Volden, E., and Fernandez, D.: A Digital Twin of the terrestrial water cycle: a glimpse into the future through high-resolution Earth observations, *Front. Sci.*, 1, <https://doi.org/10.3389/fsci.2023.1190191>, publisher: Frontiers, 2024a.
- 900 Brocca, L., Gaona, J., Bavera, D., Fioravanti, G., Puca, S., Ciabatta, L., Filippucci, P., Mosaffa, H., Esposito, G., Roberto, N., Dari, J., Vreugdenhil, M., and Wagner, W.: Exploring the actual spatial resolution of 1 km satellite soil moisture products, *Science of The Total Environment*, 945, 174 087, <https://doi.org/10.1016/j.scitotenv.2024.174087>, 2024b.
- Brunner, M. I. and Chartier-Rescan, C.: Drought Spatial Extent and Dependence Increase During Drought Propagation From the At-
905 mosphere to the Hydrosphere, *Geophysical Research Letters*, 51, e2023GL107 918, <https://doi.org/10.1029/2023GL107918>, _eprint: <https://onlinelibrary.wiley.com/doi/pdf/10.1029/2023GL107918>, 2024.
- Brunner, M. I., Björnson Gurung, A., Zappa, M., Zekollari, H., Farinotti, D., and Stähli, M.: Present and future water scarcity in Switzerland: Potential for alleviation through reservoirs and lakes, *Science of The Total Environment*, 666, 1033–1047, <https://doi.org/10.1016/j.scitotenv.2019.02.169>, 2019a.
- 910 Brunner, M. I., Farinotti, D., Zekollari, H., Huss, M., and Zappa, M.: Future shifts in extreme flow regimes in Alpine regions, *Hydrology and Earth System Sciences*, 23, 4471–4489, <https://doi.org/10.5194/hess-23-4471-2019>, publisher: Copernicus GmbH, 2019b.
- Brunner, M. I., Liechti, K., and Zappa, M.: Extremeness of recent drought events in Switzerland: dependence on variable and return period choice, *Natural Hazards and Earth System Sciences*, 19, 2311–2323, <https://doi.org/10.5194/nhess-19-2311-2019>, publisher: Copernicus GmbH, 2019c.
- 915 Brunner, M. I., Slater, L., Tallaksen, L. M., and Clark, M.: Challenges in modeling and predicting floods and droughts: A review, *WIREs Water*, 8, e1520, <https://doi.org/10.1002/wat2.1520>, _eprint: <https://onlinelibrary.wiley.com/doi/pdf/10.1002/wat2.1520>, 2021.
- Brunner, M. I., Van Loon, A. F., and Stahl, K.: Moderate and Severe Hydrological Droughts in Europe Differ in Their Hydrometeorological Drivers, *Water Resources Research*, 58, e2022WR032 871, <https://doi.org/10.1029/2022WR032871>, _eprint: <https://onlinelibrary.wiley.com/doi/pdf/10.1029/2022WR032871>, 2022.
- 920 Brunner, M. I., Götze, J., Schlemper, C., and Van Loon, A. F.: Hydrological Drought Generation Processes and Severity Are Changing in the Alps, *Geophysical Research Letters*, 50, e2022GL101 776, <https://doi.org/10.1029/2022GL101776>, _eprint: <https://onlinelibrary.wiley.com/doi/pdf/10.1029/2022GL101776>, 2023.
- BUWAL, BWG, MeteoSchweiz: Auswirkungen des Hitzesommers 2003 auf die Gewässer. Schriftenreihe Umwelt Nr. 369. Bern: Bundesamt für Umwelt, Wald und Landschaft, 174 S., Tech. rep., 2004.
- 925 Calanca, P.: Climate change and drought occurrence in the Alpine region: How severe are becoming the extremes?, *Global and Planetary Change*, 57, 151–160, <https://doi.org/10.1016/j.gloplacha.2006.11.001>, 2007.
- Cammalleri, C., Barbosa, P., and Vogt, J. V.: Analysing the Relationship between Multiple-Timescale SPI and GRACE Terrestrial Water Storage in the Framework of Drought Monitoring, *Water*, 11, 1672, <https://doi.org/10.3390/w11081672>, number: 8 Publisher: Multidisciplinary Digital Publishing Institute, 2019.
- 930 CH2018: CH2018 – Climate Scenarios for Switzerland, Technical Report, National Centre for Climate Services, Zurich, 271 pp. ISBN: 978-3-9525031-4-0., Tech. rep., 2018.
- Clerc-Schwarzenbach, F., Selleri, G., Neri, M., Toth, E., van Meerveld, I., and Seibert, J.: Large-sample hydrology – a few camels or a whole caravan?, *Hydrology and Earth System Sciences*, 28, 4219–4237, <https://doi.org/10.5194/hess-28-4219-2024>, publisher: Copernicus GmbH, 2024.

- 935 Cui, G., Ma, Q., and Bales, R.: Assessing multi-year-drought vulnerability in dense Mediterranean-climate forests using water-balance-based indicators, *Journal of Hydrology*, 606, 127 431, <https://doi.org/10.1016/j.jhydrol.2022.127431>, 2022.
- Dalla Torre, D., Di Marco, N., Menapace, A., Avesani, D., Righetti, M., and Majone, B.: Suitability of ERA5-Land re-analysis dataset for hydrological modelling in the Alpine region, *Journal of Hydrology: Regional Studies*, 52, 101 718, <https://doi.org/10.1016/j.ejrh.2024.101718>, 2024.
- 940 Das, B. C., Islam, A., and Sarkar, B.: Drainage Basin Shape Indices to Understanding Channel Hydraulics, *Water Resour Manage*, 36, 2523–2547, <https://doi.org/10.1007/s11269-022-03121-4>, 2022.
- de Jager, A., Corbane, C., and Szabo, F.: Recent Developments in Some Long-Term Drought Drivers, *Climate*, 10, 31, <https://doi.org/10.3390/cli10030031>, number: 3 Publisher: Multidisciplinary Digital Publishing Institute, 2022.
- Ding, Y., Gong, X., Xing, Z., Cai, H., Zhou, Z., Zhang, D., Sun, P., and Shi, H.: Attribution of meteorological, hydrological and agricultural drought propagation in different climatic regions of China, *Agricultural Water Management*, 255, 106 996, <https://doi.org/10.1016/j.agwat.2021.106996>, 2021.
- 945 Dingman, S. L.: Drainage density and streamflow: A closer look, *Water Resources Research*, 14, 1183–1187, <https://doi.org/10.1029/WR014i006p01183>, _eprint: <https://onlinelibrary.wiley.com/doi/pdf/10.1029/WR014i006p01183>, 1978.
- Eekhout, J. P. C., Hunink, J. E., Terink, W., and de Vente, J.: Why increased extreme precipitation under climate change negatively affects water security, *Hydrology and Earth System Sciences*, 22, 5935–5946, <https://doi.org/10.5194/hess-22-5935-2018>, publisher: Copernicus GmbH, 2018.
- 950 European Commission: Standardized Precipitation Index (SPI). EDO Indicator Factsheet. European Drought Observatory (EDO)., https://edo.jrc.ec.europa.eu/documents/factsheets/factsheet_spi.pdf, 2020.
- Floriantic, M. G., Berghuijs, W. R., Jonas, T., Kirchner, J. W., and Molnar, P.: Effects of climate anomalies on warm-season low flows in Switzerland, *Hydrology and Earth System Sciences*, 24, 5423–5438, <https://doi.org/10.5194/hess-24-5423-2020>, publisher: Copernicus GmbH, 2020.
- 955 Floriantic, M. G., Spies, D., van Meerveld, I. H. J., and Molnar, P.: A multi-scale study of the dominant catchment characteristics impacting low-flow metrics, *Hydrological Processes*, 36, e14 462, <https://doi.org/10.1002/hyp.14462>, _eprint: <https://onlinelibrary.wiley.com/doi/pdf/10.1002/hyp.14462>, 2022.
- 960 Fluhrer, A., Baur, M. J., Piles, M., Bayat, B., Rahmati, M., Chaparro, D., Dubois, C., Hellwig, F. M., Montzka, C., Kübert, A., Mueller, M. M., Augscheller, I., Jonard, F., Schellenberg, K., and Jagdhuber, T.: Assessing evapotranspiration dynamics across central Europe in the context of land–atmosphere drivers, *Biogeosciences*, 22, 3721–3746, <https://doi.org/10.5194/bg-22-3721-2025>, publisher: Copernicus GmbH, 2025.
- Fowler, K., Peel, M., Saft, M., Nathan, R., Horne, A., Wilby, R., McCutcheon, C., and Peterson, T.: Hydrological Shifts Threaten Water Resources, *Water Resources Research*, 58, e2021WR031 210, <https://doi.org/10.1029/2021WR031210>, _eprint: <https://onlinelibrary.wiley.com/doi/pdf/10.1029/2021WR031210>, 2022.
- 965 Frei, C.: Interpolation of temperature in a mountainous region using nonlinear profiles and non-Euclidean distances, *International Journal of Climatology*, 34, 1585–1605, <https://doi.org/10.1002/joc.3786>, _eprint: <https://onlinelibrary.wiley.com/doi/pdf/10.1002/joc.3786>, 2014.
- Frei, C. and Schär, C.: A precipitation climatology of the Alps from high-resolution rain-gauge observations, *International Journal of Climatology*, 18, 873–900, [https://doi.org/10.1002/\(SICI\)1097-0088\(19980630\)18:8<873::AID-JOC255>3.0.CO;2-9](https://doi.org/10.1002/(SICI)1097-0088(19980630)18:8<873::AID-JOC255>3.0.CO;2-9), _eprint: <https://onlinelibrary.wiley.com/doi/pdf/10.1002/%28SICI%291097-0088%2819980630%2918%3A8%3C873%3A%3AAID-JOC255%3E3.0.CO%3B2-9>, 1998.
- 970

- Gebrechorkos, S. H., Sheffield, J., Vicente-Serrano, S. M., Funk, C., Miralles, D. G., Peng, J., Dyer, E., Talib, J., Beck, H. E., Singer, M. B., and Dadson, S. J.: Warming accelerates global drought severity, *Nature*, 642, 628–635, <https://doi.org/10.1038/s41586-025-09047-2>, publisher: Nature Publishing Group, 2025.
- 975 Gudmundsson, L. and Stagge, J. H.: SCI: Standardized Climate Indices such as SPI, SRI or SPEIR package version 1.0-2., 2016.
- Guo, Y., Zhang, Y., Zhang, L., and Wang, Z.: Regionalization of hydrological modeling for predicting streamflow in ungauged catchments: A comprehensive review, *WIREs Water*, 8, e1487, <https://doi.org/10.1002/wat2.1487>, _eprint: <https://onlinelibrary.wiley.com/doi/pdf/10.1002/wat2.1487>, 2021.
- 980 Haile, G. G., Tang, Q., Li, W., Liu, X., and Zhang, X.: Drought: Progress in broadening its understanding, *WIREs Water*, 7, e1407, <https://doi.org/10.1002/wat2.1407>, _eprint: <https://onlinelibrary.wiley.com/doi/pdf/10.1002/wat2.1407>, 2020.
- Hammond, J. C., Simeone, C., Hecht, J. S., Hodgkins, G. A., Lombard, M., McCabe, G., Wolock, D., Wieczorek, M., Olson, C., Caldwell, T., Dudley, R., and Price, A. N.: Going Beyond Low Flows: Streamflow Drought Deficit and Duration Illuminate Distinct Spatiotemporal Drought Patterns and Trends in the U.S. During the Last Century, *Water Resources Research*, 58, e2022WR031930, <https://doi.org/10.1029/2022WR031930>, _eprint: <https://onlinelibrary.wiley.com/doi/pdf/10.1029/2022WR031930>, 2022.
- 985 Hao, Z. and Singh, V. P.: Drought characterization from a multivariate perspective: A review, *Journal of Hydrology*, 527, 668–678, <https://doi.org/10.1016/j.jhydrol.2015.05.031>, 2015.
- Haslinger, K., Koffler, D., Schöner, W., and Laaha, G.: Exploring the link between meteorological drought and streamflow: Effects of climate-catchment interaction, *Water Resources Research*, 50, 2468–2487, <https://doi.org/10.1002/2013WR015051>, _eprint: <https://onlinelibrary.wiley.com/doi/pdf/10.1002/2013WR015051>, 2014.
- 990 Haslinger, K., Holawe, F., and Blöschl, G.: Spatial characteristics of precipitation shortfalls in the Greater Alpine Region—a data-based analysis from observations, *Theor Appl Climatol*, 136, 717–731, <https://doi.org/10.1007/s00704-018-2506-5>, 2019.
- Henne, P. D., Bigalke, M., Büntgen, U., Colombaroli, D., Conedera, M., Feller, U., Frank, D., Fuhrer, J., Grosjean, M., Heiri, O., Luterbacher, J., Mestrot, A., Rigling, A., Rössler, O., Rohr, C., Rutishauser, T., Schwikowski, M., Stampfli, A., Szidat, S., Theurillat, J.-P., Weingartner, R., Wilcke, W., and Tinner, W.: An empirical perspective for understanding climate change impacts in Switzerland, *Reg Environ Change*, 18, 205–221, <https://doi.org/10.1007/s10113-017-1182-9>, 2018.
- 995 Hersbach, H., Bell, B., Berrisford, P., Hirahara, S., Horányi, A., Muñoz-Sabater, J., Nicolas, J., Peubey, C., Radu, R., Schepers, D., Simmons, A., Soci, C., Abdalla, S., Abellan, X., Balsamo, G., Bechtold, P., Biavati, G., Bidlot, J., Bonavita, M., De Chiara, G., Dahlgren, P., Dee, D., Diamantakis, M., Dragani, R., Flemming, J., Forbes, R., Fuentes, M., Geer, A., Haimberger, L., Healy, S., Hogan, R. J., Hólm, E., Janisková, M., Keeley, S., Laloyaux, P., Lopez, P., Lupu, C., Radnoti, G., de Rosnay, P., Rozum, I., Vamborg, F., Villaume, S., and Thépaut, J.-N.: The ERA5 global reanalysis, *Quarterly Journal of the Royal Meteorological Society*, 146, 1999–2049, <https://doi.org/10.1002/qj.3803>, _eprint: <https://onlinelibrary.wiley.com/doi/pdf/10.1002/qj.3803>, 2020.
- 1000 Hijmans, R.: terra: Spatial Data Analysis. R package version 1.7-29., <https://cran.r-project.org/web/packages/terra/>, 2023.
- Hirschi, M., Davin, E. L., Schwingshackl, C., Wartenburger, R., Meier, R., Gudmundsson, L., and Seneviratne, S. I.: Soil moisture and evapotranspiration, Report, ETH Zurich, <https://doi.org/10.3929/ethz-b-000389455>, accepted: 2020-06-05T07:44:43Z, 2020.
- 1005 Hisdal, H. and Tallaksen, L. M.: Drought event definition. Technical Report to the ARIDE project No. 6. Department of Geophysics, University of Oslo., Tech. rep., 2000.
- Horton, R. E.: Drainage-basin characteristics, *Eos, Transactions American Geophysical Union*, 13, 350–361, <https://doi.org/10.1029/TR013i001p00350>, _eprint: <https://agupubs.onlinelibrary.wiley.com/doi/pdf/10.1029/TR013i001p00350>, 1932.

- 1010 Höge, M., Kauzlaric, M., Siber, R., Schönenberger, U., Horton, P., Schwanbeck, J., Floriancic, M. G., Viviroli, D., Wilhelm, S., Sikorska-Senoner, A. E., Addor, N., Brunner, M., Pool, S., Zappa, M., and Fenicia, F.: CAMELS-CH: hydro-meteorological time series and landscape attributes for 331 catchments in hydrologic Switzerland, *Earth System Science Data*, 15, 5755–5784, <https://doi.org/10.5194/essd-15-5755-2023>, publisher: Copernicus GmbH, 2023a.
- Höge, M., Kauzlaric, M., Siber, R., Schönenberger, U., Horton, P., Schwanbeck, J., Floriancic, M. G., Viviroli, D., Wilhelm, S., Sikorska-Senoner, A. E., Addor, N., Brunner, M., Pool, S., Zappa, M., and Fenicia, F.: Catchment attributes and hydro-meteorological time series for large-sample studies across hydrologic Switzerland (CAMELS-CH), <https://doi.org/10.5281/zenodo.10354485>, 2023b.
- 1015 Imfeld, N., Stucki, P., Brönnimann, S., Bürgi, M., Calanca, P., Holzkämper, A., Isotta, F., Nussbaumer, S. U., Scherrer, S., Staub, K., Vicedo-Cabrera, A., Wohlgenuth, T., and Zumbühl, H. J.: 2022: Ein ziemlich normaler zukünftiger Sommer, *Geographica Bernensia*, G100, 1–3, <https://doi.org/10.4480/GB2022.G100>, publisher: Geographisches Institut Universität Bern, 2022.
- 1020 Jehn, F. U., Bestian, K., Breuer, L., Kraft, P., and Houska, T.: Using hydrological and climatic catchment clusters to explore drivers of catchment behavior, *Hydrology and Earth System Sciences*, 24, 1081–1100, <https://doi.org/10.5194/hess-24-1081-2020>, publisher: Copernicus GmbH, 2020.
- Kchouk, S., Melsen, L. A., Walker, D. W., and van Oel, P. R.: A geography of drought indices: mismatch between indicators of drought and its impacts on water and food securities, *Natural Hazards and Earth System Sciences*, 22, 323–344, <https://doi.org/10.5194/nhess-22-323-2022>, publisher: Copernicus GmbH, 2022.
- 1025 Koehler, J., Dietz, A. J., Zellner, P., Baumhoer, C. A., Dirscherl, M., Cattani, L., Vlahović, , Alasawedah, M. H., Mayer, K., Haslinger, K., Bertoldi, G., Jacob, A., and Kuenzer, C.: Drought in Northern Italy: Long Earth Observation Time Series Reveal Snow Line Elevation to Be Several Hundred Meters Above Long-Term Average in 2022, *Remote Sensing*, 14, 6091, <https://doi.org/10.3390/rs14236091>, number: 23 Publisher: Multidisciplinary Digital Publishing Institute, 2022.
- 1030 Kotlarski, S., Gobiet, A., Morin, S., Olefs, M., Rajczak, J., and Samacoits, R.: 21st Century alpine climate change, *Clim Dyn*, 60, 65–86, <https://doi.org/10.1007/s00382-022-06303-3>, 2023.
- Kratzert, F., Klotz, D., Brenner, C., Schulz, K., and Herrnegger, M.: Rainfall–runoff modelling using Long Short-Term Memory (LSTM) networks, *Hydrology and Earth System Sciences*, 22, 6005–6022, <https://doi.org/10.5194/hess-22-6005-2018>, publisher: Copernicus GmbH, 2018.
- 1035 Kratzert, F., Klotz, D., Shalev, G., Klambauer, G., Hochreiter, S., and Nearing, G.: Towards learning universal, regional, and local hydrological behaviors via machine learning applied to large-sample datasets, *Hydrology and Earth System Sciences*, 23, 5089–5110, <https://doi.org/10.5194/hess-23-5089-2019>, publisher: Copernicus GmbH, 2019.
- Kratzert, F., Nearing, G., Addor, N., Erickson, T., Gauch, M., Gilon, O., Gudmundsson, L., Hassidim, A., Klotz, D., Nevo, S., Shalev, G., and Matias, Y.: Caravan - A global community dataset for large-sample hydrology, *Sci Data*, 10, 61, <https://doi.org/10.1038/s41597-023-01975-w>, publisher: Nature Publishing Group, 2023.
- 1040 Laaha, G. and Koffler, D.: lfstat: Calculation of Low Flow Statistics for Daily Stream Flow Data. R package version 0.9.12, 2022.
- Lee, S. and Ajami, H.: Comprehensive assessment of baseflow responses to long-term meteorological droughts across the United States, *Journal of Hydrology*, 626, 130–256, <https://doi.org/10.1016/j.jhydrol.2023.130256>, 2023.
- Lees, T., Reece, S., Kratzert, F., Klotz, D., Gauch, M., De Bruijn, J., Kumar Sahu, R., Greve, P., Slater, L., and Dadson, S. J.: Hydrological concept formation inside long short-term memory (LSTM) networks, *Hydrology and Earth System Sciences*, 26, 3079–3101, <https://doi.org/10.5194/hess-26-3079-2022>, publisher: Copernicus GmbH, 2022.

- Mahto, S. S. and Mishra, V.: Global evidence of rapid flash drought recovery by extreme precipitation, *Environ. Res. Lett.*, 19, 044 031, <https://doi.org/10.1088/1748-9326/ad300c>, publisher: IOP Publishing, 2024.
- Marty, C., Michel, A., Jonas, T., Steijn, C., Muelchi, R., and Kotlarski, S.: SPASS – new gridded climatological snow datasets for Switzerland: Potential and limitations, *EGUsphere*, pp. 1–21, <https://doi.org/10.5194/egusphere-2025-413>, publisher: Copernicus GmbH, 2025.
- Massari, C., Avanzi, F., Bruno, G., Gabellani, S., Penna, D., and Camici, S.: Evaporation enhancement drives the European water-budget deficit during multi-year droughts, *Hydrology and Earth System Sciences*, 26, 1527–1543, <https://doi.org/10.5194/hess-26-1527-2022>, publisher: Copernicus GmbH, 2022.
- Matanó, A., Berghuijs, W. R., Mazzoleni, M., Ruiten, M. C. d., Ward, P. J., and Loon, A. F. V.: Compound and consecutive drought-flood events at a global scale, *Environ. Res. Lett.*, 19, 064 048, <https://doi.org/10.1088/1748-9326/ad4b46>, publisher: IOP Publishing, 2024.
- McKee, T., Doesken, N., and Kleist, J.: THE RELATIONSHIP OF DROUGHT FREQUENCY AND DURATION TO TIME SCALES, Eight conference on applied climatology, 17-22 January 1993, Anaheim, California, <https://www.semanticscholar.org/paper/THE-RELATIONSHIP-OF-DROUGHT-FREQUENCY-AND-DURATION-McKee-Doesken/c3f7136d6cb726b295eb34565a8270177c57f40f>, 1993.
- Melsen, L. A. and Guse, B.: Hydrological Drought Simulations: How Climate and Model Structure Control Parameter Sensitivity, *Water Resources Research*, 55, 10 527–10 547, <https://doi.org/10.1029/2019WR025230>, _eprint: <https://onlinelibrary.wiley.com/doi/pdf/10.1029/2019WR025230>, 2019.
- Menapace, A., Dhawan, P., Dalla Torre, D., Kaffas, K., Crespi, A., Larcher, M., Righetti, M., and Cannon, A. J.: Review of bias correction methods for climate model outputs in hydrology, *Journal of Hydrology*, 660, 133 213, <https://doi.org/10.1016/j.jhydrol.2025.133213>, 2025.
- MeteoSwiss: Daily Precipitation (final analysis): RhiresD, https://www.meteoswiss.admin.ch/dam/jcr:4f51f0f1-0fe3-48b5-9de0-15666327e63c/ProdDoc_RhiresD.pdf, 2021a.
- MeteoSwiss: Daily Mean, Minimum and Maximum Temperature: TabsD, TminD, TmaxD, https://www.meteoswiss.admin.ch/dam/jcr:818a4d17-cb0c-4e8b-92c6-1a1bdf5348b7/ProdDoc_TabsD.pdf, 2021b.
- MeteoSwiss: Daily Relative Sunshine Duration: SrelD, https://www.meteoswiss.admin.ch/dam/jcr:981891db-30d1-47cc-a2e1-50c270bdaf22/ProdDoc_SrelD.pdf, 2021c.
- MeteoSwiss: Spatial Climate Analyses - MeteoSwiss, <https://www.meteoswiss.admin.ch/climate/the-climate-of-switzerland/spatial-climate-analyses.html>, 2024.
- MeteoSwiss: Open Data - MeteoSchweiz, <https://www.meteoswiss.admin.ch/service-und-publikationen/service/open-data.html>, 2025.
- Michel, A., Aschauer, J., Jonas, T., Gubler, S., Kotlarski, S., and Marty, C.: SnowQM 1.0: A fast R Package for bias-correcting spatial fields of snow water equivalent using quantile mapping, *Geoscientific Model Development Discussions*, pp. 1–28, <https://doi.org/10.5194/gmd-2022-298>, publisher: Copernicus GmbH, 2023.
- Miller, V. C.: A quantitative geomorphic study of drainage basin characteristics in the Clinch Mountain Area, Virginia and Tennessee. New York: Columbia University, Office of Naval Research Project NR 389 - 042, Technical Report No. 3., Project NR 389 - 042, Technical Report 3, Columbia University, Office of Naval Research, New York, <https://apps.dtic.mil/sti/citations/tr/AD0057755>, 1953.
- Mishra, A. K. and Singh, V. P.: A review of drought concepts, *Journal of Hydrology*, 391, 202–216, <https://doi.org/10.1016/j.jhydrol.2010.07.012>, 2010.
- Mott, R.: Climatological snow data since 1998, OSHD. *EnviDat*. <https://www.doi.org/10.16904/envidat.401>, 2023.

- Mott, R., Winstral, A., Cluzet, B., Helbig, N., Magnusson, J., Mazzotti, G., Quéno, L., Schirmer, M., Webster, C., and Jonas, T.: Operational snow-hydrological modeling for Switzerland, *Front. Earth Sci.*, 11, <https://doi.org/10.3389/feart.2023.1228158>, publisher: Frontiers, 2023.
- 1085 Muelchi, R., Rössler, O., Schwanbeck, J., Weingartner, R., and Martius, O.: River runoff in Switzerland in a changing climate – changes in moderate extremes and their seasonality, *Hydrology and Earth System Sciences*, 25, 3577–3594, <https://doi.org/10.5194/hess-25-3577-2021>, publisher: Copernicus GmbH, 2021a.
- Muelchi, R., Rössler, O., Schwanbeck, J., Weingartner, R., and Martius, O.: River runoff in Switzerland in a changing climate – runoff regime changes and their time of emergence, *Hydrology and Earth System Sciences*, 25, 3071–3086, <https://doi.org/10.5194/hess-25-3071-2021>, publisher: Copernicus GmbH, 2021b.
- 1090 Mukherjee, S., Mishra, A., and Trenberth, K. E.: Climate Change and Drought: a Perspective on Drought Indices, *Curr Clim Change Rep*, 4, 145–163, <https://doi.org/10.1007/s40641-018-0098-x>, 2018.
- Muñoz-Sabater, J., Dutra, E., Agustí-Panareda, A., Albergel, C., Arduini, G., Balsamo, G., Boussetta, S., Choulga, M., Harrigan, S., Hersbach, H., Martens, B., Miralles, D. G., Piles, M., Rodríguez-Fernández, N. J., Zsoter, E., Buontempo, C., and Thépaut, J.-N.: ERA5-Land: a state-of-the-art global reanalysis dataset for land applications, *Earth System Science Data*, 13, 4349–4383, <https://doi.org/10.5194/essd-13-4349-2021>, publisher: Copernicus GmbH, 2021.
- 1095 Mwinjuma, M., Wang, R., Mtupili, M., and Twaha, M.: Comparisons of SPI and SPEI in capturing drought dynamics: A Global assessment across arid and humid regions, *Atmospheric Research*, 329, 108 475, <https://doi.org/10.1016/j.atmosres.2025.108475>, 2026.
- 1100 Myronidis, D., Fotakis, D., Ioannou, K., and Sgouropoulou, K.: Comparison of ten notable meteorological drought indices on tracking the effect of drought on streamflow, *Hydrological Sciences Journal*, 63, 2005–2019, <https://doi.org/10.1080/02626667.2018.1554285>, publisher: Taylor & Francis _eprint: <https://doi.org/10.1080/02626667.2018.1554285>, 2018.
- Najafi, H., Lagerwall, G. L., Obeysekera, J., and Liu, J.: Machine Learning in Climate Downscaling: A Critical Review of Methodologies, Physical Consistency, and Operational Applications, *Water*, 18, 271, <https://doi.org/10.3390/w18020271>, publisher: Multidisciplinary Digital Publishing Institute, 2026.
- 1105 Nathan, R. J. and McMahon, T. A.: Evaluation of automated techniques for base flow and recession analyses, *Water Resources Research*, 26, 1465–1473, <https://doi.org/10.1029/WR026i007p01465>, _eprint: <https://onlinelibrary.wiley.com/doi/pdf/10.1029/WR026i007p01465>, 1990.
- Naumann, G., Cammalleri, C., Mentaschi, L., and Feyen, L.: Increased economic drought impacts in Europe with anthropogenic warming, *Nat. Clim. Chang.*, 11, 485–491, <https://doi.org/10.1038/s41558-021-01044-3>, number: 6 Publisher: Nature Publishing Group, 2021.
- 1110 NCCS, N. C. f. C. S.: South side of the Alps - Current climate., <https://www.nccs.admin.ch/nccs/en/home/regionen/grossregionen/alpensuedseite/klima-heute-alpensuedseite.html>, 2025.
- Orth, R. and Destouni, G.: Drought reduces blue-water fluxes more strongly than green-water fluxes in Europe, *Nat Commun*, 9, 3602, <https://doi.org/10.1038/s41467-018-06013-7>, 2018.
- 1115 Otero, N., Horton, P., Martius, O., Allen, S., Zappa, M., Wechsler, T., and Schaeffli, B.: Impacts of hot-dry conditions on hydropower production in Switzerland, *Environ. Res. Lett.*, 18, 064 038, <https://doi.org/10.1088/1748-9326/acd8d7>, publisher: IOP Publishing, 2023.
- Parry, S., Prudhomme, C., Wilby, R. L., and Wood, P. J.: Drought termination: Concept and characterisation, *Progress in Physical Geography: Earth and Environment*, 40, 743–767, <https://doi.org/10.1177/0309133316652801>, publisher: SAGE Publications Ltd, 2016.
- Parry, S., Wilby, R., Prudhomme, C., Wood, P., and McKenzie, A.: Demonstrating the utility of a drought termination framework: prospects for groundwater level recovery in England and Wales in 2018 or beyond, *Environ. Res. Lett.*, 13, 064 040, <https://doi.org/10.1088/1748-9326/aac78c>, publisher: IOP Publishing, 2018.
- 1120

- Pebesma, E.: Simple Features for R: Standardized Support for Spatial Vector Data, *The R Journal*, 10, 439–446, <https://journal.r-project.org/archive/2018/RJ-2018-009/index.html>, 2018.
- 1125 Pebesma, E. and Bivand, R.: *Spatial Data Science: With Applications in R*, Chapman and Hall/CRC, New York, <https://doi.org/10.1201/9780429459016>, 2023.
- Peña-Angulo, D., Vicente-Serrano, S. M., Domínguez-Castro, F., Lorenzo-Lacruz, J., Murphy, C., Hannaford, J., Allan, R. P., Trambly, Y., Reig-Gracia, F., and El Kenawy, A.: The Complex and Spatially Diverse Patterns of Hydrological Droughts Across Europe, *Water Resources Research*, 58, e2022WR031976, <https://doi.org/10.1029/2022WR031976>, _eprint: <https://onlinelibrary.wiley.com/doi/pdf/10.1029/2022WR031976>, 2022.
- 1130 Peña-Gallardo, M., Vicente-Serrano, S. M., Hannaford, J., Lorenzo-Lacruz, J., Svoboda, M., Domínguez-Castro, F., Maneta, M., Tomas-Burguera, M., and Kenawy, A. E.: Complex influences of meteorological drought time-scales on hydrological droughts in natural basins of the contiguous United States, *Journal of Hydrology*, 568, 611–625, <https://doi.org/10.1016/j.jhydrol.2018.11.026>, 2019.
- Pisupati, S. L. and Ratnakar, P.: Morphometric analysis and prioritization of sub-watersheds in the Gosthani River Basin of southern India using PCA-WSM and geospatial techniques, *Journal of Water and Climate Change*, 16, 2006–2031, <https://doi.org/10.2166/wcc.2025.727>, 2025.
- 1135 Poussin, C., Massot, A., Ginzler, C., Weber, D., Chatenoux, B., Lacroix, P., Piller, T., Nguyen, L., and Giuliani, G.: Drying conditions in Switzerland – indication from a 35-year Landsat time-series analysis of vegetation water content estimates to support SDGs, *Big Earth Data*, 5, 445–475, <https://doi.org/10.1080/20964471.2021.1974681>, publisher: Taylor & Francis _eprint: <https://doi.org/10.1080/20964471.2021.1974681>, 2021.
- 1140 Qiu, J., Shen, Z., Leng, G., and Wei, G.: Synergistic effect of drought and rainfall events of different patterns on watershed systems, *Sci Rep*, 11, 18957, <https://doi.org/10.1038/s41598-021-97574-z>, number: 1 Publisher: Nature Publishing Group, 2021.
- Ranasinghe, R., Ruane, A. C., Vautard, R., Arnell, N., Coppola, E., Cruz, F. A., Dessai, S., Islam, A. S., Rahimi, M., Ruiz Carrascal, D., Sillmann, J., Sylla, M. B., Tebaldi, C., Wang, W., and Zaaboul, R.: Climate Change Information for Regional Impact and for Risk Assessment., in: *Climate Change 2021: The Physical Science Basis. Contribution of Working Group I to the Sixth Assessment Report of the Intergovernmental Panel on Climate Change.*, pp. 1767–1926, Cambridge University Press, Cambridge, United Kingdom and New York, NY, USA, doi:10.1017/9781009157896.014, 2021.
- 1145 Raposo, V. d. M. B., Costa, V. A. F., and Rodrigues, A. F.: A review of recent developments on drought characterization, propagation, and influential factors, *Science of The Total Environment*, 898, 165550, <https://doi.org/10.1016/j.scitotenv.2023.165550>, 2023.
- Rodell, M. and Reager, J. T.: Water cycle science enabled by the GRACE and GRACE-FO satellite missions, *Nat Water*, 1, 47–59, <https://doi.org/10.1038/s44221-022-00005-0>, publisher: Nature Publishing Group, 2023.
- 1150 Saft, M., Western, A. W., Zhang, L., Peel, M. C., and Potter, N. J.: The influence of multiyear drought on the annual rainfall-runoff relationship: An Australian perspective, *Water Resources Research*, 51, 2444–2463, <https://doi.org/10.1002/2014WR015348>, _eprint: <https://onlinelibrary.wiley.com/doi/pdf/10.1002/2014WR015348>, 2015.
- Samaniego, L., Kumar, R., and Zink, M.: Implications of Parameter Uncertainty on Soil Moisture Drought Analysis in Germany, *Journal of Hydrometeorology*, 14, 47–68, <https://doi.org/10.1175/JHM-D-12-075.1>, publisher: American Meteorological Society Section: Journal of Hydrometeorology, 2013.
- 1155 Samaniego, L., Thober, S., Kumar, R., Wanders, N., Rakovec, O., Pan, M., Zink, M., Sheffield, J., Wood, E. F., and Marx, A.: Anthropogenic warming exacerbates European soil moisture droughts, *Nature Clim Change*, 8, 421–426, <https://doi.org/10.1038/s41558-018-0138-5>, number: 5 Publisher: Nature Publishing Group, 2018.

- 1160 Sarailidis, G., Vasiliades, L., and Loukas, A.: Analysis of streamflow droughts using fixed and variable thresholds, *Hydrological Processes*, 33, 414–431, <https://doi.org/10.1002/hyp.13336>, _eprint: <https://onlinelibrary.wiley.com/doi/pdf/10.1002/hyp.13336>, 2019.
- Savelli, E., Rusca, M., Cloke, H., and Di Baldassarre, G.: Drought and society: Scientific progress, blind spots, and future prospects, *WIREs Climate Change*, 13, e761, <https://doi.org/10.1002/wcc.761>, _eprint: <https://onlinelibrary.wiley.com/doi/pdf/10.1002/wcc.761>, 2022.
- Scherrer, S. C., Hirschi, M., Spirig, C., Maurer, F., and Kotlarski, S.: Trends and drivers of recent summer drying in Switzerland, *Environ. Res. Commun.*, <https://doi.org/10.1088/2515-7620/ac4fb9>, 2022.
- 1165 Scherrer, S. C., Göldi, M., Gubler, S., Steger, C. R., and Kotlarski, S.: Towards a spatial snow climatology for Switzerland: Comparison and validation of existing datasets, *Meteorologische Zeitschrift*, <https://doi.org/10.1127/metz/2023/1210>, publisher: Schweizerbart'sche Verlagsbuchhandlung, 2023.
- Schürch, M., Kozel, R., and Jemelin, L.: Hydrogeological mapping in Switzerland, *Hydrogeol J*, 15, 799–808, <https://doi.org/10.1007/s10040-006-0136-y>, 2007.
- 1170 Shapiro, S. S. and Wilk, M. B.: An Analysis of Variance Test for Normality (Complete Samples), *Biometrika*, 52, 591–611, <https://doi.org/10.2307/2333709>, publisher: [Oxford University Press, Biometrika Trust], 1965.
- Sideris, I. V., Gabella, M., Erdin, R., and Germann, U.: Real-time radar–rain–gauge merging using spatio-temporal co-kriging with external drift in the alpine terrain of Switzerland, *Quarterly Journal of the Royal Meteorological Society*, 140, 1097–1111, <https://doi.org/10.1002/qj.2188>, _eprint: <https://onlinelibrary.wiley.com/doi/pdf/10.1002/qj.2188>, 2014.
- 1175 Stagge, J. H., Tallaksen, L. M., Gudmundsson, L., Van Loon, A. F., and Stahl, K.: Candidate Distributions for Climatological Drought Indices (SPI and SPEI), *International Journal of Climatology*, 35, 4027–4040, <https://doi.org/10.1002/joc.4267>, _eprint: <https://onlinelibrary.wiley.com/doi/pdf/10.1002/joc.4267>, 2015.
- Stahl, K., Vidal, J.-P., Hannaford, J., Tjeldeman, E., Laaha, G., Gauster, T., and Tallaksen, L. M.: The challenges of hydrological drought definition, quantification and communication: an interdisciplinary perspective, in: *Proceedings of IAHS*, vol. 383, pp. 291–295, Copernicus GmbH, <https://doi.org/10.5194/piahs-383-291-2020>, iSSN: 2199-8981, 2020.
- 1180 Staudinger, M., Stahl, K., and Seibert, J.: A drought index accounting for snow, *Water Resources Research*, 50, 7861–7872, <https://doi.org/10.1002/2013WR015143>, _eprint: <https://onlinelibrary.wiley.com/doi/pdf/10.1002/2013WR015143>, 2014.
- Staudinger, M., Stoelzle, M., Seeger, S., Seibert, J., Weiler, M., and Stahl, K.: Catchment water storage variation with elevation, *Hydrological Processes*, 31, 2000–2015, <https://doi.org/10.1002/hyp.11158>, _eprint: <https://onlinelibrary.wiley.com/doi/pdf/10.1002/hyp.11158>, 2017.
- 1185 Stocker, B. D.: *cwd v1.0: R package for cumulative water deficit calculation (v1.0)*. Zenodo. <https://doi.org/10.5281/zenodo.5359053>, 2021.
- Stocker, B. D., Tumber-Dávila, S. J., Konings, A. G., Anderson, M. C., Hain, C., and Jackson, R. B.: Global patterns of water storage in the rooting zones of vegetation, *Nat. Geosci.*, 16, 250–256, <https://doi.org/10.1038/s41561-023-01125-2>, number: 3 Publisher: Nature Publishing Group, 2023.
- 1190 Stoelzle, M., Schuetz, T., Weiler, M., Stahl, K., and Tallaksen, L. M.: Beyond binary baseflow separation: a delayed-flow index for multiple streamflow contributions, *Hydrology and Earth System Sciences*, 24, 849–867, <https://doi.org/10.5194/hess-24-849-2020>, publisher: Copernicus GmbH, 2020.
- Streeb, N., Lustenberger, F., and Zappa, M.: Beurteilung der Beeinflussung des Abflusses an NAWA-Messstellen. Detailbericht des BAFU-Projekts HydCheck., Tech. rep., Eidg. Forschungsanstalt WSL, Birmensdorf, https://www.bafu.admin.ch/dam/bafu/de/dokumente/wasser/externe-studien-berichte/beurteilung-der-beeinflussung-des-abflusses-an-nawa-messstellen.pdf.download.pdf/20241007_HydCheck_Detailbericht.pdf, 2024.
- 1195

- Sur, C., Park, S.-Y., Kim, J.-S., and Lee, J.-H.: Prognostic and diagnostic assessment of hydrological drought using water and energy budget-based indices, *Journal of Hydrology*, 591, 125–149, <https://doi.org/10.1016/j.jhydrol.2020.125549>, 2020.
- 1200 Sutanto, S. J. and Van Lanen, H. A. J.: Catchment memory explains hydrological drought forecast performance, *Sci Rep*, 12, 2689, <https://doi.org/10.1038/s41598-022-06553-5>, number: 1 Publisher: Nature Publishing Group, 2022.
- Swiss Confederation: Nationale Trockenheitsplattform, <https://www.trockenheit.admin.ch/de>, 2025.
- Swisstopo: Bodeneignungskarte der Schweiz, <https://www.bfs.admin.ch/bfs/de/home/dienstleistungen/geostat/geodaten-bundesstatistik/boden-nutzung-bedeckung-eignung/abgeleitete-und-andere-daten/bodeneignungskarte-schweiz.html>, 2020.
- Tallaksen, L. M. and Van Lanen, H. A. J., eds.: Hydrological drought: processes and estimation methods for streamflow and groundwater., no. 48 in *Developments in Water Science*, Elsevier Science B.V., Amsterdam, the Netherlands, 2004.
- 1205 Tallaksen, L. M., Madsen, H., and Clausen, B.: On the definition and modelling of streamflow drought duration and deficit volume, *Hydrological Sciences Journal*, 42, 15–33, <https://doi.org/10.1080/02626669709492003>, publisher: Taylor & Francis _eprint: <https://doi.org/10.1080/02626669709492003>, 1997.
- Tarasova, L., Gnann, S., Yang, S., Hartmann, A., and Wagener, T.: Catchment characterization: Current descriptors, knowledge gaps and future opportunities, *Earth-Science Reviews*, 252, 104–139, <https://doi.org/10.1016/j.earscirev.2024.104739>, 2024.
- 1210 Tijdeman, E., Barker, L. J., Svoboda, M. D., and Stahl, K.: Natural and Human Influences on the Link Between Meteorological and Hydrological Drought Indices for a Large Set of Catchments in the Contiguous United States, *Water Resources Research*, 54, 6005–6023, <https://doi.org/10.1029/2017WR022412>, _eprint: <https://onlinelibrary.wiley.com/doi/pdf/10.1029/2017WR022412>, 2018.
- Tijdeman, E., Stahl, K., and Tallaksen, L. M.: Drought Characteristics Derived Based on the Standardized Streamflow Index: A Large Sample Comparison for Parametric and Nonparametric Methods, *Water Resources Research*, 56, e2019WR026315, <https://doi.org/10.1029/2019WR026315>, _eprint: <https://onlinelibrary.wiley.com/doi/pdf/10.1029/2019WR026315>, 2020.
- 1215 Tijdeman, E., Blauhut, V., Stoelzle, M., Menzel, L., and Stahl, K.: Different drought types and the spatial variability in their hazard, impact, and propagation characteristics, *Natural Hazards and Earth System Sciences*, 22, 2099–2116, <https://doi.org/10.5194/nhess-22-2099-2022>, publisher: Copernicus GmbH, 2022.
- 1220 Tripathy, K. P. and Mishra, A. K.: How Unusual Is the 2022 European Compound Drought and Heat-wave Event?, *Geophysical Research Letters*, 50, e2023GL105453, <https://doi.org/10.1029/2023GL105453>, _eprint: <https://onlinelibrary.wiley.com/doi/pdf/10.1029/2023GL105453>, 2023.
- Tschurr, F., Feigenwinter, I., Fischer, A. M., and Kotlarski, S.: Climate Scenarios and Agricultural Indices: A Case Study for Switzerland, *Atmosphere*, 11, 535, <https://doi.org/10.3390/atmos11050535>, number: 5 Publisher: Multidisciplinary Digital Publishing Institute, 2020.
- 1225 USGS: Drainage Density | U.S. Geological Survey, <https://www.usgs.gov/media/images/drainage-density>, 2023.
- Van Lanen, H. a. J., Wanders, N., Tallaksen, L. M., and Van Loon, A. F.: Hydrological drought across the world: impact of climate and physical catchment structure, *Hydrology and Earth System Sciences*, 17, 1715–1732, <https://doi.org/10.5194/hess-17-1715-2013>, publisher: Copernicus GmbH, 2013.
- Van Loon, A. F.: Hydrological drought explained, *WIREs Water*, 2, 359–392, <https://doi.org/10.1002/wat2.1085>, _eprint: <https://onlinelibrary.wiley.com/doi/pdf/10.1002/wat2.1085>, 2015.
- 1230 Van Loon, A. F. and Laaha, G.: Hydrological drought severity explained by climate and catchment characteristics, *Journal of Hydrology*, 526, 3–14, <https://doi.org/10.1016/j.jhydrol.2014.10.059>, 2015.
- Van Loon, A. F. and Van Lanen, H. a. J.: A process-based typology of hydrological drought, *Hydrology and Earth System Sciences*, 16, 1915–1946, <https://doi.org/10.5194/hess-16-1915-2012>, publisher: Copernicus GmbH, 2012.

- 1235 Vicente-Serrano, S. M., Beguería, S., and López-Moreno, J. I.: A Multiscalar Drought Index Sensitive to Global Warming: The Standardized Precipitation Evapotranspiration Index, *Journal of Climate*, 23, 1696–1718, <https://doi.org/10.1175/2009JCLI2909.1>, publisher: American Meteorological Society Section: *Journal of Climate*, 2010.
- Vicente-Serrano, S. M., Peña-Angulo, D., Beguería, S., Domínguez-Castro, F., Tomás-Burguera, M., Noguera, I., Gimeno-Sotelo, L., and El Kenawy, A.: Global drought trends and future projections, *Philosophical Transactions of the Royal Society A: Mathematical, Physical and Engineering Sciences*, 380, 20210285, <https://doi.org/10.1098/rsta.2021.0285>, publisher: Royal Society, 2022.
- 1240 Viviroli, D., Zappa, M., Gurtz, J., and Weingartner, R.: An introduction to the hydrological modelling system PREVAH and its pre- and post-processing-tools, *Environmental Modelling & Software*, 24, 1209–1222, <https://doi.org/10.1016/j.envsoft.2009.04.001>, 2009.
- von Matt, C. N., Muelchi, R., Gudmundsson, L., and Martius, O.: Compound droughts under climate change in Switzerland, *Natural Hazards and Earth System Sciences*, 24, 1975–2001, <https://doi.org/10.5194/nhess-24-1975-2024>, publisher: Copernicus GmbH, 2024.
- 1245 von Matt, C. N., Martius, O., and Stocker, B.: HYD-RESPONSES: High-resolution daily catchment-level time series for relevant hydro-meteorological variables, (water) deficit accumulation and streamflow droughts for Switzerland, <https://doi.org/10.5281/zenodo.15748821>, 2026.
- Weingartner, R. and Schwanbeck, J.: Veränderung der Niedrigwasserabflüsse und der kleinsten saisonalen Abflüsse in der Schweiz im Zeitraum 1961 – 2018. Im Auftrag des Bundesamts für Umwelt (BAFU), Bern, Schweiz, 41 S., Tech. rep., Bern, Schweiz, 2020.
- 1250 Wickham, H., Averick, M., Bryan, J., Chang, W., McGowan, L. D., François, R., Grolemund, G., Hayes, A., Henry, L., Hester, J., Kuhn, M., Pedersen, T. L., Miller, E., Bache, S. M., Müller, K., Ooms, J., Robinson, D., Seidel, D. P., Spinu, V., Takahashi, K., Vaughan, D., Wilke, C., Woo, K., and Yutani, H.: Welcome to the Tidyverse, *Journal of Open Source Software*, 4, 1686, <https://doi.org/10.21105/joss.01686>, 2019.
- WMO and GWP: Handbook of Drought Indicators and Indices (M. Svoboda and B. A. Fuchs). Integrated Drought Management Programme (IDMP), Integrated Drought Management Tools and Guidelines Series 2. Geneva., 2016.
- 1255 Wood, R. R., Janzing, J., van Hamel, A., Götte, J., Schumacher, D. L., and Brunner, M. I.: Comparison of high-resolution climate reanalysis datasets for hydro-climatic impact studies, *Hydrology and Earth System Sciences*, 29, 4153–4178, <https://doi.org/10.5194/hess-29-4153-2025>, publisher: Copernicus GmbH, 2025.
- Wu, J., Chen, X., Love, C. A., Yao, H., Chen, X., and AghaKouchak, A.: Determination of water required to recover from hydrological drought: Perspective from drought propagation and non-standardized indices, *Journal of Hydrology*, 590, 125227, <https://doi.org/10.1016/j.jhydrol.2020.125227>, 2020.
- 1260 Wu, J., Chen, X., Yuan, X., Yao, H., Zhao, Y., and AghaKouchak, A.: The interactions between hydrological drought evolution and precipitation-streamflow relationship, *Journal of Hydrology*, 597, 126210, <https://doi.org/10.1016/j.jhydrol.2021.126210>, 2021.
- Wu, J., Mallakpour, I., Yuan, X., Yao, H., Wang, G., and Chen, X.: Impact of the false intensification and recovery on the hydrological drought internal propagation, *Weather and Climate Extremes*, 36, 100430, <https://doi.org/10.1016/j.wace.2022.100430>, 2022.
- 1265 Xu, Z., Wu, Z., Guo, X., and He, H.: Estimation of water required to recover from agricultural drought: Perspective from regression and probabilistic analysis methods, *Journal of Hydrology*, 617, 128888, <https://doi.org/10.1016/j.jhydrol.2022.128888>, 2023.
- Yi, K., Senay, G. B., Fisher, J. B., Wang, L., Suvočarev, K., Chu, H., Moore, G. W., Novick, K. A., Barnes, M. L., Keenan, T. F., Mallick, K., Luo, X., Missik, J. E. C., Delwiche, K. B., Nelson, J. A., Good, S. P., Xiao, X., Kannenberg, S. A., Ahmadi, A., Wang, T., Bohrer, G., Litvak, M. E., Reed, D. E., Oishi, A. C., Torn, M. S., and Baldocchi, D.: Challenges and Future Directions in Quantifying Terrestrial Evapotranspiration, *Water Resources Research*, 60, e2024WR037622, <https://doi.org/10.1029/2024WR037622>, <https://agupubs.onlinelibrary.wiley.com/doi/pdf/10.1029/2024WR037622>, 2024.

- Yihdego, Y., Vaheddoost, B., and Al-Weshah, R. A.: Drought indices and indicators revisited, *Arab J Geosci*, 12, 69, <https://doi.org/10.1007/s12517-019-4237-z>, 2019.
- 1275 Zambrano-Bigiarini, M.: hydroTSM: Time Series Management, Analysis and Interpolation for Hydrological ModellingR package version 0.6-0. URL <https://github.com/hzambran/hydroTSM>. DOI:10.5281/zenodo.839864., 2020.
- Zhang, L., Yan, Z., Huang, K., and Zhang, W.: Evaluation and statistical bias correction of ERA5-Land meteorological variables for a humid river basin in Southwest China, *Sci Rep*, 15, 41 101, <https://doi.org/10.1038/s41598-025-24942-4>, publisher: Nature Publishing Group, 2025.
- 1280 Zhou, Z., Shi, H., Fu, Q., Ding, Y., Li, T., and Liu, S.: Investigating the Propagation From Meteorological to Hydrological Drought by Introducing the Nonlinear Dependence With Directed Information Transfer Index, *Water Resources Research*, 57, e2021WR030028, <https://doi.org/10.1029/2021WR030028>, _eprint: <https://onlinelibrary.wiley.com/doi/pdf/10.1029/2021WR030028>, 2021.